5
Phase Equilibria in Fluid Systems

Conventional chemical plants can usually be divided into a preparation, reaction, and separation step (see Figure 5.1). Although the reactor can be considered as the heart or the central unit of the chemical plant, often 60–80% of the total costs are caused by the separation step, where the various thermal separation processes are applied to obtain the products with the desired purity, to recycle the unconverted reactants and to remove the undesired by-products. Because of the many advantages (energy used as separating agent, high-density differences between the two fluid phases (liquid, vapor)) in 90% of the cases distillation processes are applied in the chemical or the petrochemical industry, whereas in the pharmaceutical industry crystallization processes are far more important [1].

Different aspects have to be considered during the synthesis of separation processes. As the preliminary step the chemical engineer has to decide which separation processes should be used. Then he has to find out if separation problems occur. In the case of distillation these problems are typically azeotropic points, which do not allow separation by ordinary distillation. To understand distillation processes, the knowledge of residue curves and boundary lines is quite helpful. In the case of azeotropic points the engineer has to find an alternative way (e.g. separation at low or high pressure or by pressure swing distillation), or to select suitable solvents for the separation of the considered system (e.g. azeotropic or extractive distillation) or to choose a hybrid process (i.e., by combination of the distillation step with another separation process, for example, membrane separation, adsorption, etc.). Furthermore, the engineer has to design the equipment (e.g. to determine the number of theoretical stages needed or the height of the packing of the separation column) and in addition, he has to choose the optimum separation sequence. To treat the different aspects mentioned above, a reliable and detailed knowledge of the phase equilibrium behavior as a function of temperature, pressure, and composition for the multicomponent system, which has to be separated, is required.

The knowledge of the phase equilibrium behavior is not only important for the design of separation processes, but also for other applications, like the design of biphasic reactors, for example, gas–liquid reactors, the estimation of the fate of persistent chemicals in the environment, and so on.

In consequence, the typical question asked by the chemical engineer in the design phase is: "What is the composition and the pressure in phase β, when

Chemical Thermodynamics: for Process Simulation. First Edition.
Jürgen Gmehling, Bärbel Kolbe, Michael Kleiber, and Jürgen Rarey.

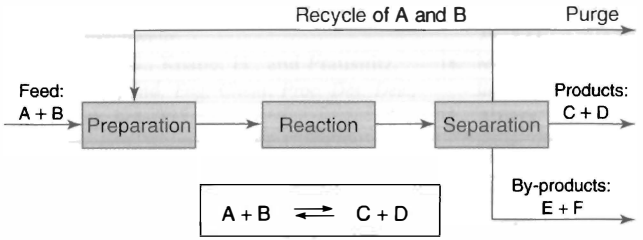

Figure 5.1 Simplified structure of a conventional chemical plant.

phase β is in equilibrium with phase α at given composition and temperature?" (see Figure 5.2). In most cases, multicomponent systems with nonpolar, polar, supercritical compounds, and electrolytes have to be considered. For example, for the system ethanol–water–sodium chloride–CO_2 several questions can be raised from Figure 5.2, such as:

- How strong does sodium chloride influence the solubility of CO_2 in the system ethanol–water?
- Does the system ethanol–water still show azeotropic behavior in the presence of sodium chloride?
- How is the solubility of sodium chloride in water influenced by the presence of ethanol and CO_2?
- Can the presence of sodium chloride cause a miscibility gap in the system ethanol–water?
- How strong is the pH-value influenced by the presence of CO_2?
- Which solvent can be applied to separate the azeotropic system ethanol–water by azeotropic or extractive distillation?
- Or can carbon dioxide directly be used for the separation of ethanol and water by supercritical extraction?

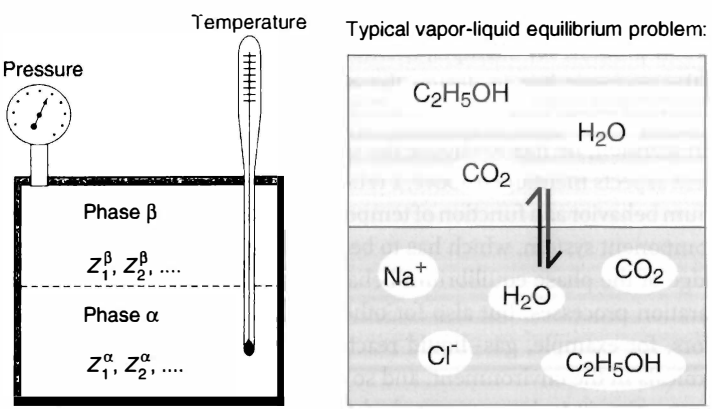

Figure 5.2 Equilibrium stage and typical separation problem.

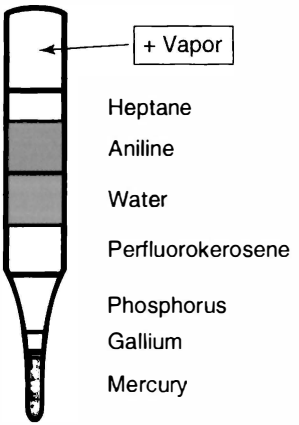

Figure 5.3 Seven liquid phases in equilibrium with the vapor phase [2].

However, the number of phases is not limited to two only. For example, in the case of hetero-azeotropic mixtures like butanol–water or ethanol–water–cyclohexane already two liquid phases exist besides the vapor phase. Hildebrand showed that in the system water–heptane–perfluorokerosene–aniline–phosphorus–gallium–mercury even seven liquid phases are in equilibrium with the vapor phase [2] (see Figure 5.3).

Depending on the state of the phases α and β vapor–liquid equilibria (VLE), liquid–liquid equilibria (LLE), solid–liquid equilibria (SLE), and so on, can be distinguished. In the case of VLE the phase equilibrium behavior is shown in Figure 5.4 as a *Pxy*-diagram for the binary system ethanol–water at 70 °C. For a given composition in the liquid phase the system pressure and the composition in

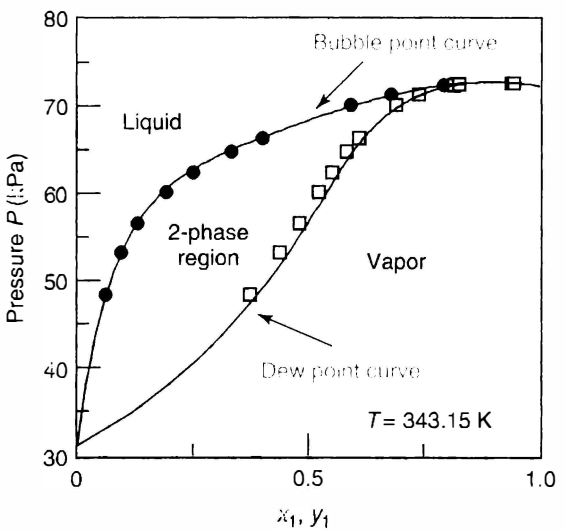

Figure 5.4 *Pxy*-diagram for the system ethanol (1)–water (2) at 70 °C [8].

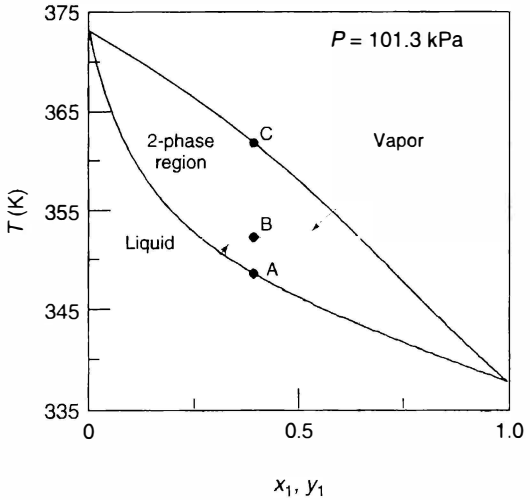

Figure 5.5 Illustration of the law of opposite lever arms on the basis of the binary system methanol (1)–water (2) at 101.3 kPa.

the vapor phase can be obtained from the diagram. Furthermore, it can be seen that at high ethanol concentrations the composition in the liquid phase is identical to the composition in the vapor phase, which makes a separation impossible by ordinary distillation.

In *Pxy*- and *Txy*-diagrams, the law of the opposite lever arms can be applied to determine the amount of vapor and liquid in the two-phase region. This is demonstrated in the *Txy*-diagram of the system methanol–water at 101.3 kPa (see Figure 5.5).

Consider a binary liquid mixture with the concentration z_0 and the temperature T_0. If the mixture is heated up, the bubble point line is reached in point A, and the first bubble is formed. When the mixture is further heated up, a further increase of temperature is obtained and more vapor is formed. At point B, the mixture consists of a liquid with the composition x_B and a vapor with the composition y_B. At point C, all liquid has been vaporized. Using n_T as the total number of moles, the mass balance yields for point B

$$n_T z_0 = \left(n^{\mathrm{L}} + n^{\mathrm{V}}\right) z_0 = n^{\mathrm{L}} x_B + n^{\mathrm{V}} y_B \tag{5.1}$$

which is equivalent to

$$\frac{n^{\mathrm{L}}}{n^{\mathrm{V}}} = \frac{y_B - z_0}{z_0 - x_B} \tag{5.2}$$

Therefore, the ratio between the amounts of vapor and liquid corresponds to the ratio of the lever arms located on the opposite side of the tie line.

From Figure 5.4 it can be seen that at 70 °C both compounds exist as liquids. Often the system temperature is above the critical temperature of one or more

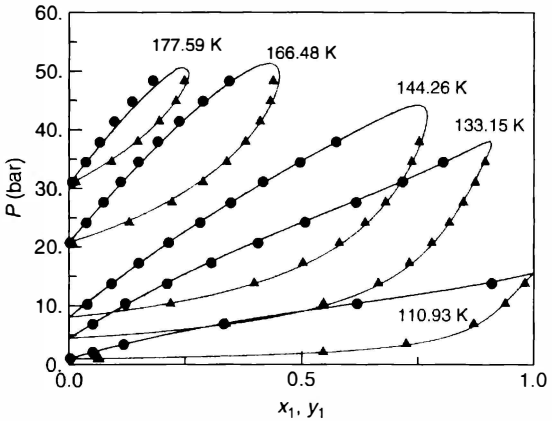

Figure 5.6 *Pxy*-diagram for the system nitrogen (1)–methane (2) at different temperatures.

components of the system considered. This is shown in Figure 5.6 for the binary system nitrogen–methane. Here the two phase regions do not cover the whole composition range for temperatures above the critical temperature of nitrogen ($T_c = 126.2$ K). Obviously now the binary system shows a critical point, where the length of the tie lines becomes zero.

But by applying the *Pxy*-diagram again the pressure and composition in the vapor phase for a given temperature and the corresponding composition in the liquid phase can be determined.

Often also the *K*-factors ($K_i = y_i/x_i$) are plotted as a function of the pressure, as shown in Figure 5.7 for the system nitrogen–methane. From this diagram the

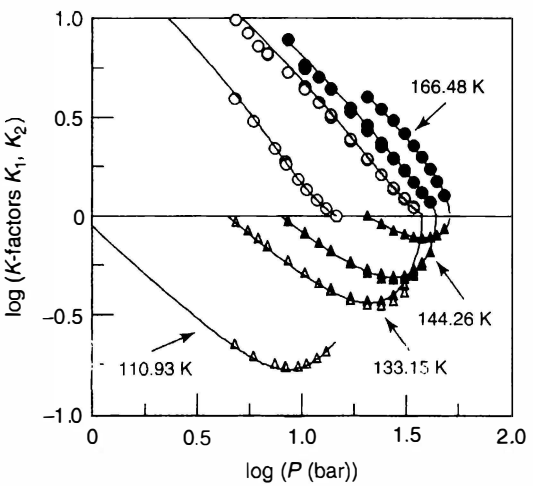

Figure 5.7 *K*-factors for the binary system nitrogen (1)–methane (2) as a function of pressure at different temperatures.

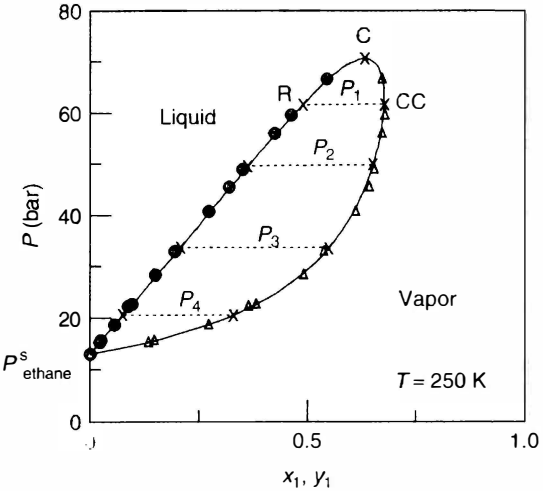

Figure 5.8 Isothermal *Px*-diagram for the binary system methane (1)–ethane (2) at 250 K.

K-factors for component 1 and 2 can be read directly for a given temperature and pressure. While for the low-boiler N_2 *K*-factors larger than one are obtained, *K*-factors smaller than one are observed for the high-boiler CH_4. At the same time the critical pressure of the mixture can be determined as the pressure where for a given isotherm both *K*-factors for the considered nonazeotropic system show a value of 1. This point can be found for all the isotherms above the critical temperature of nitrogen ($T_c = 126.2$ K).

With the help of an isothermal *Pxy*-diagram (see Figure 5.8) different phenomena which occur near the critical point, such as retrograde condensation or retrograde evaporation, can be explained.

For mole fractions lower than x_R the VLE behavior is similar to subcritical systems. Also in the range *R*–*C* a liquid and a vapor phase is obtained. But the vapor phase now is depleted of the low boiling component with increasing pressure from *CC* to *C*.

For compositions on the dew-point line in the range between *C* and *CC* a pressure decrease leads to the formation of a liquid phase. If the pressure is lowered further the amount of liquid phase will increase by condensation. At line P_1 the largest amount of liquid is found according to the law of the opposite lever arms. Below CC the system shows VLE behavior like subcritical systems again. This means vaporization instead of condensation is observed when the pressure is decreased, until the dew-point line is reached again and thus only vapor exists.

The lower limit of the region of retrograde condensation *CC* is often called *critical condensation point*. At *CC* the highest concentration of the low boiler in the vapor phase is obtained in equilibrium with the liquid phase. At this point the dew-point curve runs vertically and thus the slope for a given temperature is

$$\left(\frac{dP}{dy_1}\right)_{CC} = \infty \tag{5.3}$$

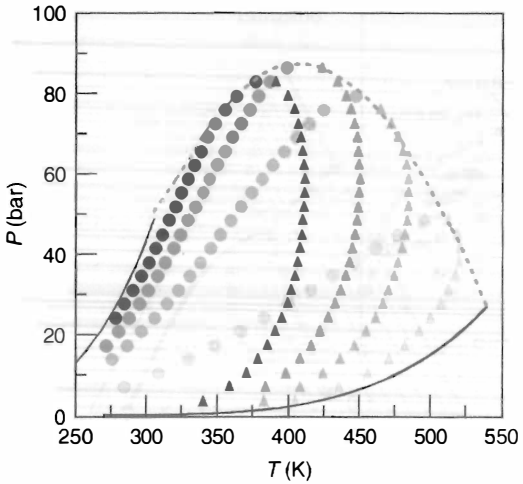

Figure 5.9 Experimental vapor pressures of ethane and heptane and experimental *PT*-data of the system ethane(1)–heptane (2) with different fixed compositions [3]—vapor pressure, ● liquid, ▲ vapor, ---- critical locus, $x_1 = y_1 = 0$, 0.2658, 0.5871, 0.7709, 0.8871, 1.

The upper limit of the retrograde region is the critical point *C*, which satisfies the following condition at constant temperature:

$$\left(\frac{dP}{dy_1}\right)_C = 0 \tag{5.4}$$

The phenomenon that a liquid is formed by lowering the pressure at constant temperature or, respectively, by increasing the temperature at constant pressure is called retrograde condensation.

Retrograde condensation plays an important role in technical applications, for example, in oil production, high-pressure pipelines, refrigeration processes and in natural gas reservoirs, where temperature and pressure are high enough to produce critical conditions.

The region in which vapor and liquid may coexist in a binary system is limited by the vapor pressure curves of the pure components and the critical line. In Figure 5.9 the vapor pressure curves of the pure compounds of the system ethane–heptane are shown together with the *PT*-curves of different fixed compositions of the liquid and the vapor phase. The intersections of the dew point and the bubble point curve for a given temperature and pressure mark the VLE for the chosen compositions in the liquid and the vapor phase. The critical points of a binary system can be found where a loop in Figure 5.9 is tangential to the envelope critical curve, also called *critical locus*.

The typical VLE behavior of a binary system above the critical temperature of one of the compounds looks like the behavior also shown in Figure 5.6

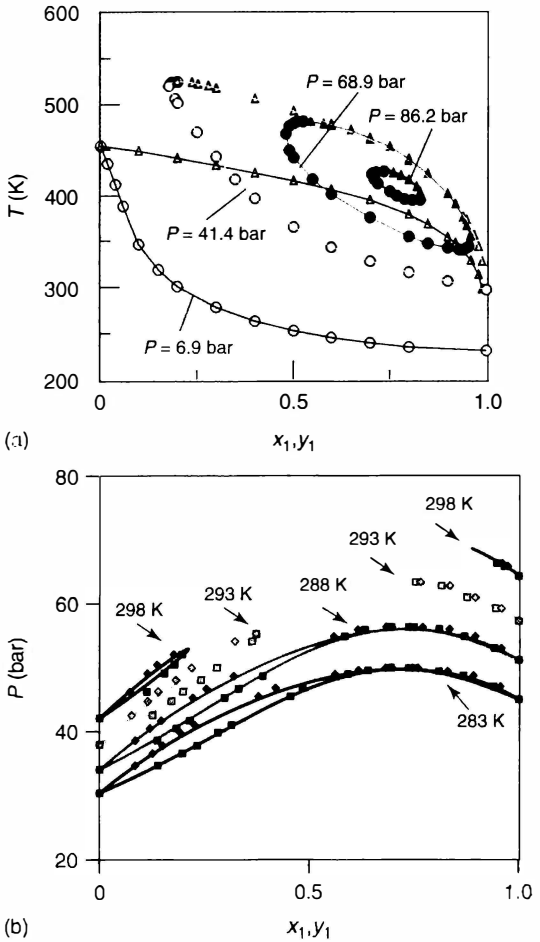

Figure 5.10 VLE behavior of the following binary systems near the critical point: (a) ethane (1)–heptane (2); (b) CO_2 (1)–ethane (2) experimental data taken from [3].

for the system nitrogen–methane. Other examples are CO_2–propane and argon–krypton.

In a few cases a different behavior is observed. In particular, this can happen if the system, for example, shows negative deviation from Raoult's law or a pressure maximum azeotrope. For the isobaric data of the system ethane–heptane and the isothermal data of the system CO_2–ethane this is shown in Figure 5.10. As can be seen for the system ethane–heptane, closed curves like islands appear at pressures of 68.9 and 86.2 bar. The reason is that at these pressures both components are supercritical (ethane: $P_c = 48.8$ bar, $T_c = 305.4$ K; heptane: $P_c = 27.3$ bar, $T_c = 540.3$ K) but the mixture is subcritical, which means coexisting liquid and vapor phase. For the system CO_2–ethane, the isotherms at 293 K and 298 K show

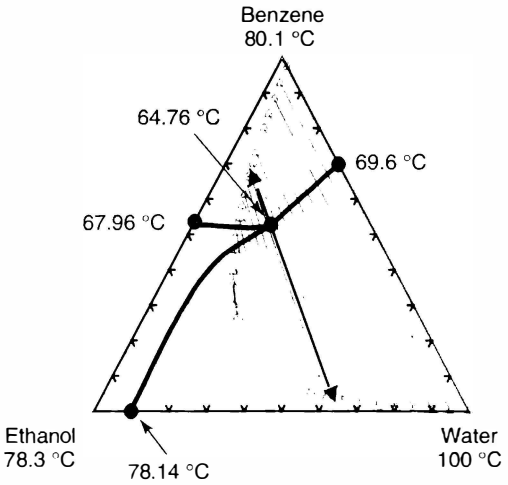

Figure 5.11 Ternary phase equilibrium diagram for the system ethanol–water–benzene at atmospheric pressure, • – azeotropic points.

two critical points, one on the right and the other on the left-hand side, and thus no coexisting phases in the medium concentration range between the two critical points. This is caused by the fact that the system shows a pressure maximum azeotrope.

For multicomponent systems, the phase equilibrium behavior can become much more complicated. The phase equilibrium behavior of the ternary system ethanol–water–benzene at atmospheric pressure is shown in Figure 5.11. It can be seen that a ternary azeotrope exists besides three binary azeotropes. The binary system benzene–water shows a large miscibility gap, which results in a miscibility gap in the ternary system. In the diagram the binodal curve and a few tie lines are shown. The tie lines connect the two liquid phases in equilibrium. While the azeotropes ethanol–water and ethanol–benzene are homogeneous, the binary azeotrope benzene–water and the ternary azeotrope are heterogeneous azeotropes. The ternary azeotrope shows the lowest boiling point. This can be used to separate the azeotropic system ethanol–water by the so-called azeotropic distillation[1] (see Section 11.4). After condensation, the ternary azeotrope forms two liquid phases, a benzene and a water-rich phase. The compositions of the two liquid phases are marked in Figure 5.11 by the arrows. The occurrence of azeotropic behavior and the selection of suitable solvents for azeotropic distillation are discussed in more detail in Sections 5.6 and 11.4. In Figure 5.11 additionally the so-called boundary residual curves are shown. While in binary systems the azeotropic point cannot be crossed by ordinary distillation, boundary lines in ternary systems, and boundary

1) Nowadays, benzene is no more used because of its toxicity. In commercial plants, it has been widely replaced by cyclohexane.

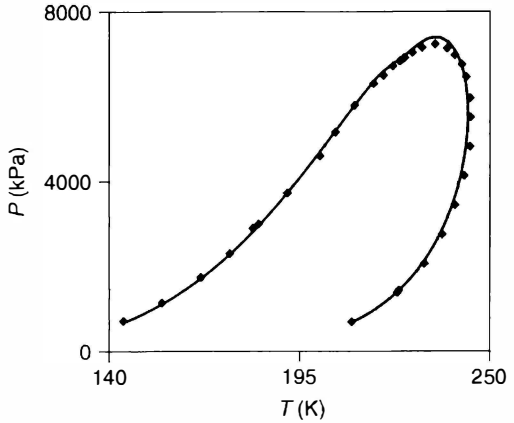

Figure 5.12 *PT*-diagram of a natural gas mixture consisting of 85.11 mol% methane, 10.07 mol% ethane, and 4.82 mol% propane [4].

surfaces in quaternary systems have the same consequences. How these residual curves are calculated is discussed in Section 11.3 in detail.

A natural gas is a typical multicomponent mixture; thus, a diagram like Figure 5.8 is not appropriate for illustration. Therefore, often *PT*-projections of phase diagrams, which are valid for a fixed overall concentration, are used (see Figure 5.12).

5.1 Thermodynamic Fundamentals

While a large number of phase equilibrium data are available for binary systems, much less data have been published for ternary systems and almost no data can be found for multicomponent systems. Of course the various phase equilibria for binary and multicomponent systems can be measured as a function of temperature or pressure and composition. Today highly sophisticated, reliable, and often computer-driven lab facilities are available to do so. Nevertheless, the measurement of the phase equilibrium behavior of multicomponent systems is very time consuming. For a ten component system, the number of experimental VLE data required is listed in Table 5.1, assuming the data are taken at constant pressure (e.g., atmospheric pressure) in 10 mol%-steps. For the pure components this means that only 10 normal boiling points have to be measured. Then there are 45 binary systems for which nine data points between 10 and 90 mol% are measured, so that in total 405 data points have to be measured. As can be seen in Table 5.1 there are additionally 120 ternary, 210 quaternary, 252 quinary, and many higher systems. For the 10-component system only one data point with 10 mol% of every component has to be experimentally determined. A total number of 92378

Table 5.1 Number of experimental data required for a ten-component system at a given pressure (e.g., atmospheric pressure), when the data are measured in 10 mol% steps.

Number of components	Number of systems	Data points/ system	Total number of data points/system	Total number of data points
1	10	1	10	10
2	45	9	405	415
3	120	36	4320	4735
4	210	84	17640	22375
5	252	126	31752	54127
6	210	126	26460	80587
7	120	84	10080	90667
8	45	36	1620	92287
9	10	9	90	92377
10	1	1	1	92378

data points results, which have to be measured. If 10 data points can be measured per working day, the measurements would last ~37 years [5].

Because of this time consuming effort reliable thermodynamic models are required, which allow the calculation of the phase equilibrium behavior of multicomponent systems using only a limited number of experimental data, for example, only binary data. From Table 5.1 it can be concluded that in this case only 42 days are required to measure all pure component and binary data of a ten-component system (in total 415 data points). Since a lot of binary VLE data can be found in the literature [3, 6], even less than 42 days of experimental work would be necessary.

Following Gibbs, phase equilibrium exists if the components show identical chemical potentials in the different phases α and β:

$$\mu_i^{\alpha} = \mu_i^{\beta} \tag{4.71}$$

The chemical potential is a thermodynamic quantity, which was first introduced by Gibbs. It is not an easily imaginable quantity. Later it was shown by Lewis (see Section 4.7.2) that the phase equilibrium condition given in Eq. (4.71) can be replaced by the following so-called isofugacity condition:

$$f_i^{\alpha} = f_i^{\beta} \tag{4.75}$$

At low pressures, except for strongly associating compounds the fugacities of the pure compounds are approximately identical to the vapor pressure or sublimation pressure depending on the state (liquid or solid). In case of mixtures, at low pressures the fugacity is nearly identical with the partial pressure of the compound considered.

For practical applications, Eqs. (4.71) and (4.75) are not very helpful, since the connection to the measurable quantities T, P and the composition in the liquid and

vapor phase is missing to be able to calculate the required *K*-factors K_i or separation factors α_{ij} for the design of the different separation processes.[2] Therefore, auxiliary quantities such as activity coefficients γ_i and fugacity coefficients φ_i have been introduced.

The *fugacity coefficient* φ_i of component *i* can be defined as the ratio of the fugacity in the liquid phase L (vapor phase V) to the product of the mole fraction x_i (y_i) and system pressure *P*. In the vapor phase the product $y_i P$ can be substituted by the partial pressure p_i:

$$\varphi_i^L \equiv \frac{f_i^L}{x_i P} \tag{5.5}$$

$$\varphi_i^V \equiv \frac{f_i^V}{y_i P} \equiv \frac{f_i^V}{p_i} \tag{5.6}$$

The *activity coefficient* γ_i is defined as follows:

$$\gamma_i \equiv \frac{f_i}{x_i f_i^0} \tag{5.7}$$

whereby the standard fugacity f_i^0 can be chosen arbitrarily.

Using the different definitions for the fugacities two different approaches can be derived for the description of phase equilibria. Starting from Eq. (4.75), the following relations for VLE are obtained [7]:

$$f_i^L = f_i^V \tag{5.8}$$

Approach A:

$$x_i \varphi_i^L = y_i \varphi_i^V \tag{5.9}$$

Approach B:

$$x_i \gamma_i f_i^0 = y_i \varphi_i^V P \tag{5.10}$$

In Approach A, the fugacity coefficients of the liquid φ_i^L and vapor phase φ_i^V are needed. They describe the deviation from ideal gas behavior and can be calculated with the help of equations of state, for example, cubic equations of state and reliable mixing rules. In Approach B, besides the activity coefficients γ_i a value for the standard fugacity f_i^0 is required. In the case of VLE usually the fugacity of the pure liquid at system temperature and system pressure is used as standard fugacity. For the calculation of the solubilities of supercritical compounds Henry constants are often applied as standard fugacity (see Section 5.7).

2) In the case of distillation K_i is defined as the ratio of the vapor phase mole fraction to the liquid phase mole fraction ($K_i = y_i/x_i$), and the separation factor α_{ij} is the ratio of the *K*-factors ($\alpha_{ij} = K_i/K_j$).

Using Eqs. (5.8) and (5.6), the fugacity of the pure liquid at system temperature can directly be calculated, since the pressure is identical with the vapor pressure of the pure liquid which is in equilibrium with pure vapor:

$$f_i^0\,(T, P_i^s) = \varphi_i^L P_i^s = \varphi_i^V P_i^s \equiv \varphi_i^s P_i^s \tag{5.11}$$

where the fugacity coefficient in the liquid or vapor phase in the saturation state φ_i^L or φ_i^V can be replaced by the fugacity coefficient at saturation pressure φ_i^s.

To get the fugacity of the pure liquid not at the vapor pressure P_i^s, but at system pressure P, the compression or expansion of the pure liquid from the vapor pressure to the system pressure has to be taken into account. This can be done using Eq. (2.71):

$$\left(\frac{\partial \ln f_i^L}{\partial P}\right)_T = \frac{v_i^L}{RT} \tag{5.12}$$

With the assumption that the molar liquid volume v_i^L is constant in the pressure range covered, Eq. (5.13) is obtained for the standard fugacity at system temperature and system pressure, where the exponential term in Eq. (5.13) is called *Poynting factor* Poy_i:

$$f_i^0\,(T, P) = \varphi_i^s P_i^s \exp\frac{v_i^L\,(P - P_i^s)}{RT} = \varphi_i^s P_i^s \mathrm{Poy}_i \tag{5.13}$$

Combining Eqs. (5.10) and (5.13) leads to the following relation for the description of VLE with the help of activity coefficients:

$$x_i \gamma_i \varphi_i^s P_i^s \mathrm{Poy}_i = y_i \varphi_i^V P \tag{5.14}$$

Introducing the auxiliary quantity ϕ_i gives

$$x_i \gamma_i \phi_i P_i^s = y_i P \qquad \text{with} \qquad \phi_i = \frac{\varphi_i^s \mathrm{Poy}_i}{\varphi_i^V} \tag{5.15}$$

If the pressure difference $P - P_i^s$ is not too large, the value of the Poynting factor is approximately 1. This is shown below for the system ethanol–water at 70 °C.

Example 5.1

Calculate the Poynting factor for ethanol and water at 70 °C for pressure differences of 1, 10 and 100 bar. At 70 °C, the following molar volumes can be used:
ethanol: 61.81 $\mathrm{cm^3/mol}$, water 18.42 $\mathrm{cm^3/mol}$.

Solution

For a pressure difference of 1 bar (e.g. system pressure $P = 5$ bar, vapor pressure $P_i^s = 4$ bar) the following Poynting factors are obtained for ethanol and water:

$$\mathrm{Poy}_{\mathrm{ethanol}} = \exp\frac{0.06181 \cdot 1}{0.0831433 \cdot 343.15} = 1.0022$$

$$\mathrm{Poy}_{\mathrm{water}} = \exp\frac{0.01842 \cdot 1}{0.0831433 \cdot 343.15} = 1.0006$$

In the same way the following values are obtained for a pressure difference of 10 and 100 bar:

10 bar:	$Poy_{ethanol} = 1.022,$	$Poy_{water} = 1.006$
100 bar:	$Poy_{ethanol} = 1.242,$	$Poy_{water} = 1.067$

It can be seen that at typical pressure differences (e.g., $P - P_i^s < 1$ bar) in distillation processes the Poynting factors show values near unity. Because of the larger molar volume of ethanol, the deviation from unity is larger for ethanol than for water.

Besides the Poynting factor, the real vapor phase behavior has to be taken into account in Eqs. (5.14) and (5.15). This can be done with the help of equations of state. Since only the vapor phase nonideality has to be considered, simple equations of state, for example, the virial equation of state can be applied, which are only able to describe the *PvT* behavior of the vapor phase. For moderate pressures the use of second virial coefficients is sufficient. In the case of systems with strong associating compounds such as carboxylic acids or hydrogen fluoride this approach cannot be applied any more. In this case the deviation from ideal gas behavior caused by the strong interactions – comparable to chemical reactions – has to be taken into account by so-called chemical contributions (see Section 13.2).

Example 5.2

Calculate the fugacity coefficients φ_i^V, φ_i^s, and the auxiliary quantity ϕ_i for the system ethanol–water at 70 °C using the virial equation. At 70 °C the following second virial coefficients should be used for the system ethanol(1)–water(2):

$$B_{11} = -1100\,\text{cm}^3/\text{mol}$$
$$B_{12} = -850\,\text{cm}^3/\text{mol}$$
$$B_{22} = -650\,\text{cm}^3/\text{mol}$$

The following liquid molar volumes can be used for the calculation of the Poynting factors: water 18.42 cm^3/mol and ethanol: 61.81 cm^3/mol.

Solution

The calculation procedure for the system ethanol (1)–water (2) is demonstrated for the data point $x_1 = 0.252$, $y_1 = 0.552$, and $P = 62.39$ kPa listed in Table 5.2.

Using Eq. (4.97) for the calculation of the fugacity coefficients in the vapor phase:

$$\ln \varphi_i^V = \left[2 \sum_j y_j B_{ij} - B \right] \frac{P}{RT} \tag{4.97}$$

Table 5.2 Vapor–liquid equilibrium data for the system ethanol (1)–water (2) at 70 C [8].

x_1	y_1	P (kPa)
0.0	0.0	31.09[3]
0.062	0.374	48.33
0.095	0.439	53.2
0.131	0.482	56.53
0.194	0.524	60.12
0.252	0.552	62.39
0.334	0.583	64.73
0.401	0.611	66.34
0.593	0.691	70.11
0.680	0.739	71.23
0.793	0.816	72.35
0.810	0.826	72.41
0.943	0.941	72.59
0.947	0.945	72.59
1.0	1.0	72.3[3]

and for the pure compounds:

$$\ln \varphi_i^s = \frac{B_{ii} P_i^s}{RT} \tag{2.108}$$

where the second virial coefficient B of the mixture can be obtained using the following relation:

$$B = \sum_i \sum_j y_i y_j B_{ij} \tag{4.89}$$

Using Eq. (4.89) the following virial coefficient is obtained for the given vapor phase composition:

$$\begin{aligned} \mathrm{B} &= 0.552^2 \cdot (-1100) + 2 \cdot 0.552 \cdot 0.448 \cdot (-850) + 0.448^2 \cdot (-650) \\ &= -886\,\mathrm{cm}^3/\mathrm{mol} \end{aligned}$$

Using this value the fugacity coefficient of ethanol can be calculated directly using Eq. (4.97):

$$\begin{aligned} \ln \varphi_1^V &= [2\,(0.552 \cdot (-1100) + 0.448 \cdot (-850)) + 886] \frac{62.39}{8314.33 \cdot 343.15} \\ &= -0.0238 \\ \varphi_1^V &= 0.9764 \end{aligned}$$

3) Unfortunately, in [8] the pure component vapor pressures were not measured. Therefore, these values were added by using the available constants for the Antoine equation (see Figure 5.30).

The fugacity coefficient of ethanol (1) in the saturation state is obtained as

$$\ln \varphi_1^s = \frac{-1100 \cdot 72.30}{8314.33 \cdot 343.15} = -0.02787$$
$$\varphi_1^s = 0.9725$$

In a similar way, the following values are obtained for water (2):

$$\varphi_2^V = 0.9862$$
$$\varphi_2^s = 0.9929$$

With the Poynting factors

$$\text{Poy}_{\text{ethanol}} = \exp\frac{0.06181 \cdot (0.6239 - 0.723)}{0.0831433 \cdot 343.15} = 0.9998$$
$$\text{Poy}_{\text{water}} = \exp\frac{0.01842 \cdot (0.6239 - 0.3109)}{0.0831433 \cdot 343.15} = 1.0002$$

the following ϕ_i values are obtained for this data point:

$$\phi_{\text{ethanol}} = \frac{0.9725 \cdot 0.9998}{0.9764} = 0.9958$$
$$\phi_{\text{water}} = \frac{0.9929 \cdot 1.0002}{0.9862} = 1.0070$$

For the whole composition range the ϕ_i-values are shown in Figure 5.13. It can be seen that in the whole composition range, the ϕ_i-values are between 0.98 and 1.01.

As shown in Example 5.2, for nonassociating compounds in contrast to strongly associating compounds such as carboxylic acids or HF the fugacity coefficients in the vapor phase φ_i^V and in the saturation state φ_i^s show very similar values at moderate pressures, so that ϕ_i-values around unity are obtained. This means that for nonassociating systems the following simplified relation can often be used to describe the VLE behavior:

$$x_i \gamma_i P_i^s \approx \gamma_i P \tag{5.16}$$

Using the different approaches, the following relations are obtained to calculate the required K-factors K_i and relative volatilities (separation factors) α_{ij}:

$$K_i = \frac{\gamma_i}{x_i} = \frac{\varphi_i^L}{\varphi_i^V} \qquad \alpha_{ij} = \frac{K_i}{K_j} = \frac{\gamma_i/x_i}{\gamma_j/x_j} = \frac{\varphi_i^L \varphi_j^V}{\varphi_i^V \varphi_j^L} \tag{5.17}$$

$$K_i = \frac{\gamma_i}{x_i} \approx \frac{\gamma_i P_i^s}{P} \qquad \alpha_{ij} = \frac{K_i}{K_j} = \frac{\gamma_i/x_i}{\gamma_j/x_j} \approx \frac{\gamma_i P_i^s}{\gamma_j P_j^s} \tag{5.18}$$

As can be seen later, both approaches allow the calculation of the VLE behavior of multicomponent systems using binary data alone.

When the advantages and disadvantages of different approaches are compared, approach A ($\varphi-\varphi$ approach) shows various important advantages over Approach B, for example, that the same auxiliary quantities are used to describe the real behavior

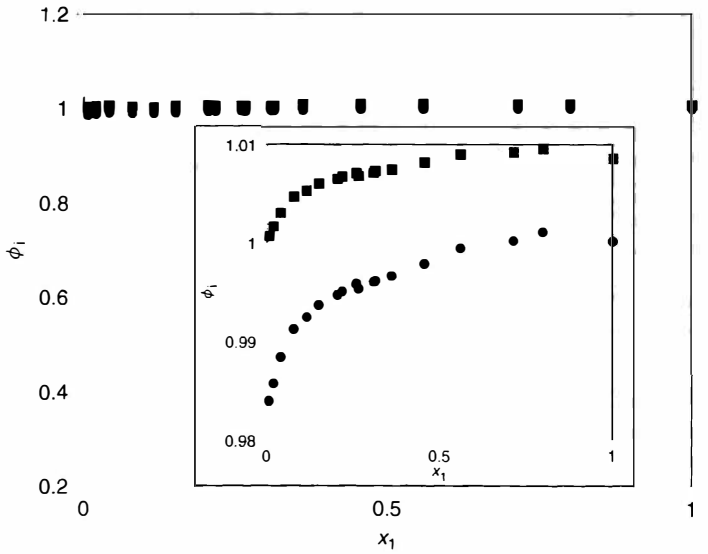

Figure 5.13 ϕ_i-values for the system ethanol(1)–water (2) at 70 C.

in the liquid and vapor phase. No additional model is required to account for the real behavior of the vapor phase. Furthermore, no problem arises with supercritical compounds, since no standard fugacity (vapor pressure) is required. At the same time densities, enthalpies (including heats of vaporization), heat capacities, and so on, as a function of temperature, pressure, and composition can be calculated for both phases, which are required as additional information in Approach B – the so-called $\gamma-\varphi$-approach (see Section 5.2). The disadvantage is that for the calculation a computer is required. On the other hand, the strength of Approach B is its relative simplicity and the opportunity to have independent correlations for each quantity, which can be fitted as accurately as possible and as necessary.

5.2
Application of Activity Coefficient Models

The equation of state approach is very attractive for the calculation of VLE. But it requires an equation of state and reliable mixing rules, which are able to describe the *PvT* behavior not only of the vapor but also of the liquid phase with the required accuracy. In spite of the progress achieved in the last 20 years, up to now there is no universal equation of state and mixing rule which can be successfully applied to all kind of systems in a wide temperature and pressure range for pure compounds and mixtures.

For the calculation of VLE with Approach B often the simplified Eq. (5.16) is applied. Then besides the activity coefficients as a function of composition and temperature only the vapor pressures of the components are required for the calculation.

Using Eq. (5.16) the required activity coefficients and the excess Gibbs energies can directly be derived from complete experimental VLE data. This is shown in Example 5.3 for the binary system ethanol–water measured at 70 °C.

Example 5.3

Calculate the activity coefficients and the excess Gibbs energies for the system ethanol (1)–water (2) at 70 °C as a function of composition using Eq. (5.16) and Table 5.2.

Solution

For the system ethanol (1)–water (2), the calculation of the activity coefficients and the excess Gibbs energy is demonstrated for a mole fraction $x_1 = 0.252$.

Using the simplified Eq. (5.16), the activity coefficients can be calculated by the following relation:

$$\gamma_i \approx \frac{\gamma_i P}{x_i P_i^s}$$

For the selected composition the following activity coefficients are obtained for ethanol (1) and water (2):

$$\gamma_1 = \frac{0.552 \cdot 62.39}{0.252 \cdot 72.30} = 1.890$$

$$\gamma_2 = \frac{0.448 \cdot 62.39}{0.748 \cdot 31.09} = 1.202$$

With the help of these activity coefficients the excess Gibbs energy can be calculated using Eq. (4.86).

$$g^E = RT\left(x_1 \ln \gamma_1 + x_2 \ln \gamma_2\right)$$

$$g^E = 8.31433 \cdot 343.15(0.252 \ln 1.890 + 0.748 \ln 1.202) = 850.2 \text{ J/mol}$$

$$\frac{g^E}{RT} = 0.252 \ln 1.890 + 0.748 \ln 1.202 = 0.298$$

For the other compositions the activity coefficients, the excess Gibbs energies and the dimensionless excess Gibbs energies (g^E/RT) are listed in Table 5.3. Furthermore the values are shown in the graphical form in Figure 5.14 together with the correlation results using the Wilson model (see Chapter 5.3).

Depending on the values of the activity coefficients γ_1 and γ_2 and the vapor pressures P_1^s and P_2^s, a very different VLE behavior is observed. In Figure 5.15, the vapor phase composition y_1, the activity coefficients $\ln \gamma_i$, the pressure P at isothermal conditions and the temperature T at isobaric conditions as a function of the mole fraction of component 1[4] in the liquid (vapor) phase are shown for binary

4) In the case of binary VLE the low boiling substance is always designated as component 1.

Table 5.3 Experimental data [8] for the system ethanol (1)–water (2) at 70 °C and the derived activity coefficients and excess Gibbs energies.

x_1	y_1	P (kPa)	γ_1	γ_2	g^E (J/mol)	g^E/RT
0	0	31.09		1.000	0	0
0.062	0.374	48.33	4.032	1.037	345.0	0.1209
0.095	0.439	53.2	3.400	1.061	483.9	0.1696
0.131	0.482	56.53	2.877	1.084	594.6	0.2084
0.194	0.524	60.12	2.246	1.142	753.2	0.2640
0.252	0.552	62.39	1.890	1.202	850.2	0.2980
0.334	0.583	64.73	1.563	1.304	929.2	0.3257
0.401	0.611	66.34	1.398	1.386	940.9	0.3298
0.593	0.691	70.11	1.130	1.712	831.1	0.2913
0.68	0.739	71.23	1.071	1.869	703.3	0.2465
0.793	0.816	72.35	1.030	2.069	495.5	0.1737
0.81	0.826	72.41	1.021	2.133	459.3	0.1610
0.943	0.941	72.59	1.002	2.417	148.6	0.0521
0.947	0.945	72.59	1.002	2.423	138.9	0.0487
1	1	72.3	1.000		0	0

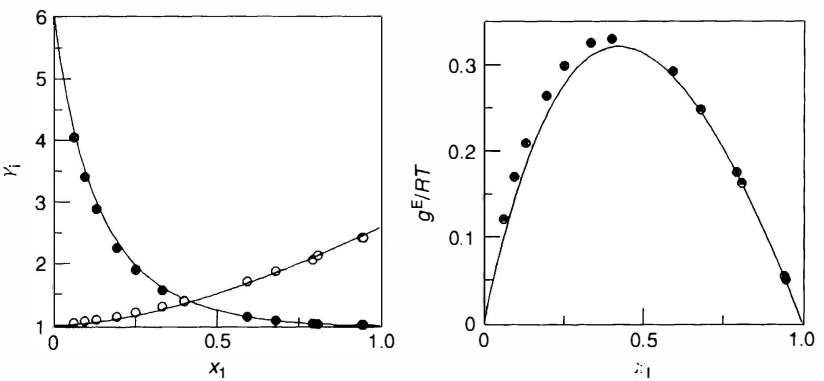

Figure 5.14 Concentration dependence of the activity coefficients and of the dimensionless excess Gibbs energy for the system ethanol (1)–water (2) at 70 °C [8] — Wilson model.

systems with very different real behavior. In the two diagrams on the right-hand side the pressure and temperature are not only given as a function of the liquid phase (continuous boiling point line) but also as a function of the vapor phase composition (dashed dew-point line).

While the first system benzene–toluene shows nearly ideal behavior ($\gamma_i \approx 1$), the activity coefficients for the next three systems steadily increase (positive deviation from Raoult's law). The influence of the activity coefficients can particularly be

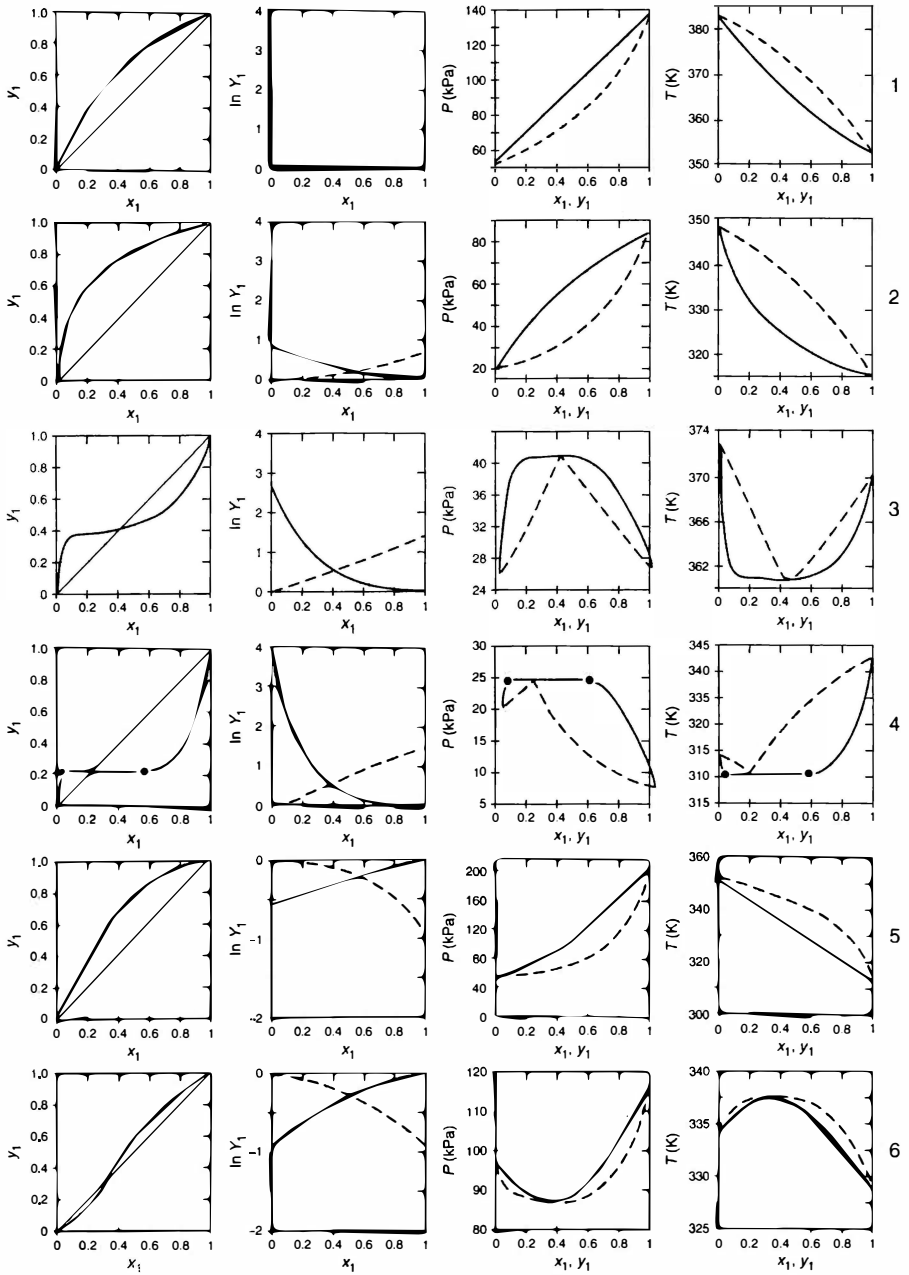

Figure 5.15 Different types of vapor–liquid equilibrium diagrams for the following binary systems: (1) benzene (1) -toluene (2); (2) methanol (1)–water (2); (3) 1 -propanol (1)–water (2); (4) 1–butanol (1)–water (2); (5) dichloromethane (1)–2–butanone (2); (6) acetone (1)–chloroform (2).

recognized from the pressure as a function of the liquid phase mole fraction x_1 at a given temperature. While a straight line for the pressure is obtained in the case of the nearly ideal system benzene–toluene following Raoult's law, higher pressures than the values obtained using Raoult's law are observed for the system methanol–water ($\gamma_i > 1$). With increasing activity coefficients as in the case of the system 1-propanol–water ($\gamma_i \gg 1$) the pressure even shows a maximum. At the same time a minimum of the temperature is observed in the isobaric case. At the pressure maximum (respectively minimum of the temperature) the boiling point line and the dew-point line meet. This means that the composition in the liquid and the vapor phase becomes identical and in the y–x-diagram an intersection of the 45° line is observed. These points are called *azeotropic points*. Systems with an azeotropic point cannot be separated by ordinary distillation.

When the values of the activity coefficients further increase, two liquid phases can occur, as in the case of the system 1-butanol–water. If the two liquid phase region (shown by the horizontal line) intersect the 45° line in the y–x-diagram, a so-called heterogeneous azeotropic point occurs. In the case of heterogeneous azeotropic points the condensation of the vapor leads to the formation of two liquid phases. In the system 1-butanol–water a butanol-rich and a water-rich phase is formed. The pressure (temperature) and the vapor phase composition show constant values for the binary system in the whole heterogeneous region.

Besides the large number of systems with positive deviation from Raoult's law ($\gamma_i > 1$), sometimes systems with negative deviation from Raoult's law ($\gamma_i < 1$), are observed. In Figure 5.15, the systems dichloromethane–2-butanone and acetone–chloroform were chosen as examples. Because of the strong hydrogen bonding effects between the two compounds, associates with low volatility are formed in these systems. This results in the fact that the pressure above the liquid mixture is lower than the pressure assuming ideal behavior ($\gamma_i = 1$). Depending on the vapor pressures azeotropic behavior can also occur in systems with negative deviations from Raoult's law, as in the system acetone–chloroform. However, in contrast to systems with positive deviations from Raoult's law, in these systems azeotropic points with a pressure minimum (temperature maximum) are formed. Binary systems with negative deviation from Raoult's law ($\gamma_i < 1$) cannot show two liquid phases. The occurrence and disappearance of binary azeotropes are discussed in more detail in Section 5.6.

5.3
Calculation of Vapor–Liquid Equilibria Using g^E-Models

As discussed in Section 5.1, besides the vapor pressure of the pure compounds an activity coefficient model is required, which allows the calculation of the VLE behavior using only binary experimental data. Using Eq. (4.85) an analytical expression for the activity coefficients can be derived if an expression for the excess Gibbs energy is available. By definition, the expression for the excess Gibbs energy

must obey the following boundary condition:

$$g^E \rightarrow 0 \text{ for } x_i \rightarrow 1$$

For the binary case the excess Gibbs energy g^E shows a value of 0 for $x_1 = 1$ and $x_2 = 1$. The simplest expression which obeys the boundary conditions is the Porter equation [9]:

$$\frac{g^E}{RT} = Ax_1x_2 \tag{5.19}$$

In this equation, A is a parameter which can be fitted to experimental data. Using Eq. (4.85) an analytical expression for the activity coefficients can be derived directly from Porter's expression [9]. For the derivation it is advisable to replace the mole fractions by the mole numbers:

$$\frac{(n_1 + n_2)\, g^E}{RT} = \frac{G^E}{RT} = \frac{An_1n_2}{n_1 + n_2}$$

$$\ln \gamma_1 = \left(\frac{\partial G^E/RT}{\partial n_1} \right)_{T,P,n_2} = \frac{An_2(n_1 + n_2) - An_1n_2}{(n_1 + n_2)^2}$$

$$\ln \gamma_1 = Ax_2^2$$

In the same way, the following expression is obtained for component 2:

$$\ln \gamma_2 = Ax_1^2$$

Porter's equation can be applied if g^E shows a symmetric curvature, this means an extreme value at equimolar composition ($x_1 = 0.5$). This behavior is only observed for chemically similar compounds of similar size.

For the description of g^E/RT for all other binary systems a more flexible expression is required. The simplest way is the introduction of further adjustable parameters, as in the Redlich–Kister expansion [10]:

$$\frac{g^E}{RT} = x_1x_2\left[A + B(x_1 - x_2) + C(x_1 - x_2)^2 + \cdots\right] \tag{5.20}$$

With the help of the flexible Redlich–Kister expansion all kinds of concentration dependencies of g^E for binary systems can be described. The contribution of the different parameters to the value of the excess Gibbs energy is shown in Figure 5.16. However, both the Porter and the Redlich–Kister model can only be used for binary systems. Furthermore, the correct temperature dependence of the activity coefficients cannot be described using temperature-independent parameters.

In practice, g^E-models are required which allow the calculation of the real behavior of multicomponent systems in the whole composition and a wide temperature range using binary data alone. The largest part of the VLE data (88.5%) has been published for binary systems. Only 10.3% of the VLE data published are for ternary and approx. 1% for quaternary systems [3]. This means there is nearly no chance to find the required experimental VLE data for quaternary and higher systems.

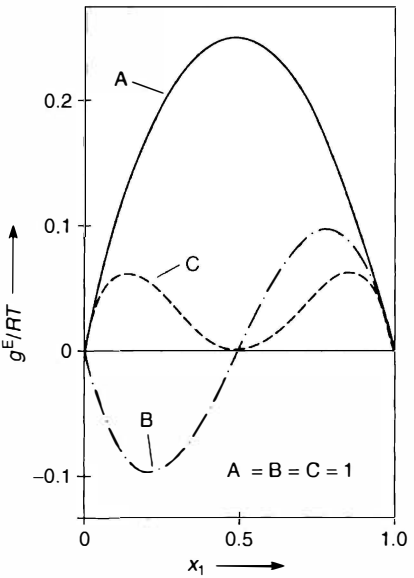

Figure 5.16 Contribution of the different parameters of the Redlich–Kister expansion to the value of the excess Gibbs energy.

A sophisticated thermodynamic model should take into account the various contributions to the excess Gibbs energy to be able to describe not only the concentration, but also the temperature and pressure dependence correctly:

$$g^E = h^E - Ts^E = u^E + Pv^E - Ts^E \tag{5.21}$$

Most of the excess properties are available experimentally. While the g^E-values can be obtained from VLE measurements (see Example 5.3), the excess enthalpies h^E are obtained from calorimetric and the excess volumes v^E from density measurements. When the excess properties mentioned before are known, other excess properties, for example the excess entropy s^E, can directly be derived, as shown in the next example.

Example 5.4

Construct a diagram with the thermodynamic excess properties g^E, h^E, and $-Ts^E$ for the system ethanol (1)–water (2) from the VLE data of Mertl [8] (Tables 5.2 and 5.3) and the excess enthalpies [11] in Table 5.4.

Solution

The g^E-values can directly be calculated from the activity coefficients derived from the experimental VLE-data. The values for g^E/RT were already listed in Table 5.3. At a concentration of $x_1 = 0.252$ the following value for the excess Gibbs energy is obtained:

$$g^E = 8.31433 \quad 343.15 \cdot 0.298 = 850.2 \text{ J/mol}.$$

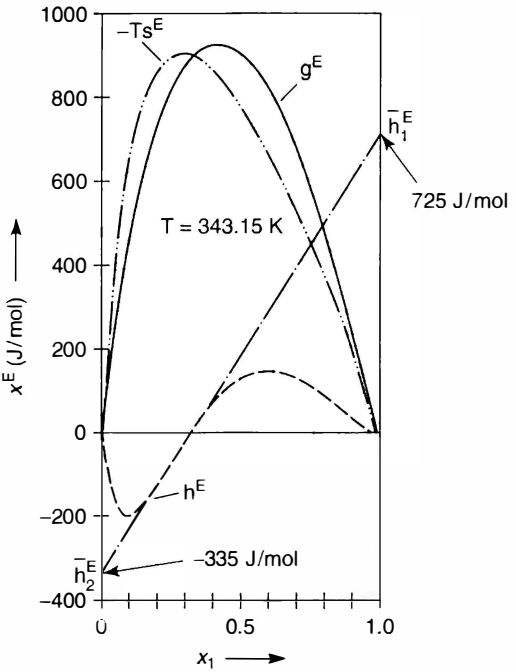

Figure 5.17 Excess Gibbs energy, excess enthalpy, and $-Ts^E$ for the system ethanol (1)–water (2) at 70 °C.

The value for $-Ts^E$ can be calculated from the difference $g^E - h^E$:

$$-Ts^E = g^E - h^E$$

For the whole composition range the results are shown in Figure 5.17.

When the excess properties are known, the values of the activity coefficients can be extrapolated to other conditions. Applying the van't Hoff equation (see Appendix C), the following temperature and pressure dependences of the excess Gibbs energy are obtained:

$$\left(\frac{\partial\,(g^E/T)}{\partial T}\right)_{P,x} = -\frac{h^E}{T^2} \tag{5.22}$$

respectively:

$$\left(\frac{\partial\,(g^E/T)}{\partial\,(1/T)}\right)_{P,x} = h^E \tag{5.23}$$

and

$$\left(\frac{\partial g^E}{\partial P}\right)_{T,x} = v^E \tag{5.24}$$

The temperature dependence of the molar excess enthalpy can be expressed by the molar excess heat capacity c_p^E.

$$\left(\frac{\partial h^E}{\partial T}\right)_{P,x} = c_p^E \tag{5.25}$$

With the help of these expressions, the temperature and pressure dependence of the activity coefficients can be derived directly:

$$\left(\frac{\partial \ln \gamma_i}{\partial (1/T)}\right)_{P,x} = \frac{\bar{h}_i^E}{R} \tag{5.26}$$

$$\left(\frac{\partial \ln \gamma_i}{\partial P}\right)_{T,x} = \frac{\bar{v}_i^E}{RT} \tag{5.27}$$

The partial molar excess properties vary with composition. They can be derived directly from the curvature of the excess enthalpies h^E or excess volumes v^E as a function of the mole fraction. How the partial molar properties can be determined by the tangent line for the excess enthalpy and a composition of $x_1 = 0.252$ is shown in Figure 5.17. Using the partial molar excess values $\bar{h}_i^E$ and $\bar{v}_i^E$ the activity coefficient at a different temperature or pressure can be determined. But it has to be considered that these partial molar excess properties do not only depend on composition but also on temperature and pressure.

While the pressure influence on the activity coefficient can usually be neglected in the case of VLE, the temperature dependence should be considered. This is shown in Example 5.5.

Example 5.5

Estimate the activity coefficients for $x_1 = 0.252$ at 50 °C for the system ethanol (1)–water (2) using the activity coefficients given in Table 5.3 and the experimental excess enthalpy data from Table 5.4. Simplifying, it should be assumed that the excess enthalpy h^E is constant in the temperature range considered.

Activity coefficients at 70 °C:

$$\gamma_1 = 1.890$$
$$\gamma_2 = 1.202$$

Solution

For a mole fraction of $x_1 = 0.252$, the following values for the partial molar excess enthalpy can be read from Figure 5.17:

$$\bar{h}_1^E = 725 \text{ J/mol}$$
$$\bar{h}_2^E = -335 \text{ J/mol}$$

Table 5.4 Excess enthalpy data [11] for the system ethanol (1)–water (2) at 70 °C.

x_1	h^E (J/mol)	x_1	h^E (J/mol)
0.0303	−108.7	0.3962	61.6
0.0596	−173.7	0.4502	101.3
0.0896	−200.1	0.4980	129.7
0.1238	−194.0	0.5802	151.3
0.1239	−196.4	0.5889	153.3
0.1697	−160.9	0.6976	135.8
0.1905	−149.9	0.7439	115.0
0.2402	−92.2	0.8022	84.0
0.3021	−24.8	0.8457	62.0
0.3514	22.8	0.8957	39.3

While for the partial molar excess enthalpy of ethanol (1) a positive value is obtained, a negative value is obtained for water (2) for this composition. Following Eq. (5.26) one obtains with the help of these values

$$\ln \gamma_i(T_2) = \ln \gamma_i(T_1) + \frac{\bar{h}_i^E}{R}\left(\frac{1}{T_2} - \frac{1}{T_1}\right),$$

the values for the activity coefficients at 50 °C can be calculated:

$$\ln \gamma_1(323.15\text{K}) = \ln 1.890 + \frac{725}{8.31433}\left(\frac{1}{323.15} - \frac{1}{343.15}\right)$$

$$\gamma_1(323.15\text{K}) = 1.920$$

$$\ln \gamma_2(323.15\text{K}) = \ln 1.202 - \frac{335}{8.31433}\left(\frac{1}{323.15} - \frac{1}{343.15}\right)$$

$$\gamma_2(323.15\text{K}) = 1.193.$$

It can be recognized that different temperature dependencies are observed for the two compounds involved, caused by the different sign of the partial molar excess enthalpies. While the activity coefficient for ethanol decreases, the activity coefficient for water increases with increasing temperature in the temperature range covered. But as can be seen from Figure 5.17 the temperature dependence of the partial molar excess enthalpies strongly depends on composition. For example, for compositions $x_1 < 0.1$ negative partial molar excess enthalpies for ethanol would result.

Example 5.6

Calculate the activity coefficient at infinite dilution of ethanol (1) in *n*-decane (2) at 353.15 and 433.15 K from the γ_1^∞ value at 338.65 K [3]:

$$\gamma_1^\infty = 15.9$$

assuming that the value of the partial molar excess enthalpy of ethanol $\bar{h}_1^{E,\infty} = 19000$ J/mol [3] is constant in the temperature range covered.

Solution

Using Eq. (5.26), the following activity coefficients result:

$$\ln \gamma_1^{\infty}(353.15\,\mathrm{K}) = \ln 15.9 + \frac{19000}{8.31433}\left(\frac{1}{353.15} - \frac{1}{338.65}\right)$$
$$= 2.7663 - 0.2771 = 2.4892$$
$$\gamma_1^{\infty}(353.15\,\mathrm{K}) = 12.05$$
$$\ln \gamma_1^{\infty}(433.15\mathrm{K}) = \ln 15.9 + \frac{19000}{8.31433}\left(\frac{1}{433.15} - \frac{1}{338.65}\right)$$
$$= 2.7663 - 1.4722 = 1.2941$$
$$\gamma_1^{\infty}(433.15\,\mathrm{K}) = 3.65$$

It can be seen that the activity coefficient at infinite dilution of ethanol in *n*-decane decreases by a factor greater than 4 when the temperature is increased from 338 to 433 K.

From these results it can be concluded that the temperature dependence cannot be neglected. While positive values of the partial molar excess enthalpies lead to a decrease of the activity coefficients with increasing temperature, negative values of the partial molar excess enthalpies lead to an increase of the activity coefficients with increasing temperature. The variation of the molar excess enthalpy with composition and temperature is often very complex. In the system ethanol–water around 70 °C even the sign changes with composition, as shown in Figure 5.18.

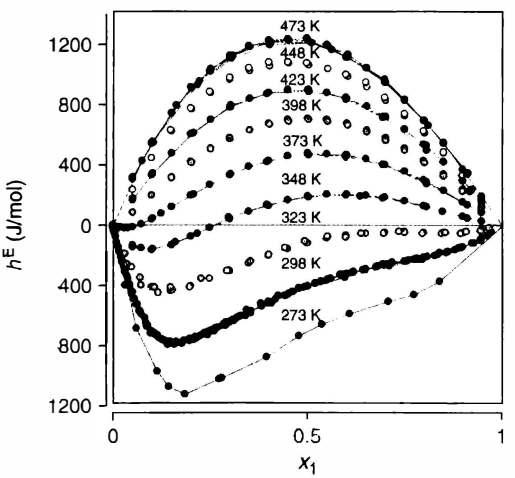

Figure 5.18 Selected excess enthalpy data at different temperatures for the system ethanol–water [3].

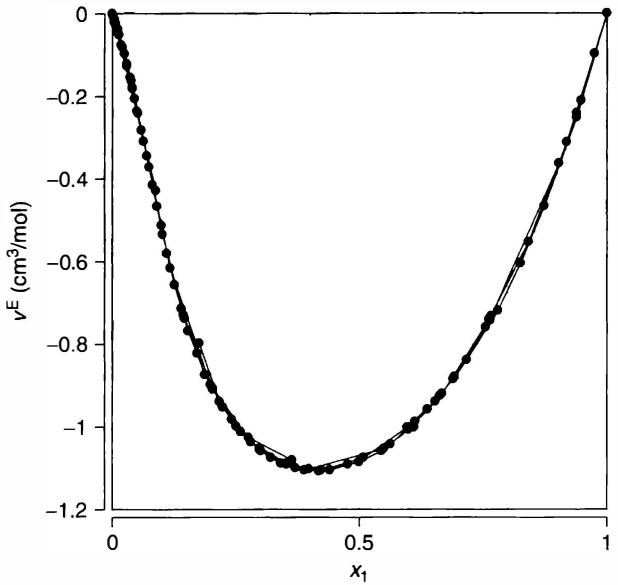

Figure 5.19 Excess volumes of the system ethanol (1)–water (2) at 20 °C [3].

Example 5.7

Estimate the difference between the sum of the volumes of the pure compounds and the volume of the resulting binary mixture of 0.4 mol ethanol and 0.6 mol water at 20 °C. Additionally please check the influence of a pressure difference of 2 bar on the activity coefficient qualitatively.

In the table below the densities at 20 °C and the molar masses are given [3]. (see also Example 4.1)

Compound	Density (g/cm³)	Molar mass (g/mol)
Ethanol	0.7893	46.069
Water	0.9982	18.015

The excess volumes for the system ethanol (1)–water (2) at 20 °C are shown in Figure 5.19.

Solution

To determine the volume of the pure compounds first the masses have to be calculated:

$$m_{\text{ethanol}} = 0.4 \cdot 46.069 = 18.43 \text{ g} \qquad V_{\text{ethanol}} = \frac{18.43}{0.7893} = 23.35 \text{ cm}^3$$

$$m_{H_2O} = 0.6 \cdot 18.015 = 10.81 \text{ g} \qquad V_{H_2O} = \frac{10.81}{0.9982} = 10.83 \text{ cm}^3$$

This means that the total volume of the pure compounds under ideal conditions is $34.18\,cm^3$.

For the calculation of the correct mixture volume the excess volume has to be known. From Figure 5.19 an excess volume of $-1.10\,cm^3/mol$ for a composition of $x_1 = 0.4$ can be read. Using this value the volume of the mixture can be calculated using Eq. (4.57):

$$v = \sum x_i v_i + v^E$$
$$v = 34.18 - 1.10 = 33.08\ cm^3/mol$$

This means that the volume of the mixture is approx. 3.2% lower than the volume of the pure compounds, this means starting from $100\,cm^3$ only $96.8\,cm^3$ remain.

For $x_1 = 0.4$ for both components a partial molar excess volume of $-1.1\,cm^3/mol$ (intersection at $x_1 = 0$ and $x_1 = 1$ of the slope at $x_1 = 0.4$) is obtained. Using this value the following change of the activity coefficients is obtained, when the pressure is increased by 2 bar:

$$\ln \frac{\gamma_i(P_2)}{\gamma_i(P_1)} = \frac{\bar{v}_i^E}{RT}(P_2 - P_1) = \frac{-0.0011 \cdot 2}{0.0831433 \cdot 293.15} = -9.026 \cdot 10^{-5}$$
$$\frac{\gamma_i(P_2)}{\gamma_i(P_1)} = 0.9999$$

Because of the negative sign of the partial molar excess volume the activity coefficient decrease with increasing pressure. But it can be seen that in contrast to the temperature influence caused by h^E, the pressure influence on the activity coefficients is negligible for typical pressure differences observed for VLE. But for large pressure differences the effect has to be taken into account. This is demonstrated in Section 5.8 for LLE.

The excess properties h^E and v^E do not only depend on temperature but also on pressure. This is shown in Figure 5.20 for the excess volumes of the system ethanol–water at 298 K. While for an equimolar mixture approximately a value of $-1\,cm^3/mol$ is observed at low pressures, the excess volume decreases to values smaller than $-0.3\,cm^3/mol$ at pressures above 2000 bar.

The temperature dependence of the excess Gibbs energy and the activity coefficients can be derived from a g^E–h^E-diagram (Figure 5.21). Depending on the sign of the excess properties g^E and h^E four quadrants are obtained.[5]

5) However, following Eq. 5.26 not the excess enthalpy but the partial molar excess enthalpy is the determining property to describe the temperature dependence of the activity coefficients. Depending on the curvature of h^E as a function of composition for positive (negative) values of h^E negative (positive) partial molar excess enthalpies can be obtained, for example, if an S-shaped curvature occurs as shown in Figure 5.18. Therefore, the following statements are only valid conditionally. But in most cases the sign of the partial molar and the molar excess enthalpy are identical (exception for S-shaped curves).

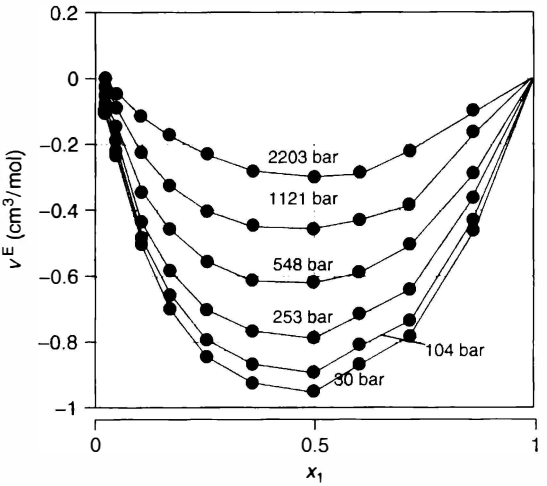

Figure 5.20 Excess volume of the system ethanol (1)–water (2) at 323 K as a function of pressure [3, 12].

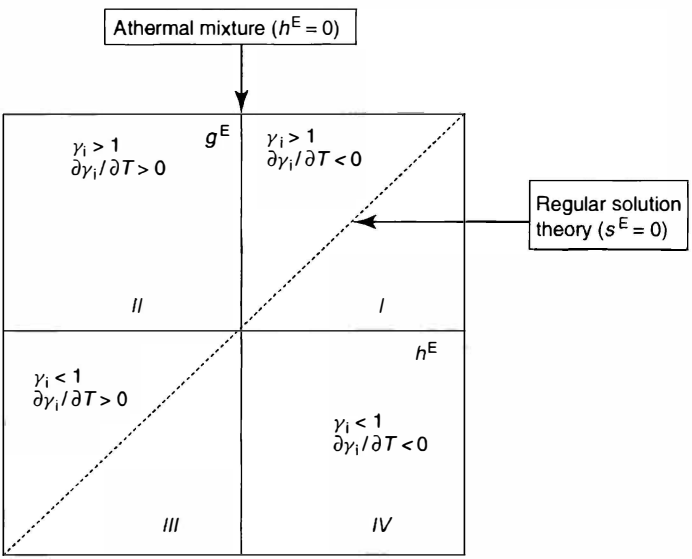

Figure 5.21 Representation of the temperature dependence of the activity coefficients in a g^E–h^E-diagram.

For positive deviations from Raoult's law ($g^E > 0$, $\gamma_i > 1$), depending on the sign of the excess enthalpy two cases can be distinguished. In the case of endothermic behavior ($h^E > 0$), the excess Gibbs energy and therewith, the values of the activity coefficient decrease with increasing temperature.

Most of the binary systems belong to quadrant I, this means they show positive deviations from Raoult's law and endothermic h^E behavior. This means that these systems become more ideal with increasing temperature. In the case of exothermal behavior (quadrant II), the activity coefficient will increase with temperature; this means stronger deviation from Raoult's law is obtained with increasing temperature. Only a few systems belong to quadrant II ($g^E > 0$, $h^E < 0$).[6] Just these systems, for example, alcohol–water-, alkyl amine–water systems, and so on, are of great technical importance. Systems with negative deviation from Raoult's law ($g^E < 0$ (quadrants III and IV)) are significantly more rare. In these systems the interaction energies between different components are stronger than those between the pure components, as for example, in the system acetone–chloroform. Because of the strong hydrogen bondings complexes are formed, which are less volatile. The systems which belong to quadrant III become more ideal, since for the excess Gibbs energy less negative values are obtained with increasing temperature. For systems in quadrant IV stronger negative deviation from Raoult's law are observed with increasing temperature. In Figure 5.21 also the lines for the so-called athermal mixture ($h^E = 0$, i.e., $g^E = -Ts^E$) and the regular solution ($s^E = 0$, i. e., $g^E = h^E$) are shown.

It would be desirable to apply analytical expressions for the activity coefficient, which are not only able to describe the concentration dependence, but also the temperature dependence correctly. Presently, there is no approach completely fulfilling this task. But the newer approaches, as for example, the Wilson [13], NRTL (nonrandom two liquid theory) [14], and UNIQUAC (universal quasi-chemical theory) equation [15] allow for an improved description of the real behavior of multicomponent systems from the information of the binary systems. These approaches are based on the concept of local composition, introduced by Wilson [13]. This concept assumes that the local composition is different from the overall composition because of the interacting forces. For this approach, different boundary cases can be distinguished:

- Because of the very similar interacting forces, the local composition is identical with the macroscopic composition (random mixture, almost ideal behavior $\gamma_i \approx 1$).
- Two liquid phases are formed, since molecule 2 has no tendency to locate near molecule 1 and vice versa (strong positive deviation from Raoult's law, $\gamma_i \gg 1$).
- The interacting forces between the different molecules are much larger than those between the same molecules, so that complexes are formed (negative deviation from Raoult's law, $\gamma_i < 1$).

The different equations are represented in detail in the literature. To derive a reliable g^E- resp. activity coefficient model using Eq. (4.85) the different excess properties (h^E, s^E, v^E) should be taken into account. Flory [16] and Huggins [17, 18] independently derived an expression for g^E starting from the excess entropy

6) Sometimes only in a limited concentration range (see Figure 5.18).

of athermal polymer solutions that means $h^E = 0$ using the lattice theory. In these mixtures with molecules very different in size, volume fractions ϕ_i instead of mole fractions are used. In binary systems the volume fraction can be calculated by the following expressions using the molar volumes v_i:

$$\phi_1 = \frac{x_1 v_1}{x_1 v_1 + x_2 v_2} \qquad \phi_2 = \frac{x_2 v_2}{x_1 v_1 + x_2 v_2} \tag{5.28}$$

Using the expression for the excess entropy:

$$s^E = -R\left(x_1 \ln \frac{\phi_1}{x_1} + x_2 \ln \frac{\phi_2}{x_2}\right) \tag{5.29}$$

an expression for the excess Gibbs energy can be derived,

$$g^E = -Ts^E = RT\left(x_1 \ln \frac{\phi_1}{x_1} + x_2 \ln \frac{\phi_2}{x_2}\right) \tag{5.30}$$

which can be used to derive an expression for the activity coefficients γ_i with the help of Eq. (4.85) for an athermal solution ($h^E = 0$, see Figure 5.21):

$$\ln \gamma_i = \ln \frac{\phi_i}{x_i} + 1 - \frac{\phi_i}{x_i} \tag{5.31}$$

With the help of this expression it can be shown that strong negative deviations from Raoult's law result for systems with compounds very different in size. From Eq. (5.31) it can easily be understood why the removal of the remaining monomers from polymer solutions is much more difficult than expected.

Example 5.8

Calculate the activity coefficient of the monomer in a polymer using the athermal Flory–Huggins equation. For the calculation the following volumes should be used:

$$v_1 = 70\ \text{cm}^3/\text{mol} \quad v_2 = 70000\ \text{cm}^3/\text{mol}$$

Solution

The calculation is performed for a mole fraction of $x_1 = 0.2$. For this composition the following volume fractions are obtained:

$$\phi_1 = \frac{0.2 \cdot 70}{0.2 \cdot 70 + 0.8 \cdot 70000} = 2.499 \cdot 10^{-4} \qquad \phi_2 = 0.99975$$

Using these values the activity coefficient γ_1 can be calculated directly:

$$\ln \gamma_1 = \ln \frac{2.499 \cdot 10^{-4}}{0.2} + 1 - \frac{2.499 \cdot 10^{-4}}{0.2} = -5.686$$

$$\gamma_1 = 3.39 \cdot 10^{-3}$$

For the whole composition range the activity coefficient of the monomer (1) as a function of the weight fraction of the polymer is shown in Figure 5.22. It can be

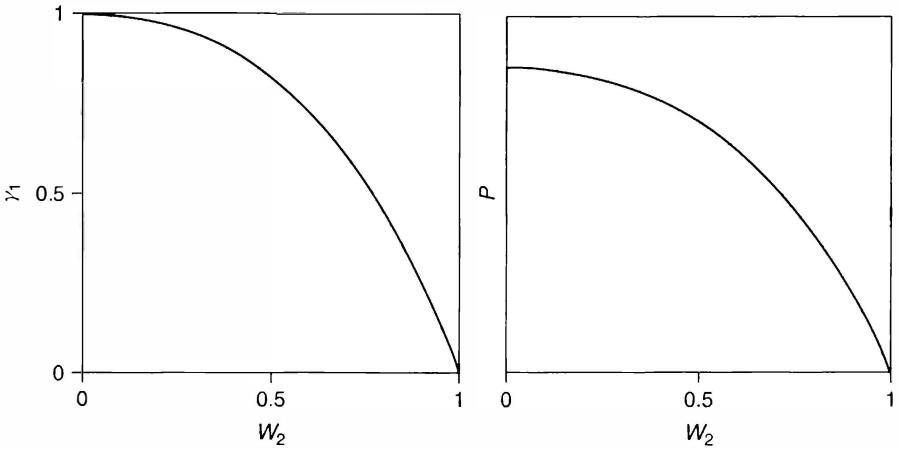

Figure 5.22 Calculated activity coefficients of the monomer and resulting system pressures as a function of the weight fraction of the polymer for a polymer solution using the Flory–Huggins equation.

seen that the volatility (activity coefficient) of the monomer drastically decreases with decreasing composition of the monomer.

To be able to account for contributions caused by the excess enthalpy h^E, a simple one parameter term was added to the Flory–Huggins equation:

$$\frac{g^E}{RT} = x_1 \ln \frac{\phi_1}{x_1} + x_2 \ln \frac{\phi_2}{x_2} + \phi_1 \phi_2 \chi \tag{5.32}$$

Starting from Eq. (5.32) the following expression is obtained for the activity coefficient of the monomer:

$$\ln \gamma_1 = \ln \frac{\phi_1}{x_1} + 1 - \frac{\phi_1}{x_1} + \chi \phi_2^2 \tag{5.33}$$

Wilson started from a similar equation as Flory and Huggins for the derivation of his equation for arbitrary mixtures apart from polymers [13]. However, instead of the true volume fractions Wilson used the so-called local volume fraction ξ_i in the expression for the excess Gibbs energy:

$$\frac{g^E}{RT} = \sum_i x_i \ln \frac{\xi_i}{x_i} \tag{5.34}$$

Local mole fractions were introduced by Wilson to define the local volume fraction, where the deviation from the macroscopic concentration is taken into account with the help of interaction energies between the different compounds using Boltzmann factors. With the introduction of the auxiliary quantities Λ_{ij} the equations for g^E and γ_i can be derived.[7] The great advantage of the Wilson equation is that only binary

7) The detailed derivation of the expression for the activity coefficients of the Wilson equation starting from Eq. (5.34) is given in Appendix C, E1.

and no ternary or higher parameters are required for the calculation of the real behavior of multicomponent systems. But the Wilson equation has the disadvantage, as in contrast to other g^E-models it cannot be applied to calculate LLE (see Appendix C, E3).

Example 5.9

Compare the experimental vapor phase mole fractions published by Hiaki *et al.* [19] for the system acetone (1)–chloroform (2)–methanol (3) at 1 atm with the calculated ones using the binary Wilson parameters $\Delta\lambda_{ij}$ listed in Table 5.5 assuming ideal vapor phase behavior.

For the calculation, the following molar volumes:

$$v_1 = 74.04\ \text{cm}^3\ \text{mol}^{-1};\ v_2 = 80.67\ \text{cm}^3\ \text{mol}^{-1};\ v_3 = 40.73\ \text{cm}^3\ \text{mol}^{-1}$$

and constants for the Antoine equation ($\log P_i^s(\text{mm Hg}) = A - B/(\vartheta(^\circ\text{C}) + C)$ should be used to calculate the vapor pressures.

Component	*A*	*B*	*C*
Acetone	7.1327	1219.97	230.653
Chloroform	6.95465	1170.97	226.232
Methanol	8.08097	1582.27	239.7

Solution

The calculation should be performed for the following composition at $T = 331.42$ K:

$$x_1 = 0.229, x_2 = 0.175, x_3 = 0.596,\ y_1 = 0.250,\ y_2 = 0.211,\ y_3 = 0.539.$$

Using the Wilson interaction parameters listed in Table 5.5 at 331.42 K the following values for $\Delta\lambda_{ij}$ are obtained:

$$\Delta\lambda_{12} = 375.2835 - 3.78434 \cdot 331.42 + 0.0079107 \cdot 331.42^2 = -10.02\ \text{K}$$

Table 5.5 Wilson interaction parameters (K) for the ternary system acetone (1)–chloroform (2)–methanol (3) (definition of a_{ij}, b_{ij}, c_{ij}, see Eq. (5.35).

i	*j*	a_{ij} (K)	a_{ji} (K)	b_{ij}	b_{ji}	c_{ij} (K^{-1})	c_{ji} (K^{-1})
1	2	375.2835	−1722.58	−3.78434	6.405502	7.91073E−03	−7.47788E−03
1	3	31.1208	747.217	−0.67704	−0.256645	8.68371E−04	−1.24796E−03
2	3	−1140.79	3596.17	2.59359	−6.2234	3.10E−05	3.00E−05

In the same way one obtains

$$\Delta\lambda_{21} = -421.03\,\text{K},\ \Delta\lambda_{13} = -97.88\,\text{K},\ \Delta\lambda_{31} = 525.08\,\text{K},$$
$$\Delta\lambda_{23} = -277.82\,\text{K},\ \Delta\lambda_{32} = 1536.91\,\text{K}.$$

In the next step the Wilson parameters Λ_{ij} used in Table 5.6 can be determined:

$$\Lambda_{ij} = \frac{v_j}{v_i} \cdot \exp\left[-\frac{\Delta\lambda_{ij}}{T}\right]$$
$$\Lambda_{12} = \frac{80.67}{74.04} \cdot \exp\left[\frac{10.02}{331.42}\right] = 1.1230$$

In the same way the other Wilson parameters are obtained:

$$\Lambda_{21} = 3.2695$$
$$\Lambda_{13} = 0.7391,\ \Lambda_{31} = 0.3728$$
$$\Lambda_{23} = 1.1675,\ \Lambda_{32} = 0.01918$$

With the help of these parameters Λ_{ij} the required activity coefficients can be calculated. For γ_1 one obtains

$$\ln\gamma_1 = -\ln\left(x_1\Lambda_{11} + x_2\Lambda_{12} + x_3\Lambda_{13}\right) + 1 - \frac{x_1\Lambda_{11}}{x_1\Lambda_{11} + x_2\Lambda_{12} + x_3\Lambda_{13}} - \frac{x_2\Lambda_{21}}{x_1\Lambda_{21} + x_2\Lambda_{22} + x_3\Lambda_{23}} - \frac{x_3\Lambda_{31}}{x_1\Lambda_{31} + x_2\Lambda_{32} + x_3\Lambda_{33}}$$

For the selected composition of $x_1 = 0.229$, $x_2 = 0.175$, and $x_3 = 0.596$ the following activity coefficient is obtained:

$$\ln\gamma_1 = -\ln\left(0.229 + 0.175 \cdot 1.123 + 0.596 \cdot 0.7391\right) + 1 - \frac{0.229}{0.229 + 0.175 \cdot 1.123 + 0.596 \cdot 0.7391} - \frac{0.175 \cdot 3.2695}{0.229 \cdot 3.2695 + 0.175 + 0.596 \cdot 1.1675} - \frac{0.596 \cdot 0.3728}{0.229 \cdot 0.3728 + 0.175 \cdot 0.01918 + 0.596} = 0.2016$$
$$\gamma_1 = 1.223$$

Similarly the other activity coefficients are calculated as

$$\gamma_2 = 1.101,\ \gamma_3 = 1.205$$

For the vapor pressures one obtains at the measured temperature of 331.42 K:

$$P_i^s = 10^{A_i - \frac{B_i}{\vartheta + C_i}}$$
$$P_1^s = 10^{7.1327 - \frac{1219.97}{58.27 + 230.653}} = 813.25\ \text{mm Hg},\ P_2^s = 689.91\ \text{mm Hg},$$
$$P_3^s = 589.94\ \text{mm Hg}$$

Then the partial pressures and the total pressure can be calculated:

$$p_i = x_i \cdot \gamma_i \cdot P_i^s$$

$$P = 0.229 \cdot 1.223 \cdot 813.25 + 0.175 \cdot 1.101 \cdot 689.91 + 0.596 \cdot 1.205 \cdot 589.94$$
$$P = 227.76 + 132.93 + 423.68 = 784.37 \text{ mm Hg}$$

The vapor phase composition is obtained from the ratio of the partial and the total pressure:

$$y_1 = \frac{p_1}{P} = \frac{227.76}{784.37} = 0.2904,\ y_2 = 0.1694,\ y_3 = 0.5402$$

Since the calculated pressure is greater than the constant experimental pressure of 760 mm Hg the calculated temperature has to be decreased in the next step until the experimental and the calculated pressure are identical. For the liquid composition considered this is fulfilled at a temperature of 330.60 K, where nearly the same values are obtained for the vapor phase mole fraction.

In the same way the vapor phase mole fractions can be calculated for all other data published by Hiaki *et al.* [19]. The experimental and calculated values are shown in Figure 5.23.

It can be seen that nearly perfect agreement between the experimental and calculated vapor phase mole fractions is obtained. Furthermore, the complex topology and the ternary saddle point are predicted correctly, as shown in Figure 5.24.

This means that the Wilson equation based on the local composition concept allows the prediction of the VLE behavior of multicomponent systems from binary data.

Later, further g^E-models based on the local composition concept were published, such as the NRTL [14] and the UNIQUAC [15] equation, which also allow the prediction of the activity coefficients of multicomponent systems using only binary parameters. In the case of the UNIQUAC equation the activity coefficient is calculated by a combinatorial and a residual part. While the temperature-independent combinatorial part takes into account the size and the shape of the molecule, the interactions between the different compounds are considered by the residual part. In contrast to the Wilson equation the NRTL und UNIQUAC equation can also be used for the calculation of LLE.

The analytical expressions of the activity coefficients for binary and multicomponent systems for the three g^E-models are given in Table 5.6. While for the Wilson and the UNIQUAC model two binary interaction parameters ($\Delta\lambda_{12}, \Delta\lambda_{21}$ resp. $\Delta u_{12}, \Delta u_{21}$) are used, in the case of the NRTL equation besides the two binary interaction parameters ($\Delta g_{12}, \Delta g_{21}$) additionally a nonrandomness factor α_{12} is required for a binary system, which is often not fitted but set to a defined value. For the Wilson equation additionally molar volumes and for the UNIQUAC equation relative van der Waals volumes and surface areas are required. These values are easily available.

Table 5.6 Important expressions for the excess Gibbs energy and the derived activity coefficients.

Model	Parameters	Expressions for the activity coefficients
Wilson [13]		$\frac{g^E}{RT} = \sum_i x_i \ln \frac{\xi_i}{x_i}$ or $\frac{g^E}{RT} = -\sum_i x_i \ln \sum_j x_j \Lambda_{ij}$
	$\Delta\lambda_{12}$[a]	$\ln \gamma_1 = -\ln (x_1 + \Lambda_{12} x_2) + x_2 \left(\frac{\Lambda_{12}}{x_1 + \Lambda_{12} x_2} - \frac{\Lambda_{21}}{\Lambda_{21} x_1 + x_2} \right)$
	$\Delta\lambda_{21}$	$\ln \gamma_2 = -\ln (x_2 + \Lambda_{21} x_1) - x_1 \left(\frac{\Lambda_{12}}{x_1 + \Lambda_{12} x_2} - \frac{\Lambda_{21}}{\Lambda_{21} x_1 + x_2} \right)$
	$\Delta\lambda_{ij}$	$\ln \gamma_i = -\ln \left(\sum_j x_j \Lambda_{ij} \right) + 1 - \sum_k \frac{x_k \Lambda_{ki}}{\sum_j x_j \Lambda_{kj}}$
		$\ln \gamma_1^\infty = 1 - \ln \Lambda_{12} - \Lambda_{21}$
		$\ln \gamma_2^\infty = 1 - \ln \Lambda_{21} - \Lambda_{12}$
NRTL [14]		$\frac{g^E}{RT} = \sum_i x_i \frac{\sum_j \tau_{ji} G_{ji} x_j}{\sum_j G_{ji} x_j}$
	Δg_{12}[b]	$\ln \gamma_1 = x_2^2 \left[\tau_{21} \left(\frac{G_{21}}{x_1 + x_2 G_{21}} \right)^2 + \frac{\tau_{12} G_{12}}{(x_2 + x_1 G_{12})^2} \right]$
	Δg_{21}	
	α_{12}	$\ln \gamma_2 = x_1^2 \left[\tau_{12} \left(\frac{G_{12}}{x_2 + x_1 G_{12}} \right)^2 + \frac{\tau_{21} G_{21}}{(x_1 + x_2 G_{21})^2} \right]$
	$\Delta g_{ij}, \alpha_{ij}$	$\ln \gamma_i = \frac{\sum_j \tau_{ji} G_{ji} x_j}{\sum_k G_{ki} x_k} + \sum_j \frac{x_j G_{ij}}{\sum_k G_{kj} x_k} \left(\tau_{ij} - \frac{\sum_n x_n \tau_{nj} G_{nj}}{\sum_k G_{kj} x_k} \right)$
UNIQUAC [15]		$g^E = g^{E,C} + g^{E,R}$
		$\frac{g^{E,C}}{RT} = \sum_i x_i \ln \frac{\phi_i}{x_i} + \frac{z}{2} \sum_i q_i x_i \ln \frac{\theta_i}{\phi_i}$
		$\frac{g^{E,R}}{RT} = -\sum_i q_i x_i \ln \left(\sum_j \theta_j \tau_{ji} \right)$
	Δu_{12}[c]	$\ln \gamma_1 = \ln \gamma_1^C + \ln \gamma_1^R$
	Δu_{21}	$\ln \gamma_1^C = 1 - V_1 + \ln V_1 - 5 q_1 \left(1 - \frac{V_1}{F_1} + \ln \frac{V_1}{F_1} \right)$
		$\ln \gamma_1^R = -q_1 \ln \frac{q_1 x_1 + q_2 x_2 \tau_{21}}{q_1 x_1 + q_2 x_2} + q_1 q_2 x_2 \left[\frac{\tau_{21}}{q_1 x_1 + q_2 x_2 \tau_{21}} - \frac{\tau_{12}}{q_1 x_1 \tau_{12} + q_2 x_2} \right]$
		$\ln \gamma_2 = \ln \gamma_2^C + \ln \gamma_2^R$
		$\ln \gamma_2^C = 1 - V_2 + \ln V_2 - 5 q_2 \left(1 - \frac{V_2}{F_2} + \ln \frac{V_2}{F_2} \right)$
		$\ln \gamma_2^R = -q_2 \ln \frac{q_1 x_1 \tau_{12} + q_2 x_2}{q_1 x_1 + q_2 x_2} + q_1 q_2 x_1 \left[\frac{\tau_{12}}{q_1 x_1 \tau_{12} + q_2 x_2} - \frac{\tau_{21}}{q_1 x_1 + q_2 x_2 \tau_{21}} \right]$

(continued overleaf)

Table 5.6 *(continued)*

Model	Parameters	Expressions for the activity coefficients
	Δu_{ij}	$\ln \gamma_i = \ln \gamma_i^C + \ln \gamma_i^R$
		$\ln \gamma_i^C = 1 - V_i + \ln V_i - 5q_i \left(1 - \frac{V_i}{F_i} + \ln \frac{V_i}{F_i}\right)$
		$\ln \gamma_i^R = q_i \left(1 - \ln \frac{\sum_j q_j x_j \tau_{ji}}{\sum_j q_j x_j} - \sum_j \frac{q_j x_j \tau_{ij}}{\sum_k q_k x_k \tau_{kj}}\right)$

[a] $\Lambda_{ij} = \frac{v_j}{v_i} \exp(-\Delta\lambda_{ij}/T)$, $\Lambda_{ii} = 1$;
v_i molar volume of component i[8];
$\Delta\lambda_{ij}$ interaction parameter between component i and j (K).

[b] $\tau_{ij} = \Delta g_{ij}/T$, $\tau_{ii} = 0$; $G_{ij} = \exp(-\alpha_{ij}\tau_{ij})$, $G_{ii} = 1$;
Δg_{ij} interaction parameter between component i and j (K):
α_{ij} nonrandomness parameter: $\alpha_{ij} = \alpha_{ji}$.

[c] γ_i^C combinatorial part of the activity coefficient of component i;
γ_i^R residual part of the activity coefficient of component i;
$\tau_{ij} = \exp(-\Delta u_{ij}/T)$, $\tau_{ii} = 1$.
Δu_{ij} interaction parameter between component i and j (K)
r_i relative van der Waals volume of component i
q_i relative van der Waals surface area of component i
$V_i = \frac{r_i}{\sum_j r_j x_j}$ volume fraction/mole fraction of component i
$F_i = \frac{q_i}{\sum_j q_i x_j}$ surface area fraction/mole fraction of component i

While for the interaction parameters $\Delta\lambda_{ij}$, Δg_{ij}, Δu_{ij} the unit K can be used, often for the published interaction parameters, for example, given in [6] the unit of a molar energy can be found. That is the case when in the denominator of the exponential term RT instead of T is used. The unit then depends on the choice of the unit of the general gas constant R (J/mol K, cal/mol K, etc.). When a large temperature range is covered, temperature-dependent parameters have to be used to describe the temperature dependence of the activity coefficients with the required accuracy, this means, following the Gibbs–Helmholtz relation the excess enthalpies resp. partial molar excess enthalpies in the temperature range covered. In this textbook the following temperature dependence of the binary interaction parameters is used:

$$\Delta\lambda_{ij}(T) = \Delta g_{ij}(T) = \Delta u_{ij}(T) = a_{ij} + b_{ij}T + c_{ij}T^2 \tag{5.35}$$

The application of the g^E-models is also explained in Appendix C, E2.

8) In practice usually constant, this means temperature-independent molar volumes v_i are used.

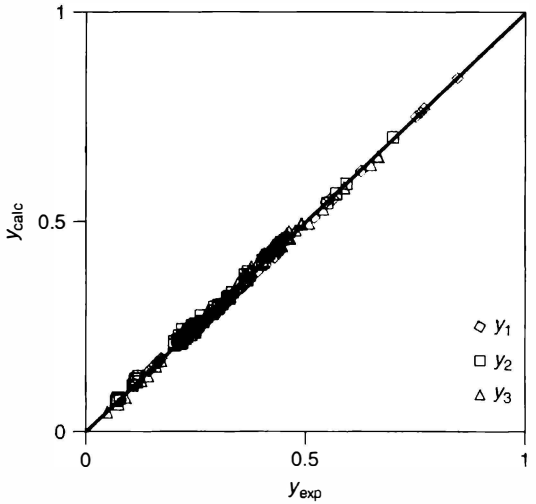

Figure 5.23 Experimental [3, 19] and calculated vapor phase mole fractions for the system acetone (1)–chloroform (2)–methanol (3) at atmospheric pressure.

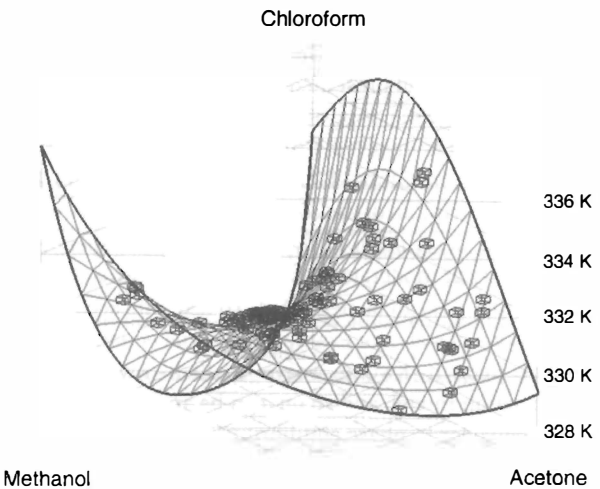

Figure 5.24 Experimental *Tx*-data [3, 19] and calculated *Tx* behavior of the ternary system acetone–chloroform–methanol at 1 atm using binary Wilson parameters.

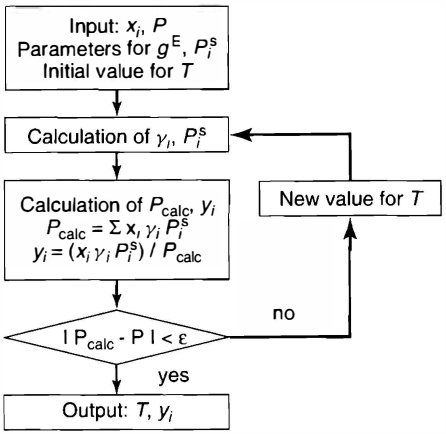

Figure 5.25 Flow diagram for the calculation of isobaric VLE data assuming ideal behavior in the vapor phase.

5.4 Fitting of g^E-Model Parameters

The quality of the design of a distillation column by solving the MESH equations[9] mainly depends on the accuracy of the *K*-factors (separation factors) [1]. Using one of the g^E-models given in Table 5.6 these values can be calculated for the system to be separated, if the binary parameters are available. However, for the proper design binary parameters have to be used which describe the *K*-factors resp. separation factors α_{ij} of the system to be separated over the entire composition and temperature range considered reliably.

The separation factors mainly depend on composition and temperature. The correct composition dependence is described with the help of activity coefficients. Following the Clausius–Clapeyron equation presented in Section 2.4.4 the temperature dependence is mainly influenced by the slope of the vapor pressure curves (enthalpy of vaporization) of the components involved. But also the activity coefficients are temperature-dependent following the Gibbs–Helmholtz equation (Eq. (5.26)). This means that besides a correct description of the composition dependence of the activity coefficients also an accurate description of their temperature dependence is required. For distillation processes at moderate pressures, the pressure effect on the activity coefficients (see Example 5.7) can be neglected. To take into account the real vapor phase behavior, equations of state, for example, the virial equation, cubic equations of state, such as the Redlich–Kwong, Soave–Redlich–Kwong (SRK), Peng–Robinson (PR), the association model, and so on, can be applied.

Assuming ideal vapor phase behavior in phase equilibrium calculations, besides carefully chosen binary g^E-model parameters only reliable vapor pressures are needed. The simple calculation procedure for the isobaric case is shown in Figure 5.25. In the isobaric case initial values for the temperature are required. During the calculation the temperature has to be changed in a way that the difference

9) MESH equations: these are the resulting balance equations for the ideal stage concept for the material balance (*M*), equilibrium conditions (*E*), summation conditions (*S*), and the heat balance (*H*).

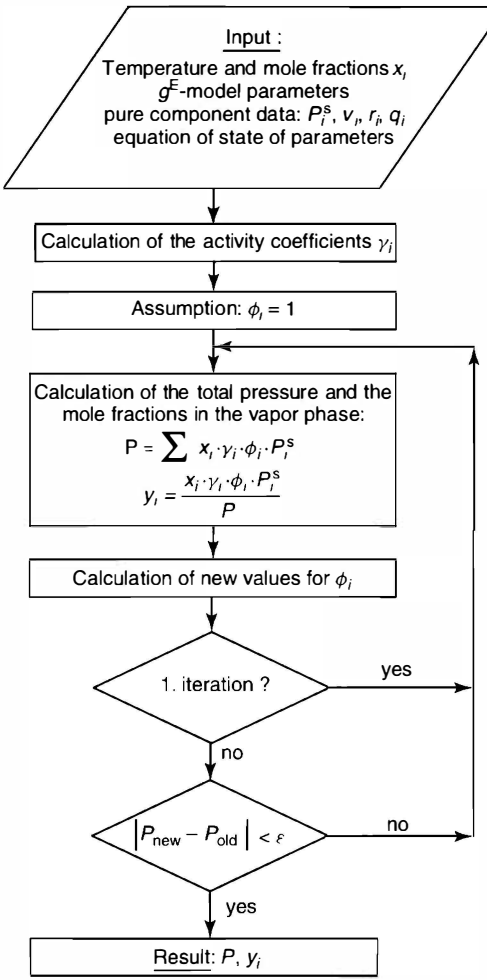

Figure 5.26 Flow diagram for the calculation of isothermal VLE taking into account the nonideal behavior of the vapor phase.

between the calculated and the desired pressure is smaller than a chosen value ε. The calculation for the isothermal case is still simpler, since the temperature does not have to be guessed and then adjusted by iteration. The calculation procedure shown in Figure 5.25 can also be applied for multicomponent systems.

If the real vapor phase behavior and the Poynting factor have to be taken into account, the procedure is a little more complicated. The procedure is shown in Figure 5.26. As input, information about the molar volumes and the real vapor phase behavior is required additionally, for example, the parameters of the equation of state chosen, the parameters for the association constants, and so on. With the help of this information, the Poynting factors and the fugacity coefficients for the mixture and the pure compounds are calculated.

A prerequisite for the correct description of the real behavior of multicomponent systems is a reliable description of the binary subsystems with the help of the fitted binary g^E-model parameters.

For fitting the binary interaction parameters nonlinear regression methods are applied, which allow adjusting the parameters in such a way that a minimum deviation of an arbitrary chosen objective function F is obtained. For this job, for example, the Simplex–Nelder–Mead method [21] can be applied successfully. The Simplex–Nelder–Mead method in contrast to many other methods [22] is a simple search routine, which does not need the first and the second derivate of the objective function with respect to the different variables. This has the great advantage that computational problems, such as "underflow" or "overflow" with the arbitrarily chosen initial parameters can be avoided.

As objective function for fitting the required g^E-model parameters different types of objective functions and experimental or derived properties X, for example, vapor phase mole fraction, pressure, temperature, K-factor K_i, separation factor α_{12}, and so on, can be selected, where either the relative or the absolute deviation of the experimental and correlated values (pressure, temperature, vapor phase composition, etc.) can be minimized,

$$F = \frac{1}{n}\sum\sum\left(X_{\mathrm{calc},i,j} - X_{\mathrm{exp},i,j}\right)^2 \stackrel{!}{=} \mathrm{Min}$$

$$F = \frac{1}{n}\sum\sum\left|X_{\mathrm{calc},i,j} - X_{\mathrm{exp},i,j}\right| \stackrel{!}{=} \mathrm{Min}$$

$$F = \frac{1}{n}\sum\sum\left[\frac{X_{\mathrm{calc},i,j} - X_{\mathrm{exp},i,j}}{X_{\mathrm{exp},i,j}}\right]^2 \stackrel{!}{=} \mathrm{Min}$$

$$F = \frac{1}{n}\sum\sum\left|\frac{X_{\mathrm{calc},i,j} - X_{\mathrm{exp},i,j}}{X_{\mathrm{exp},i,j}}\right| \stackrel{!}{=} \mathrm{Min}$$

In the case of complete data, this means VLE data, where P, T, x_i, y_i is given, also the deviation between the experimental and predicted activity coefficients or excess Gibbs energies can be used to fit the required binary parameters. Furthermore the parameters can be determined by a simultaneous fit to different properties to cover properly the composition and temperature dependence of the activity coefficients. For example, the deviation of the derived activity coefficients can be minimized together with the deviations of the activity coefficients at infinite dilution, excess enthalpies, and so on. Accurate activity coefficients at infinite dilution measured with sophisticated experimental techniques are of special importance, since they deliver the only reliable information about the real behavior in the dilute range [23],[10] for example, at the top or the bottom of a distillation column. Excess enthalpies measured using flow calorimetry are important too, since they provide the most reliable information about the temperature dependence of the activity

10) With the required care it is quite simple to measure reliable activity coefficients at infinite dilution of a low boiling substance in a high boiling compound, for example, with the help of the dilutor technique, gas–liquid chromatography, ebulliometry, Rayleigh distillation, and so on. It is much more difficult to measure these values for high boiling components in low boiling compounds, for example, water in ethylene oxide, NMP in benzene, etc. But these values are of special importance for the proper design of distillation columns. In the case of positive deviation from Raoult's law the greatest separation effort is required for the removal of the last traces of the high boiling compounds at the top of the column.

coefficients via the Gibbs–Helmholtz equation (see Eq. (5.26)), and thus for the separation factors and *K*-factors.

In the past in different papers e.g. [70] the maximum likelihood method was recommended. In this method the experimental errors of all measured quantities are taken into account in the objective function. But later it was found out that this procedure did not improve the results for ternary, quaternary, and higher systems using the fitted binary parameters.

The impact of inaccurate g^E-model parameters can be very serious. The parameters have a major influence on the investment and operating costs (number of stages, reflux ratio). The influence of the g^E-model parameters on the results is especially large if the separation factor is close to unity. Poor parameters can either lead to the calculation of nonexisting azeotropes in zeotropic systems (see Section 11.1) or the calculation of zeotropic behavior in azeotropic systems. Poor parameters can also lead to a miscibility gap which does not exist.[11] In the case of positive deviation from Raoult's law a separation problem often occurs at the top of the column, where the high boiler has to be removed, since at the top of a distillation column the most unfortunate separation factors are obtained.

Starting from Eq. (5.18), the following separation factors at the top and the bottom of a distillation column (low boiler: component 1) are obtained:
top of the column ($x_1 \rightarrow 1$):

$$\alpha_{12}^{\infty} = \frac{P_1^s}{\gamma_2^{\infty} P_2^s}$$

bottom of the column ($x_2 \rightarrow 1$):

$$\alpha_{12}^{\infty} = \frac{\gamma_1^{\infty} P_1^s}{P_2^s}$$

From these equations it can easily be seen that for positive deviation from Raoult's law ($\gamma_i > 1$) the smallest separation factors and therewith the greatest separation problems occur at the top of the column. To determine the separation factor at the top of the column, one divides by a number larger than unity (γ_2^{∞}), while in the bottom of the column one multiplies with a number larger than unity (γ_1^{∞}). While, for example, for the system acetone–water separation factors a little above unity are obtained at the top of the column at atmospheric pressure, separation factors greater than 40 are observed at the bottom of the column (see Chapter 11). In the

11) Process simulators often contain extensive data banks with pure component and mixture parameters, for example, default g^E-model parameters. This allows for generating the required input very fast. But the user should use these data and parameters with care. Even the simulator companies mention that these default values should not directly be used for process simulation. The user should ask the company expert for phase equilibrium thermodynamics to check the pure component data and mixture parameters carefully. In Figures 5.31 and 5.34 it is shown what can happen when the default values provided by the process simulator companies are used. An additional example for bad default values is given in Appendix F.

In Section 11.1 it is shown how the thermophysical properties should be checked prior to process simulation.

Table 5.7 Type of VLE data published.

Type of VLE data	Measured values				Percentage of the published VLE data
	x_i	y_i	P	T	
Isothermal complete	√	√	√	constant	18.33
Isobaric complete	√	√	constant	√	28.37
Isothermal Px data	√	–	√	constant	29.66
Isobaric Tx data	√	–	constant	√	9.11
Isothermal xy data	√	√	–	constant	3.12
Isobaric xy data	√	√	constant	–	2.03
Isothermal yP data	–	√	√	constant	0.54
Isobaric yT data	–	√	constant	√	0.16
Isoplethic PT data	constant	–	√	√	6.84
Complete data	√	√	√	√	1.85

case of negative deviations from Raoult's law the separation problem usually occurs at the bottom of the column.

Published VLE data are often of questionable quality. For fitting reliable g^E-model parameters accurate experimental VLE data should be used. An overview about the different types of VLE data published together with the proportion of such data from all published VLE data is given in Table 5.7.

In most cases the measurements are performed at isothermal or isobaric conditions. Occasionally measurements are also performed at constant composition. Sometimes none of the properties is kept constant. In less than 50% of the cases all values (x_i, y_i, T, P) are measured. The reason is that any three of the four values (x_i, y_i, T, P) are sufficient to derive the fourth quantity. Because of the greater experimental effort required, seldom dew-point data (T, P, y_i) are measured. But these data are of special importance to determine reliable separation factors for high boiling compounds (e.g., water) in low boiling compounds (ethylene oxide) at the top of the column, which at the end mainly determine the number of stages of a distillation column (see Chapter 11).

As can be seen from Table 5.7, the measurement of complete isobaric data is very popular. The reason is that a great number of chemical engineers prefer isobaric data, since distillation columns run at nearly isobaric conditions. But the measurement of isobaric data shows several disadvantages compared to isothermal data. This was already discussed in detail by Van Ness [24]. For example, the temperature dependence of the vapor pressure P_i^s has to be taken into account. At the same time the temperature and composition dependence of the g^E-model has to be regarded. Therefore Van Ness [24] comes to the following conclusion:

In the early unsophisticated days of chemical engineering VLE data were taken at constant pressure for direct application in the design of distillation columns, which were treated as though they operated at uniform pressure. There is no longer excuse for taking isobaric data, but regrettably the practice persists. Rigorous thermodynamic treatment of isobaric data presents problems that do not arise with isothermal data. Their origin is the need to take into account not only the composition dependence of the excess Gibbs energy but also its temperature dependence.

Since the measurement of temperature and pressure is more accurate than concentration measurements, Van Ness recommended the measurement of *Px*-data at isothermal conditions. Indeed, today mainly isothermal *Px*-data are measured. In the cell of the static equipments the precise liquid composition is usually achieved by injection of the degassed liquids with the help of precise piston pumps. The change of the feed composition by evaporation can easily be taken into account, when the volume of the cell and the pressure is known. Depending on the vapor volume the change of the feed composition is smaller than 0.1 mol% at moderate pressures. By this method a much more precise determination of the liquid composition is achieved than by analytical measurements. The measurement of the pressure and the temperature can be realized very precisely.

5.4.1
Check of VLE Data for Thermodynamic Consistency

Not in all cases, the quality of the published data is sufficient. The quality of complete data (P, T, x_i, γ_i) can be checked with the help of thermodynamic consistency tests. A large number of consistency tests have been developed. Most often the so-called area test is applied. The derivation of the required equations for the area test is started from the following equation (see Section 4.3):

$$\frac{dG^E}{RT} = \left(\frac{\partial G^E/RT}{\partial P}\right)_{T,n_i} dP + \left(\frac{\partial G^E/RT}{\partial T}\right)_{P,n_i} dT + \sum \left(\frac{\partial G^E/RT}{\partial n_i}\right)_{T,P,n_j \neq n_i} dn_i \tag{5.36}$$

By substitution

$$\left(\frac{\partial G^E}{\partial P}\right)_{T,n_i} = V^E \tag{5.37}$$

$$\left(\frac{\partial G^E/T}{\partial T}\right)_{P,n_i} = -\frac{H^E}{T^2} \tag{5.38}$$

$$\left(\frac{\partial G^E/RT}{\partial n_i}\right)_{T,P,n_j \neq n_i} = \ln \gamma_i \tag{5.39}$$

and applying of molar properties, the following relation is obtained for a binary system ($dx_1 = -dx_2$).

$$\frac{dg^E}{RT} = \frac{v^E}{RT}dP - \frac{h^E}{RT^2}dT + \ln\frac{\gamma_1}{\gamma_2}dx_1 \tag{5.40}$$

After integration from $x_1 = 0$ to $x_1 = 1$ an expression is obtained, which can be applied for the graphical examination of complete VLE data[12] for thermodynamic consistency.

$$\int_{x_1=0}^{x_1=1}\frac{dg^E}{RT} = \int_{x_1=0}^{x_1=1}\ln\frac{\gamma_1}{\gamma_2}dx_1 - \int_{x_1=0}^{x_1=1}\frac{h^E}{RT^2}dT + \int_{x_1=0}^{x_1=1}\frac{v^E}{RT}dP = 0 \tag{5.41}$$

In the case of isothermal or isobaric data one term in the equation above can be cancelled. Since the pressure dependence can usually be neglected, in the case of isothermal VLE data the following simple relation can be used for checking the thermodynamic consistency of VLE data:

$$\int_{x_1=0}^{x_1=1}\ln\frac{\gamma_1}{\gamma_2}dx_1 = 0 \tag{5.42}$$

The consistency test (Redlich–Kister test) is performed by plotting the logarithmic value of the ratio of the activity coefficients as a function of the mole fraction x_1. If the VLE data are thermodynamically consistent the area above and below the x-axis should be equal.

In the case of isobaric data the excess enthalpy part has to be taken into account. This can be done if the excess enthalpies for the system investigated are known. Since the excess enthalpies are usually not known, in the area test the contribution is taken into account empirically using the quantity J as suggested by Redlich and Kister [25]:

$$J = 150\frac{|\Delta T_{max}|}{T_{min}}(\%) \tag{5.43}$$

The value of J strongly depends on the temperature difference ΔT_{max}. In the case of zeotropic systems this is the difference of the boiling points.

In the DECHEMA Chemistry Data Series [6] a deviation of $D < 10\%$ is allowed to pass the thermodynamic consistency test successfully,

$$D = \frac{|A - B|}{A + B}100(\%) \tag{5.44}$$

where A is the area above the x-axis and B is the area below the x-axis.

12) As well isothermal VLE data, where only the liquid and vapor phase mole fractions, this means K-factors are measured (e.g., by headspace gas-chromatography) can be checked for thermodynamic consistency with the help of the area test, since the system pressure cancels out when the ratio of the activity coefficients is calculated.

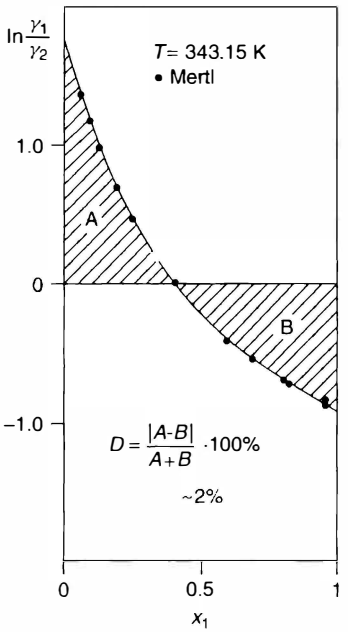

Figure 5.27 Check of isothermal complete VLE data of the system ethanol (1)-water (2) [8] for thermodynamic consistency with the help of the area test.

While in the isothermal case a deviation of $D < 10\%$ is accepted, in the isobaric case a larger area deviation is allowed to take into account the contribution of the excess enthalpy by Eq. (5.43):

$$D - J < 10\%$$

Example 5.10

Check the isothermal VLE data of the system ethanol (1)–water (2) measured by Mertl [8] at 70 °C (see Table 5.3) for thermodynamic consistency using the area test.

Solution

For the judgment of the quality of the VLE data the logarithmic values of the ratio of the activity coefficients $\ln \gamma_1/\gamma_2$ have to be plotted against the mole fraction of ethanol. The required activity coefficients are given in Table 5.3. For example, for a mole fraction of $x_1 = 0.252$ the following ratio is obtained:

$$\ln \frac{\gamma_1}{\gamma_2} = \ln \frac{1.890}{1.202} = 0.453$$

For the whole composition range the values are shown in Figure 5.27. It can be seen that the areas above and below the x-axis are nearly identical ($\approx$ 2% deviation). This means that the data published by Mertl [8] can be considered as thermodynamically consistent.

Another option to check complete VLE data for thermodynamic consistency was developed by Van Ness *et al.* [26] resp. Fredenslund *et al.* [27]. In this consistency

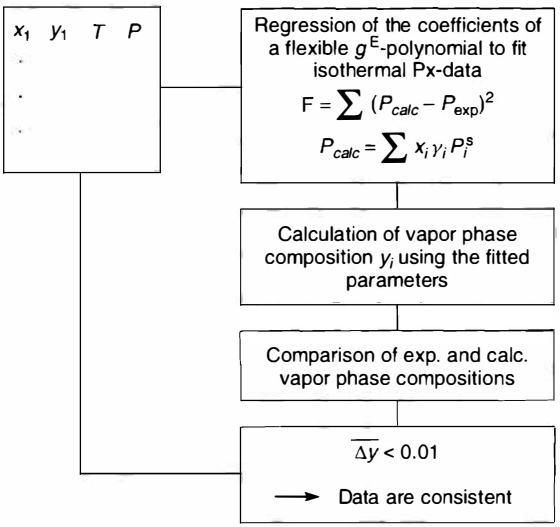

Figure 5.28 Flow diagram of the consistency test of Van Ness *et al.* [26] and Fredenslund *et al.* [27].

test only a part of the redundant phase equilibrium data, usually the *TPx*-data, are used to fit the g^E-model parameters of a flexible g^E-model, such as the Redlich–Kister expansion to minimize, for example, the deviation in pressure. In the next step the fitted parameters are used to calculate the data, which were not used for fitting the parameters, this means the corresponding vapor phase compositions. When a mean deviation between the experimental and calculated vapor phase mole fraction of <0.01 is obtained, the VLE data are considered as thermodynamically consistent. A flow diagram of this consistency test is shown in Figure 5.28.

Often isothermal *Px*-data are measured (see Table 5.7). They cannot be checked for thermodynamic consistency. But if the data can be described very accurately with the help of a consistent g^E-model, these VLE data can also be considered as thermodynamically consistent. The same is true for other incomplete VLE data listed in Table 5.7.

With the help of the g^E-model only the deviations from Raoult's law should be described. The correct deviations from Raoult's law can only be obtained, if the exact values of the pure component vapor pressures are used during the fitting procedure. This is shown below for fitting the NRTL parameters for the nearly ideal but nevertheless azeotropic system 2-propanol–*tert*-butanol simultaneously to two isothermal *Px*-data sets measured at 40 °C. The very different results of the fitting procedure are shown in Figure 5.29. Obviously, the two data sets show a systematic small difference in the pressure measurement. While a correct description of the *Px*-data and the azeotropic VLE behavior is obtained, if the vapor pressure data of the authors are used for fitting the parameters. Total disagreement is observed if the VLE calculation is performed using the vapor pressures calculated by Antoine

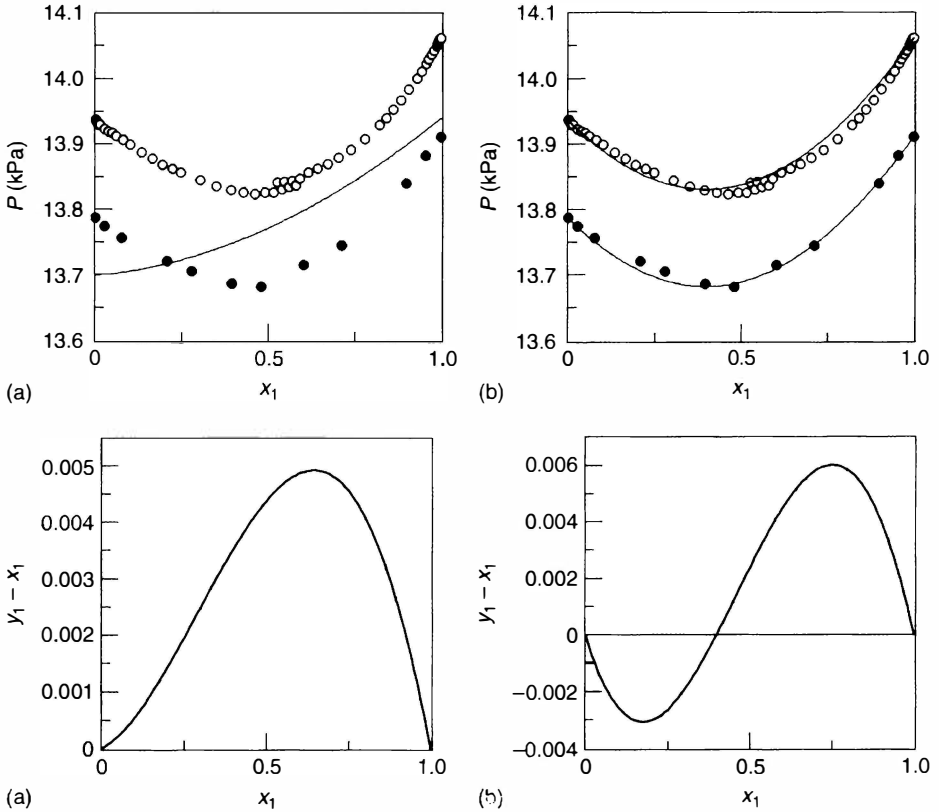

Figure 5.29 Results for the binary system 2-propanol (1) –*tert*-butanol (2) at 40 °C. (a) Using Antoine constants for both compounds ($\Delta g_{12} = -37.984$ cal/mol, $\Delta g_{21} = 29.94$ cal/mol, $\alpha_{12} = 0.3642$), (b) using the pure component vapor pressures of the authors ($\Delta g_{12} = -54.254$ cal/mol, $\Delta g_{21} = 26.41$ cal/mol, $\alpha_{12} = 0.3680$) for fitting the NRTL-parameters.

constants from literature. From Figure 5.29 it can directly be seen that of course for the objective function F:

$$F = \sum_i \left(\frac{P_{\text{exp},i} - P_{\text{calc},i}}{P_{\text{exp},i}} \right)^2$$

a much lower value is obtained, if the pure component vapor pressures given by the authors are used.

For a large number of binary systems the required binary g^E-model parameters for the Wilson, NRTL, and UNIQUAC equation and the results of the consistency tests can be found in the VLE Data Collection of the DECHEMA Chemistry Data Series published by Gmehling *et al.* [6]. One example page is shown in Figure 5.30. It shows the VLE data for the system ethanol and water at 70 °C published by Mertl [8]. On every page of this data compilation the reader will find the system, the reference, the Antoine constants with the range of validity, the experimental

$$\log P_i^s \text{ [mmHg]} = A - \frac{B}{\vartheta[°C] + C}$$

(1) ETHANOL C_2H_6O

(2) WATER H_2O

+++++ ANTOINE CONSTANTS REGION +++++ CONSISTENCY

(1)	8.11220	1592.864	226.184	20– 93 C	METHOD 1	+
(2)	8.07131	1730.630	233.426	1– 100 C	METHOD 2	+

TEMPERATURE = 70.00 DEGREE C

LIT: MERTL I., COLLECT.CZECH.CHEM.COMMUN. 37,366(1972).

Appendix:

$v_1 = 58.69$ cm^3/mol

$v_2 = 18.07$ cm^3/mol

$r_1 = 2.1055$ $q_1 = 1.972$

$r_2 = 0.9200$ $q_2 = 1.400$

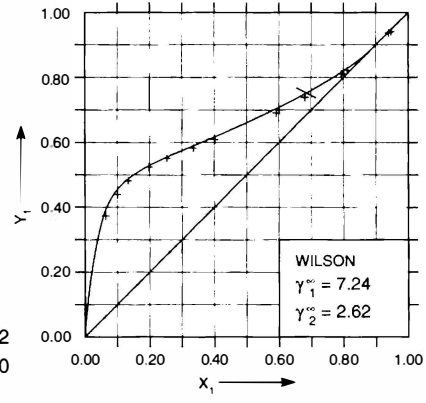

CONSTANTS:	A12	A21	ALPHA12
MARGULES	1.6346	0.8563	
VAN LAAR	1.7966	0.9238	
WILSON	471.0433	883.7530	
NRTL	−121.2691	1337.8574	0.2974
UNIQUAC	−30.1929	337.0028	

cal/mol

$A12 = \Delta\lambda_{12}$ *resp.* Δg_{12} *resp.* Δu_{12}

EXPERIMENTAL DATA			MARGULES		VAN LAAR		WILSON		NRTL		UNIQUAC	
P MM HG	X1	Y1	DIFF P	DIFF Y1	DIFF P	DIFF Y1	DIFF P	DIFF Y1	DIFF P	DIFF Y1	DIFF P	DIFF Y1
362.50	0.0620	0.3740	11.71	0.0031	3.35	−0.0097	−1.25	−0.0149	4.27	−0.0084	3.26	−0.0098
399.00	0.0950	0.4390	9.33	−0.0080	4.45	−0.0118	4.21	−0.0083	4.82	−0.0117	4.44	−0.0117
424.00	0.1310	0.4820	4.27	−0.0166	3.53	−0.0127	6.63	−0.0043	3.31	−0.0136	3.58	−0.0125
450.90	0.1940	0.5240	−2.61	−0.0273	2.34	−0.0158	7.52	−0.0057	1.51	−0.0174	2.42	−0.0156
468.00	0.2520	0.5520	−4.13	−0.0280	3.15	−0.0144	7.80	−0.0063	2.17	−0.0160	3.20	−0.0143
485.50	0.3340	0.5830	−3.27	−0.0246	3.95	−0.0131	6.67	−0.0096	3.14	−0.0142	3.94	−0.0131
497.60	0.4010	0.6110	−1.09	−0.0156	4.70	−0.0082	5.90	−0.0081	4.12	−0.0088	4.64	−0.0083
525.90	0.5930	0.6910	3.85	−0.0020	5.31	−0.0070	4.17	−0.0112	5.24	−0.0063	5.21	−0.0072
534.30	0.6800	0.7390	3.56	0.0020	3.72	−0.0051	2.17	−0.0084	3.77	−0.0043	3.61	−0.0051
542.70	0.7930	0.8160	3.95	0.0040	2.74	−0.0007	0.97	−0.0015	2.91	−0.0003	2.65	−0.0007
543.10	0.8100	0.8260	3.54	0.0008	2.16	−0.0031	0.39	−0.0035	2.34	−0.0028	2.07	−0.0031
544.50	0.9430	0.9410	2.04	−0.0022	0.59	−0.0007	−0.44	0.0006	0.74	−0.0009	0.55	−0.0007
544.50	0.9470	0.9450	2.03	−0.0021	0.64	−0.0006	−0.34	0.0007	0.79	−0.0008	0.60	−0.0006
	MEAN DEVIATION :		4.28	0.0105	3.12	0.0079	3.73	0.0064	3.01	0.0081	3.09	0.0079
	MAX. DEVIATION :		11.71	0.0280	5.31	0.0158	7.80	0.0149	5.24	0.0174	5.21	0.0156

Figure 5.30 Example page of the VLE Data Collection [6].

VLE data, the results of two thermodynamic consistency tests, and the parameters of different g^E-models, such as the Wilson, NRTL, and UNIQUAC equation. Additionally, the parameters of the Margules [28] and van Laar [29] equation are listed.[13] Furthermore, the calculated results for the different models are given. For the model which shows the lowest mean deviation in vapor phase mole fraction the results are additionally shown in graphical form together with the experimental data and the calculated activity coefficients at infinite dilution. In the appendix of the data compilation the reader will find the additionally required pure component data, such as the molar volumes for the Wilson equation, the relative van der Waals properties for the UNIQUAC equation, and the parameters of the dimerization constants for carboxylic acids. Usually, the Antoine parameter A is adjusted to A' to start from the vapor pressure data given by the authors, and to use the g^E-model parameters only to describe the deviation from Raoult's law.[14] Since in this data compilation only VLE data up to 5000 mm Hg are presented, ideal vapor phase behavior is assumed when fitting the parameters. For systems with carboxylic acids the association model is used to describe the deviation from ideal vapor phase behavior.

In practice almost exclusively VLE data are used to fit the required parameters. Since a distillation column works nearly at constant pressure, most chemical engineers prefer thermodynamically consistent isobaric VLE-data in contrast to isothermal VLE-data to fit the model parameters. But that can cause problems, in particular if the boiling points of the two compounds considered are very different [24], as for example, for the binary system ethanol–*n*-decane. The result of the Wilson equation after fitting temperature-independent binary parameters only to reliable isobaric data at 1 atm is shown in Figure 5.31 for the system ethanol–*n*-decane, where the sum of the relative deviations of the activity coefficients was used as objective function.

From the results shown in Figure 5.31 it can be seen that already for VLE poor results are obtained. In particular large deviations are obtained at low ethanol concentrations. This is not only true for the $Tx\gamma$ behavior, but also for the activity coefficients, although the activity coefficients were used to fit the Wilson parameters. The reason for the observed large deviations is that with temperature-independent parameters the observed temperature dependence cannot be described correctly. This conclusion can also be drawn when looking at the calculated excess enthalpies shown in Figure 5.31. Reliable g^E-model parameters should be able to describe the excess enthalpies following the Gibbs–Helmholtz equation. Apparently, excess enthalpies are obtained which strongly deviate from the experimental values [3], in particular at 90 and 140 °C. Of course wrong h^E-values will mean an incorrect temperature dependence of the activity coefficients. For the activity coefficients of ethanol at infinite dilution this is shown in Figure 5.31.

13) Both models (Margules, van Laar) are hardly used for process simulation today.

14) Unfortunately, Mertl [8] has not given the pure component vapor pressures. But with Antoine constants used reliable vapor pressures are obtained as can be seen from Figure 5.4

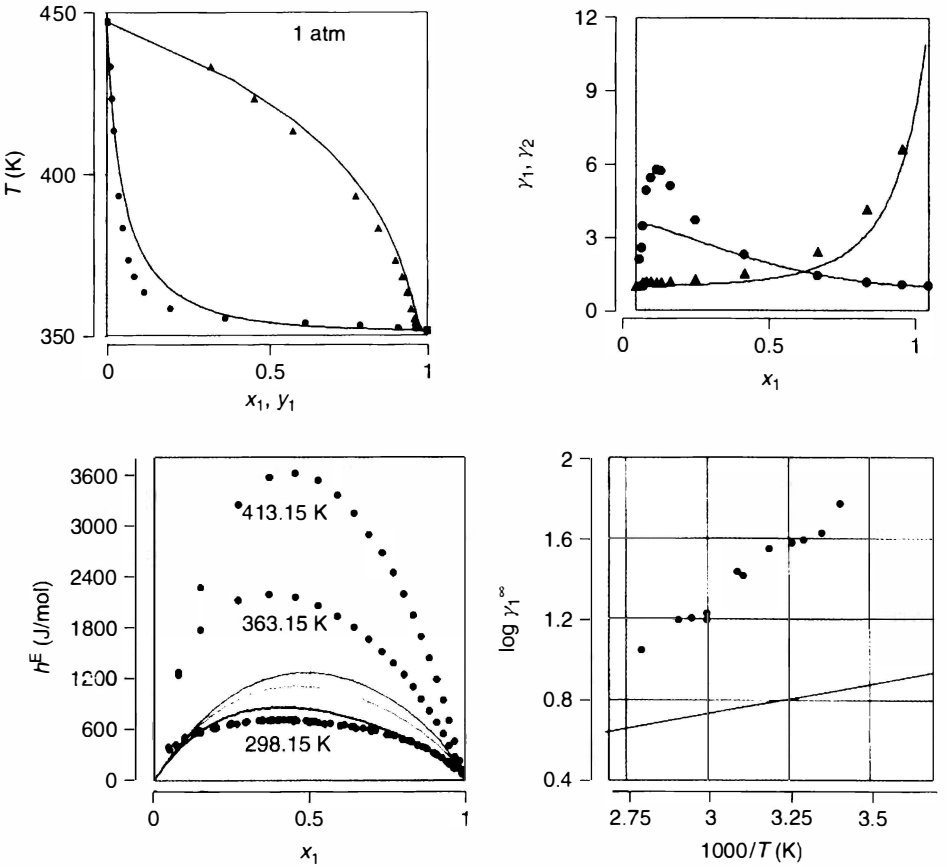

Figure 5.31 Result of the fit of temperature-independent Wilson parameters to consistent isobaric VLE data at 1 atm of the system ethanol (1)–*n*-decane (2) and calculated results for the excess enthalpies and activity coefficients at infinite dilution for the same system using the fitted parameters — Wilson (Wilson parameters: $\Delta\lambda_{12} = 1284.12$ cal/mol, $\Delta\lambda_{21} = 1172.85$ cal/mol, $v_1 = 58.68$ cm^3/mol, $v_2 = 195.92$ cm^3/mol) • experimental [3].

In the case of isobaric data the temperature will change with composition. In particular at low ethanol concentrations the temperature alters drastically. It can be seen that the temperature change between $x_1 = 0$ to $x_1 = 0.1$ is nearly 100 K. Since the system ethanol (1)–*n*-decane (2) shows strong endothermic behavior with large positive values of the partial molar excess enthalpies for ethanol ($\bar{h}_1^{E\infty} \approx 19000$ J/mol, see Figures 5.31 and 5.32), which results in a decrease of the activity coefficient of ethanol with increasing temperature (see Example 5.6) following the Gibbs–Helmholtz equation. This leads to a maximum value of γ_1 at a mole fraction of approx. $x_1 = 0.1$ for the isobaric data as shown in Figure 5.31. It can easily be understood that this curvature can not be fitted correctly using temperature-independent parameters.

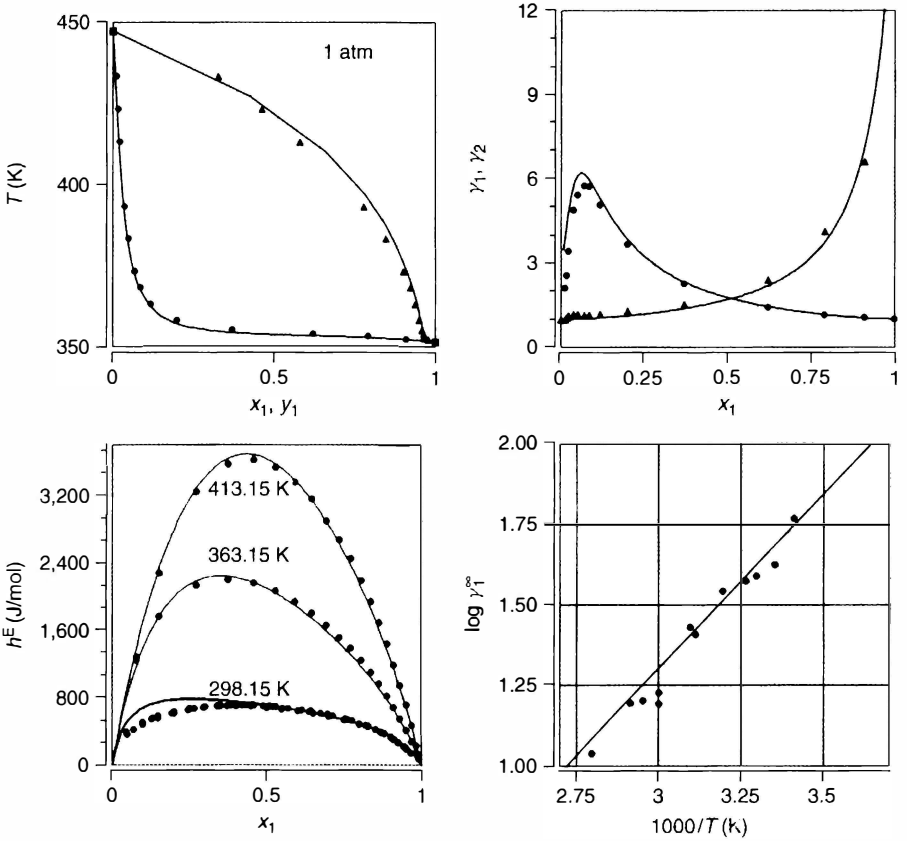

Figure 5.32 Calculated results for the VLE at 1 atm, activity coefficients γ_i, excess enthalpies as a function of composition and activity coefficients at infinite dilution as $f(T)$ for the system ethanol(1)–*n*-decane(2) using temperature-dependent Wilson parameters fitted simultaneously to VLE, h^E and γ^∞ data ● ▲ – experimental [3].

To obtain the correct values at infinite dilution and the correct temperature dependence resp. excess enthalpies, besides VLE data further reliable thermodynamic information should be taken into account for fitting temperature-dependent g^E-model parameters. Temperature-dependent Wilson parameters fitted simultaneously to VLE, excess enthalpies and activity coefficients at infinite dilution of the system ethanol–*n*-decane are given in Table 5.8. The results for VLE, activity coefficients as a function of composition and at infinite dilution and excess enthalpies obtained using these parameters are shown in Figure 5.32 together with the experimental values. It can be seen that with the temperature-dependent binary Wilson parameters (recommended values) not only the VLE behavior, but also the activity coefficients and the excess enthalpies as a function of composition and temperature are described correctly.

Table 5.8 Temperature-dependent Wilson parameters for the system ethanol (1)–*n*-decane (2): $\Delta\lambda_{ij}$ (cal/mol) $= a_{ij} + b_{ij}T + c_{ij}T^2$.

	a_{ij}	b_{ij}	$c_{ij} \cdot 10^4$
$\Delta\lambda_{12}$	4841.1	−7.9999	2.7050
$\Delta\lambda_{21}$	1276.8	−2.1230	5.4421

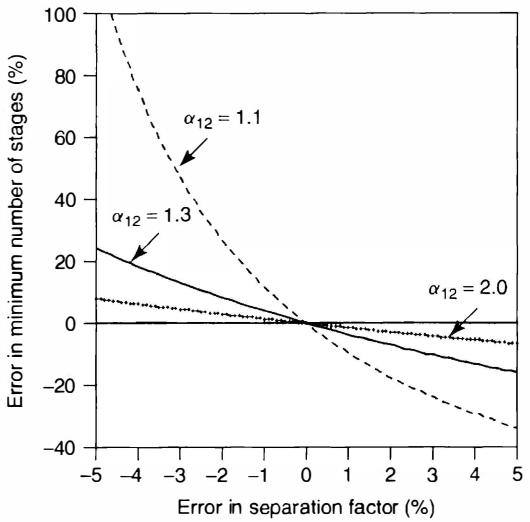

Figure 5.33 Influence of the error of the separation factor on the minimum number of theoretical stages calculated using the Fenske equation.

Already small deviations between the experimental and calculated separation factors can lead to a very different number of stages required for a given separation problem. This is especially true if the separation factor is not far away from unity. For three different separation factors the influence of an error on the minimum number of theoretical stages calculated by the Fenske equation [30] is shown in Figure 5.33,

$$N_{\text{th,min}} = \frac{\log \frac{(x_1/x_2)_d}{(x_1/x_2)_b}}{\log \alpha_{12}}$$

where d is the distillate and b the bottom product. From Figure 5.33 it can be recognized that for a separation factor of 1.1 an error of −4.5%, the minimum number of theoretical stages is nearly doubled. In the case of a separation factor of 2.0 the minimum number of theoretical stages is increased by less than 7%.

5.4.2
Recommended g^E-Model Parameters

As discussed in the chapters above reliable model parameters are most important. While mainly VLE data are used in the chemical industry, it is recommended to use all kinds of reliable data (phase equilibrium data (VLE, γ^∞, azeotropic data, SLE of eutectic systems, etc.), excess enthalpies) for fitting simultaneously g^E-model parameters, which often have to be temperature dependent. To account only for the deviations from Raoult's law, it is recommended to use the pure component vapor pressures measured by the authors for every data set. This can be done by multiplying the vapor pressure with a correction factor, for the Antoine equation, this corresponds to changing the parameter A to A'. Sometimes a large number of experimental data are available. Then of course the data used should be distributed equally over the whole temperature (pressure) range. Since often a lot of VLE data at atmospheric pressure are reported, perhaps some of the data have to be removed or at least a lower weighting factor for the numerous data should be used. The same is true for excess enthalpies. Most authors have measured excess enthalpies around room temperature. For fitting temperature-dependent model parameters the whole temperature range should be covered. While consistent VLE data (azeotropic data) provide the information about the composition

Table 5.9 Recommended NRTL interaction parameters (cal/mol) for different binary systems.

a_{12} (cal/mol)	a_{21} (cal/mol)	b_{12} (cal/(mol K))	b_{21} (cal/(mol K))	c_{12} (cal/(mol K^2))	c_{21} (cal/(mol K^2))	α_{12}
Acetone (1)–cyclohexane (2)						
1423.8	2880.0	−2.9548	−10.136	0.0008073	0.011832	0.4212
Acetone (1)–benzene (2)						
−16.064	110.25	0.37896	0.6426	−0.0004859	−0.0004819	0.6991
Benzene (1)–cyclohexane (2)						
1403.1	8.4201	−7.5455	1.8632	0.01316	−0.006295	0.3
Acetone (1)–water (2)						
833.97	−3146.5	0.83106	17.457	−0.0037816	−0.013622	0.5466
Ethanol (1)–1,4–dioxane (2)						
412.58	1334.9	0.41917	−3.7148	–	–	0.3548
Acetone (1)–chloroform (2)						
5563.9	−12824.0	−43.308	83.358	0.061888	−0.11637	0.0850
Acetone (1)–methanol (2)						
477.04	327.46	0.03815	−0.73193	−0.002931	0.0018051	0.7
Chloroform (1)–methanol (2)						
5378.5	−1471.6	6.37397	−13.015	−0.032724	0.032599	0.055

dependence of the activity coefficients, excess enthalpies deliver the most important information about the temperature dependence. Accurate activity coefficients at infinite dilution deliver the only reliable information about the dilute composition range. In the case of simple eutectic systems, also SLE data can be used. SLE data of eutectic systems deliver supporting data at low temperature, while excess enthalpies at high temperature can be used as supporting data at high temperature, to fit reliable temperature-dependent parameters for the temperature range covered. For fitting the parameters simultaneously to all kind of data, weighting factors w_i are used, so that the objective function looks like

$$F = w_{\mathrm{VLE}} \sum_{n_{\mathrm{VLE}}} \Delta \mathrm{VLE} + w_{\gamma^\infty} \sum_{n_{\gamma^\infty}} \Delta \gamma^\infty + w_{h^{\mathrm{E}}} \sum_{n_{h^{\mathrm{E}}}} \Delta h^{\mathrm{E}} + w_{\mathrm{LLE}} \sum_{n_{\mathrm{LLE}}} \Delta \mathrm{LLE} + w_{\mathrm{SLE}} \sum_{n_{\mathrm{SLE}}} \Delta \mathrm{SLE} + w_{\mathrm{AZD}} \sum_{n_{\mathrm{AZD}}} \Delta \mathrm{AZD} \tag{5.45}$$

For several binary systems recommended model parameters for the g^{E}-models Wilson, NRTL, and UNIQUAC are given in Tables 5.9–5.11. Typical results for the system acetone–water using the NRTL model are shown in Figure 5.34. It can be

Table 5.10 Recommended Wilson interaction parameters (cal/mol) for different binary systems.

a_{12} (cal/mol)	a_{21} (cal/mol)	b_{12} (cal/(mol K))	b_{21} (cal/(mol K))	c_{12} (cal/(mol K^2))	c_{21} (cal/(mol K^2))
Acetone (1)–cyclohexane (2)					
3109.2	1670.7	−10.622	−4.5189	0.013757	0.0012266
Acetone (1)–benzene (2)					
−113.72	201.96	2.5292	−1.5516	−0.0035364	0.0026447
Benzene (1)–cyclohexane (2)					
1558.96	−203.7	−8.2383	3.2140	0.012856	−0.0075245
Acetone (1)–water (2)					
−1305.7	1054.9	1.4341	3.4522	0.009414	−0.005907
Ethanol (1)–1,4-dioxane (2)					
1404.7	136.80	−3.3856	0.82783	–	–
Acetone (1)–chloroform (2)					
375.28	−1722.6	−3.7843	6.4055	0.0079107	−0.0074779
Acetone (1)–methanol (2)					
−60.756	863.79	−0.06114	−1.0533	–	–
Chloroform (1)–methanol (2)					
−1140.8	3596.2	2.5936	−6.2234	0.000031	0.000030
Ethanol (1)–*n*-decane (2)					
4841.1	1276.8	−7.9999	−2.123	0.0002705	0.0005442

Table 5.11 Recommended UNIQUAC interaction parameters (cal/mol) for different binary systems.

a_{12} (cal/mol)	a_{21} (cal/mol)	b_{12} (cal/(mol K))	b_{21} (cal/(mol K))	c_{12} (cal/(mol K^2))	c_{21} (cal/(mol K^2))
Acetone (1)–cyclohexane (2)					
259.18	560.82	−1.0167	0.041374	–	–
Acetone (1)–benzene (2)					
−75.46	120.20	−0.10062	0.44835	−0.0008052	0.0004704
Benzene (1)–cyclohexane (2)					
566.78	−116.17	−3.8155	2.2017	0.006297	−0.004641
Acetone (1)–water (2)					
2619.0	33.80	−6.3149	−4.6102	0.0008817	0.012937
Ethanol (1)–1.4-dioxane (2)					
−27.083	762.43	0.47646	−1.9128	–	–
Acetone (1)–chloroform (2)					
101.70	−853.91	−4.4866	6.9067	0.010999	−0.013211
Acetone (1)–methanol (2)					
324.48	59.98	1.2457	−0.8408	−0.003207	0.0013662
Chloroform (1)–methanol (2)					
3561.3	−416.85	−9.4697	−0.33196	0.0073773	0.002515

seen that nearly perfect agreement between experimental and correlated VLE data, activity coefficients at infinite dilution as $f(T)$, azeotropic composition as $f(T)$ and excess enthalpies as $f(T)$ is obtained. In Figure 5.35 the results for default values given in a process simulator are shown. The difference in quality can easily be recognized. For all properties much better results are obtained using the recommended NRTL parameters. This is especially true for the excess enthalpies and as consequence for the temperature dependence of the activity coefficient at infinite dilution. But reliable activity coefficients at infinite dilution are of particular importance for the design of distillation columns, where at the top (bottom) the last traces of high (low) boiler have to be removed. As described the separation factors at infinite dilution mainly influence the number of theoretical stages required for a distillation column. The procedure for fitting recommended temperature-dependent g^E-model parameters is described in more detail by Rarey–Nies *et al.* [31] and Tochigi *et al.* [32].

For some binary systems the use of temperature-dependent parameters is essential, since with temperature-independent parameters excess enthalpies above certain values cannot be described anymore with the chosen g^E-model (Novák [20]) using temperature-independent parameters. Problems can also arise if systems, such as alkane–alcohol systems, show strong deviations from Raoult's law, this means large activity coefficients at infinite dilution, but no miscibility gap. Typical

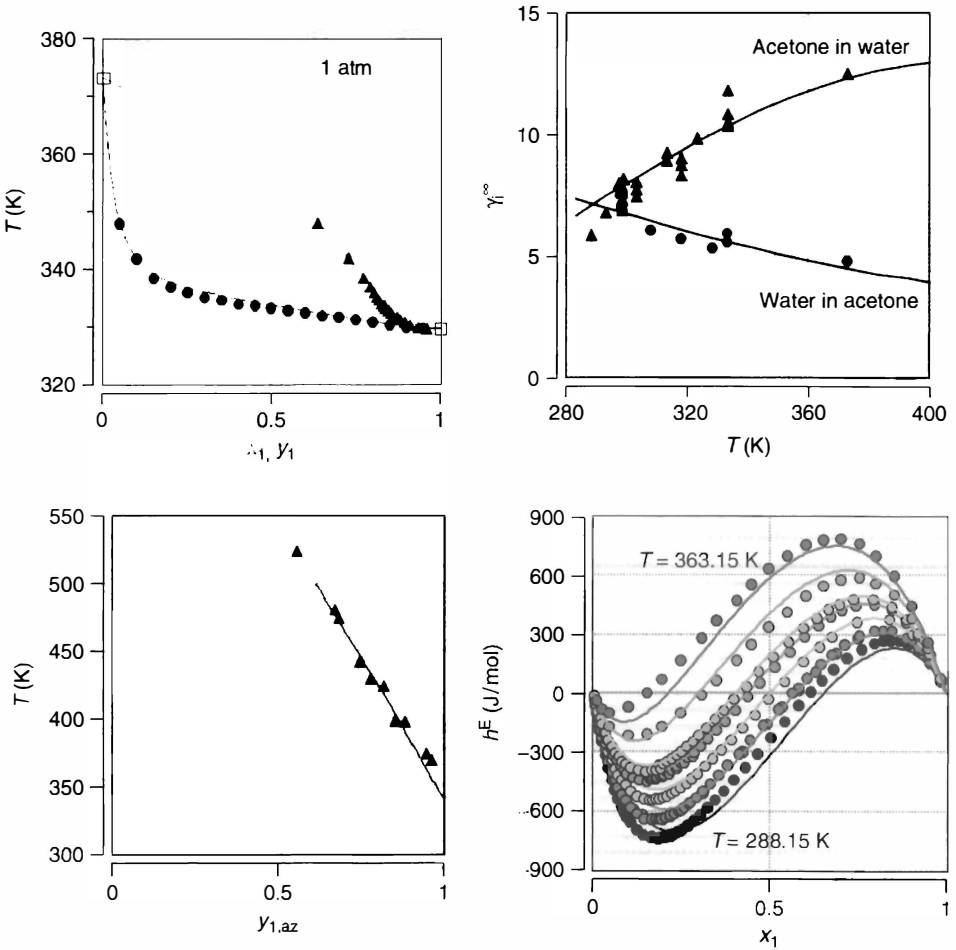

Figure 5.34 Results for acetone (1)–water (2) using recommended temperature dependent NRTL parameters fitted simultaneously to consistent VLE, h^E, and γ^∞ data.

examples are ethanol–decane or cyclohexane–1-propanol. When the activity coefficients at infinite dilution are described correctly with the NRTL or the UNIQUAC model a miscibility gap is calculated. As long as homogeneous behavior is described with these models, too low activity coefficients at infinite dilution result (Novák [20]). Only with the Wilson equation the correct activity coefficients at infinite dilution and homogeneous behavior can be described as shown before.

In Section 11.1 the importance of reliable g^E-model parameters for the synthesis and design of extractive distillation processes is demonstrated for the separation of cyclohexane from benzene using NMP as entrainer. Furthermore for the system acetone–water it is shown how default values can lead to poor separation factors or even not existing azeotropic points at the top of the column ($x_{\text{acetone}} \rightarrow 1$).

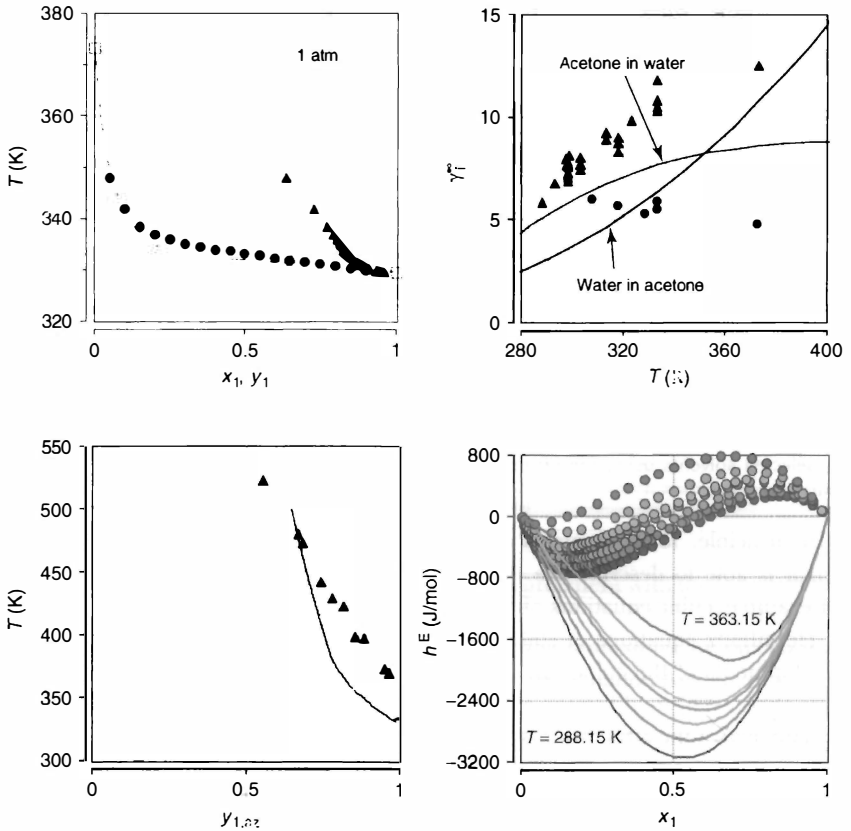

Figure 5.35 Results for acetone (1)–water (2) using the NRTL parameters provided by the process simulator.

5.5
Calculation of Vapor–Liquid Equilibria Using Equations of State

As mentioned before, Approach A (also called φ–φ approach) compared to Approach B (also called γ–φ approach) has the great advantage that supercritical compounds can be handled easily and that besides the phase equilibrium behavior various other properties such as densities, enthalpies including enthalpies of vaporization, heat capacities and a large number of other important thermodynamic properties can be calculated via residual functions for the pure compounds and their mixtures. For the calculation besides the critical data and the acentric factor for the equation of state and reliable mixing rules, only the ideal gas heat capacities of the pure compounds as a function of temperature are additionally required. A perfect equation of state with perfect mixing rules would provide perfect results. This is the reason why after the development of the van der Waals equation of state in 1873 an enormous number of different equations of state have been suggested.

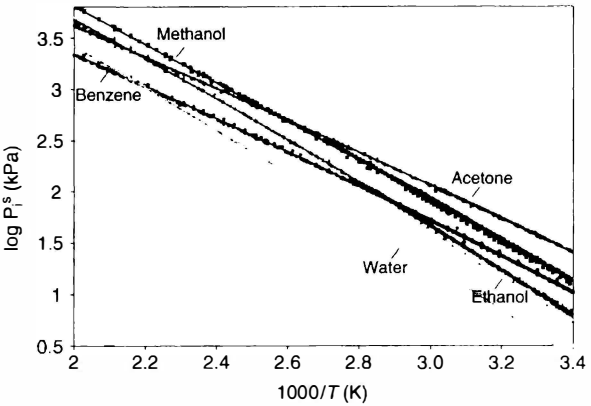

Figure 5.36 Experimental [3] and calculated vapor pressures for selected solvents using the PR equation of state and the Twu-α-function.

In principle, for the calculation of VLE any equation of state can be used which is able to describe the *PvT* behavior of the vapor and the liquid phase, for example, cubic equations of state, further developments of the virial equation, or Helmholtz equations of state. Most popular in chemical industry are further developments of the cubic van der Waals equation of state. Great improvements were obtained by modification of the attractive part, by introducing the temperature dependence of the attractive parameter with the help of a so-called α-function and the development of improved mixing rules, the so-called g^E-mixing rules, which allow the applicability to asymmetric systems and systems with polar compounds.

Exemplarily a few typical results of cubic equations of state used in practice are shown below. A prerequisite for the reliable description of VLE data of binary and multicomponent systems is the reliable description of the pure component vapor pressures. With the introduction of an α-function for the description of the temperature dependence of the attractive parameter $a(T)$ and the usage of the acentric factor ω as third parameter the results for pure component vapor pressures were significantly improved. In Figure 5.36 the experimental and calculated vapor pressures for five solvents are shown, where the PR equation of state with the Twu α-function was used. It can be seen that nearly perfect agreement is obtained in the wide temperature range covered. Even the slopes are described reliably. This means that following the Clausius–Clapeyron equation also the enthalpies of vaporization are described correctly. From the slopes it can be concluded that the enthalpies of vaporization increase from benzene to the alcohols, and then to water. This leads to the fact that in binary systems, for example, acetone–methanol, or ethanol–benzene the low boiler at low temperature can become the high boiler at higher temperatures.

In Figure 5.37 the experimental and calculated enthalpies of vaporization using the SRK and the volume translated PR equation of state for 11 different compounds in a wide temperature range up to the critical temperature are shown. It can be

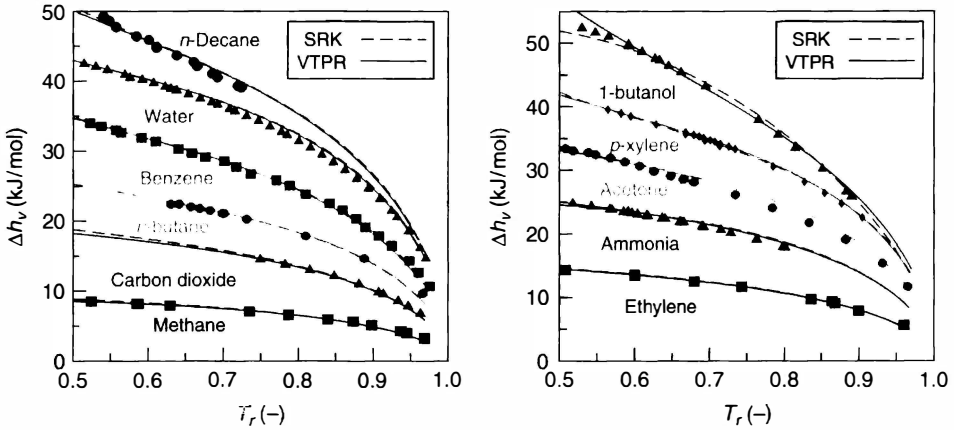

Figure 5.37 Experimental [3] and calculated enthalpies of vaporization using the Soave–Redlich–Kwong and the volume translated PR equation of state.

seen that both equations of state provide excellent agreement with the experimental findings. That is not surprising, since with the reliably calculated vapor pressures and volumes of the vapor and liquid phase, reliable enthalpies of vaporization should be obtained following the Clausius–Clapeyron equation (see Eq. (2.86)).

Example 5.11

Calculate the liquid density of cyclohexane at the normal boiling point ($T_b = 353.85$ K, $P = 1$ atm) with the help of the PR equation of state.

Pure component properties:

Component	M (g mol^{-1})	T_c (K)	P_c (bar)	ω
Cyclohexane	84.16	553.8	40.8	0.213

Solution

For the calculation of the liquid density at the normal boiling point for cyclohexane first the parameters a and b of the PR equation of state have to be determined from the critical data and the acentric factor using Eqs. (2.167)–(2.169).

$$a_c = 0.45724\frac{R^2T_c^2}{P_c} = 0.45724\frac{0.08314^2 \cdot 553.8^2}{40.8}$$

$$= 23.758\left(\text{dm}^3\right)^2 \text{bar/mol}^2$$

$$b = 0.0778\frac{RT_c}{P_c} = 0.0778\frac{0.08314 \cdot 553.8}{40.8} = 0.087798\ \text{dm}^3$$

$$T_r = \frac{T}{T_c} = \frac{353.85}{553.8} = 0.63895$$

$$\alpha(T) = \left[1 + \left(0.37464 + 1.54226\omega - 0.26992\omega^2\right)\left(1 - T_r^{0.5}\right)\right]^2$$

$$\alpha(T) = \left[1 + \left(0.37464 + 1.54226 \cdot 0.213 - 0.26992 \cdot 0.213^2\right) \cdot \left(1 - 0.63895^{0.5}\right)\right]^2 = 1.2965$$

$$a(T) = a_c \cdot \alpha(T) = 23.758 \cdot 1.2965 = 30.8022 \left(\mathrm{dm}^3\right)^2 \mathrm{bar/mol}^2$$

In the next step, the molar liquid volume has to be determined for which the right-hand side of the PR equation of state gives a value of 1 atm. This can be done iteratively or by solving the cubic equation.

$$P = \frac{RT}{v - b} - \frac{a(T)}{v(v+b) + b(v-b)}$$

For the given conditions a molar volume of $v = 0.11068\ \mathrm{dm}^3\ \mathrm{mol}^{-1}$ is obtained.

$$P = \frac{0.08314 \cdot 353.85}{0.11068 - 0.087798} - \frac{30.8022}{0.11068 \cdot (0.11068 + 0.087798) + 0.087798 \cdot (0.11068 - 0.087798)}$$

$$P = 1285.687 - 1284.681 = 1.006\ \mathrm{bar} \approx 1\ \mathrm{atm}$$

In the next step with the help of the molar liquid volume and the molar mass the liquid density at the normal boiling point can be calculated:

$$\rho = \frac{84.16}{0.11068} = 760.38\ \mathrm{g\ dm}^{-3}$$

Experimentally, a density of $719\ \mathrm{g\ dm}^{-3}$ was determined for cyclohexane at the normal boiling point [3]. This means that the calculated value using the PR equation of state is ~6% too high. In Figure 5.38 the calculated liquid densities of cyclohexane are shown together with the experimental liquid densities for a wide temperature range ($T_r = 0.5$–0.8). At the same time the experimental and liquid densities for five more solvents are shown in this diagram. It can be seen that with the exception of water the calculated liquid densities using the PR equation of state are too high. The largest density deviations are obtained for the very polar compound water. It seems that the difference between the experimental and calculated densities is nearly constant. Using the SRK equation of state, even larger deviations between the experimental and calculated liquid densities are obtained. But a reliable description of the pure component densities is a prerequisite for the calculation of reliable mixture densities for multicomponent systems. Peneloux *et al.* [33] showed that the results for the liquid densities can be improved by introducing a translation parameter c (see Section 2.5.5).

In Figure 5.39 for the temperature range $T_r = 0.5$–0.8 experimental and liquid densities for the same solvents as in Figure 5.38 are shown. But for the calculation

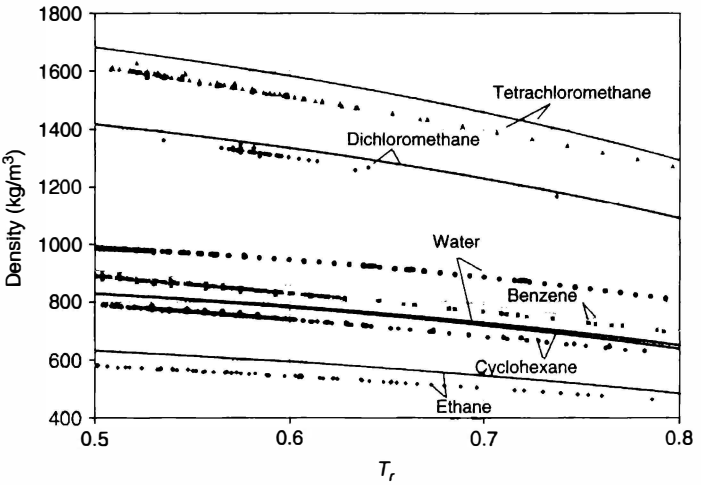

Figure 5.38 Experimental and calculated liquid densities using the PR equation of state for six different solvents in the temperature range $T_r = 0.5–0.8$.

now the volume translated PR equation of state has been used, where the translation parameter was adjusted to the experimental liquid density at $T_r = 0.7$ (see Eq. (2.178)). This ensures that with the volume translation perfect results are obtained at $T_r = 0.7$. Finally, not only for $T_r = 0.7$, but also for other temperatures improved results are obtained. From Figure 5.39 it can be seen that with the

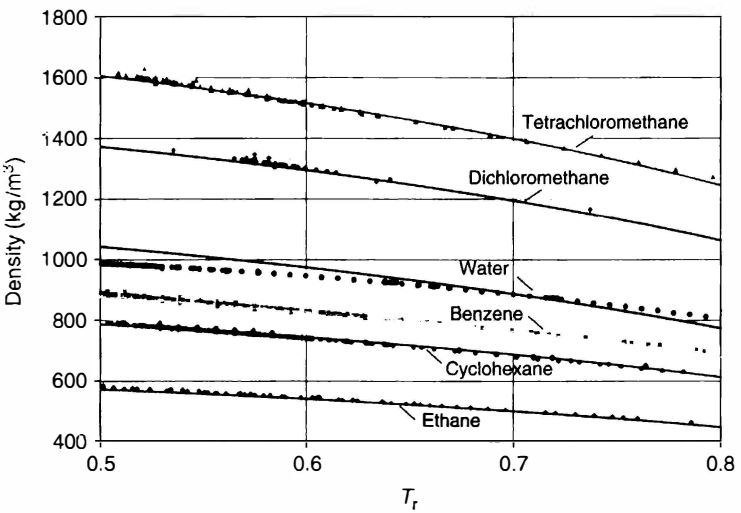

Figure 5.39 Experimental and calculated liquid densities using the volume translated PR equation of state for six different solvents in the temperature range $T_r = 0.5–0.8$.

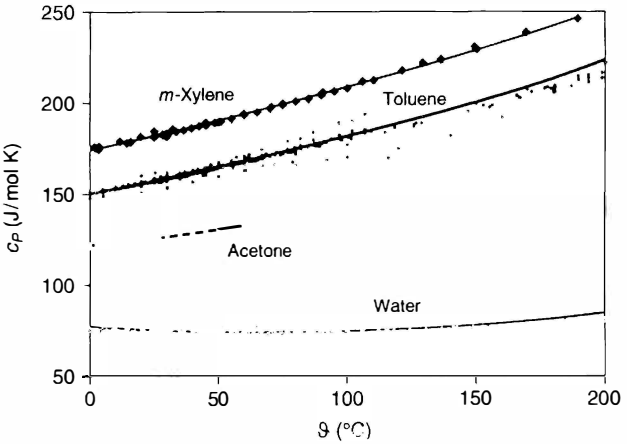

Figure 5.40 Experimental [3] and calculated liquid heat capacities using VTPR.

exception of the strong polar compound water very good agreement is obtained between the experimental and calculated densities in the whole temperature range covered. For 44 compounds investigated in the temperature range ($T_r = 0.5–0.8$) a relative mean deviation smaller than 2% was obtained. This mean relative deviation obtained for VTPR is much smaller than the deviations obtained for the PR (mean deviation approx. 6%) or the SRK equation of state (mean deviation approx. 12%) for the same 44 compounds.

Equations of state not only allow to calculate densities, enthalpies of vaporization, but also other thermodynamic properties, such as heat capacities, enthalpies, entropies, internal energy, Gibbs energy, Helmholtz energy, and other important properties, for example, Joule–Thomson coefficients, and so on. In Figure 5.40 experimental and calculated liquid heat capacities using the VTPR equation of state for five different solvents in the temperature range 0–200 °C are shown. As can be seen the agreement between experimental and calculated data is within approx. 2%. The calculated results of course depend on the quality of the heat capacities of the ideal gas, the parameters of the α-function, and further parameters. In [34] and Chapter 2 it was shown that the results can still be improved when other thermodynamic data are used in addition for fitting the parameters of the α-function.

5.5.1
Fitting of Binary Parameters of Cubic Equations of State

To describe the behavior of mixtures (enthalpies of vaporization, densities, heat capacities, phase equilibria, etc.) using equations of state, binary parameters are required. The different mixing rules suggested were already discussed in Section 4.9.2. While empirical mixing rules, for example, quadratic mixing rules could only be applied for nonpolar systems, the range of applicability of equations

of state with modern g^E-mixing rules was extended to polar systems, for example, systems with water, alcohols, ketones, and so on.

It was shown in Section 4.9.2 that in the quadratic mixing rules a binary parameter k_{12} is required to describe the behavior of the binary system. For fitting the binary parameter usually VLE data are used. With the help of all the required binary parameters k_{ij} (in the case of a ternary system: k_{12}, k_{13}, k_{23}) the ternary or multicomponent system can then be calculated.

In Figure 5.41 for the binary system *n*-butane–CO_2 the experimental results are shown together with the calculated results for $k_{12} = 0$ and for the fitted binary parameter $k_{12} = 0.1392$. It can be seen that the agreement is highly improved when going from $k_{12} = 0$ to $k_{12} = 0.1392$. Furthermore, it is remarkable that k_{12} seems to be temperature-independent over a wide temperature range. It is clear that starting from a poor description of the binary system as in the case of $k_{12} = 0$, there is no chance to obtain good results for a ternary or a multicomponent system.

For a long time the empirical quadratic mixing rules were used in gas-processing or petrochemistry. But poor results were obtained for systems with polar compounds. This is exemplarily shown for the systems acetone–water and isopropanol–water in Figures 5.42 and 5.43. It can be seen from the diagrams on the left-hand side that unsatisfactory results are obtained, if the binary parameter k_{12} of the empirical mixing rules is fitted to these systems. Huron and Vidal [35] carefully investigated the advantages of g^E-models and equations of state and developed the so-called g^E-mixing rules. Now, in g^E-mixing rules the parameters of a g^E-model, for example, of the Wilson, NRTL, or UNIQUAC model are fitted to calculate the attractive parameter of the chosen cubic equation of state. For the two systems mentioned the results are shown on the right-hand side of Figures 5.42 and 5.43. The improvements obtained are significant. The application of the new mixing rules now allowed using equations of state also for process simulation in

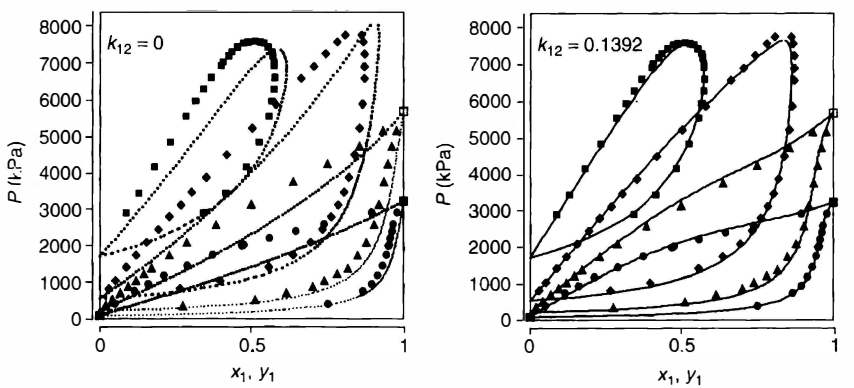

Figure 5.41 VLE results for the system *n*-butane(1) ·CO_2(2) using the binary parameter $k_{12} = 0$ and an adjusted binary parameter (● - 270 K; ▲ – 292.6 K; ♦ – 325.01 K; ■ – 377.6 K) [3].

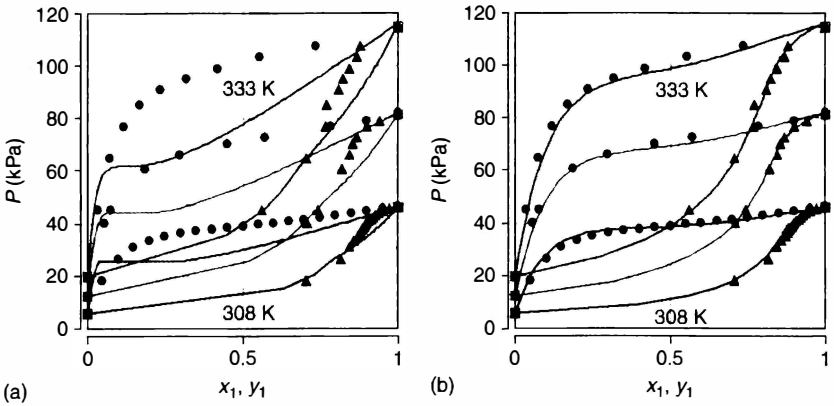

Figure 5.42 Experimental and calculated VLE data for the system acetone (1)–water (2) using the PR equation of state with classical mixing rules ($k_{12} = -0.2428$) (a) and the Soave–Redlich–Kwong equation of state with g^E-mixing rules (NRTL, $\Delta g_{12} = 257.9$ cal/mol, $\Delta g_{21} = 1069$ cal/mol, $\alpha_{12} = 0.2$) (b) at 308, 323 and 333 K.

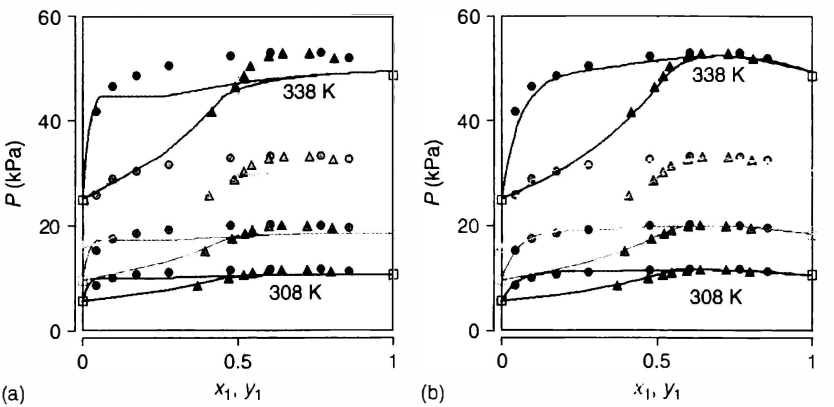

Figure 5.43 Experimental and calculated VLE data for the system isopropanol (1)–water (2) using the PR equation of state with classical mixing rules ($k_{12} = -0.168$) (a) and the Soave–Redlich–Kwong equation of state with g^E-mixing rules (NRTL, $\Delta g_{12} = -339.0$ cal/mol, $\Delta g_{21} = 1914$ cal/mol, $\alpha_{12} = 0.2$) (b) at 308, 318, 328, and 338 K.

chemical industry. Using the binary parameters derived from VLE data equations of state directly allow the calculation of all other mixture properties.

Instead of the binary parameter k_{12} in the case of g^E-mixing rules, the parameters of the Wilson, NRTL, or UNIQUAC equation are fitted. Depending on the strength of the temperature dependence either constant or temperature-dependent parameters have to be fitted. With the help of temperature-dependent parameters

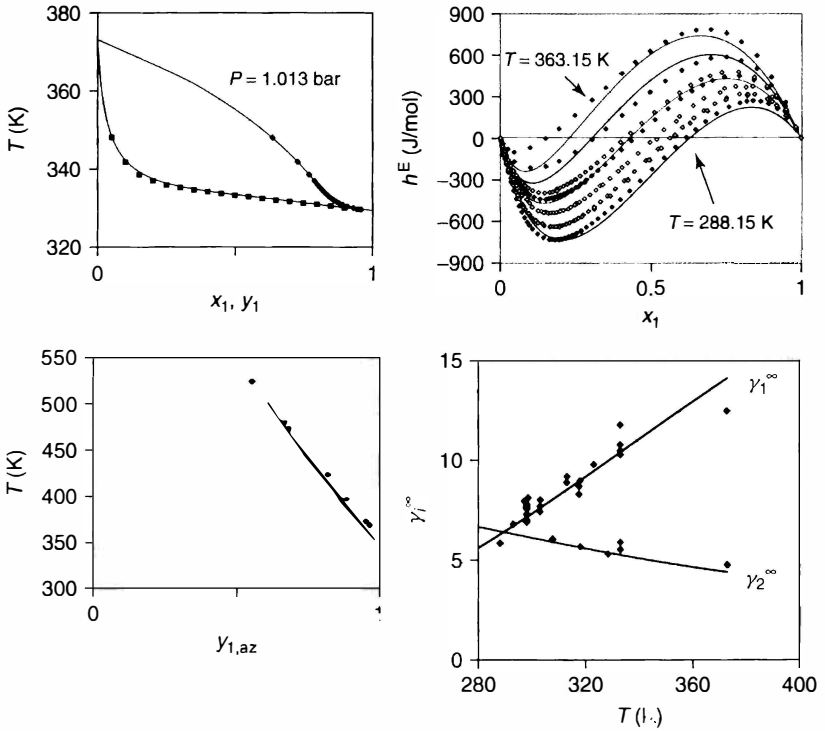

Figure 5.44 Experimental and correlated VLE, h^E, azeotropic, and γ^∞ data using the VTPR equation of state with g^E-mixing rules (UNIQUAC with temperature-dependent parameters); UNIQUAC parameters: a(acetone, H_2O) = 523.84 K, a(H_2O, acetone) = −937.99 K, b(acetone, H_2O) = −1.3221, b(H_2O, acetone) = 4.4338, c(acetone, H_2O) = 0.00125 (K^{-1}), c(H_2O, acetone) = 0.00043 (K^{-1}).

even the temperature dependence of the excess enthalpies can be described with the required accuracy. For the system acetone–water the results are shown in Figure 5.44. It can be seen that besides the VLE behavior, the excess enthalpies, activity coefficients at infinite dilution and the azeotropic data as a function of temperature can be described with the required accuracy.

With the help of the binary parameters k_{12} or g^E-model parameters now the phase equilibrium behavior, densities, enthalpies, Joule–Thomson coefficients, and so on, for binary, ternary and multicomponent systems can be calculated. For the calculation of the VLE behavior the procedure is demonstrated in the following example for the binary system nitrogen–methane using classical mixing rules. The same procedure can be applied to calculate the VLE behavior of multicomponent systems and with g^E-mixing rules as well.

Example 5.12

With the help of the SRK equation of state the system pressure and vapor phase composition for the binary system nitrogen (1)–methane (2) for a liquid mole

fraction of nitrogen $x_1 = 0.2152$ at 144.26 K should be calculated. The required pure component data and the binary parameter are given below:

Component	T_c (K)	P_c (bar)	ω
N_2	126.15	33.94	0.045
CH_4	190.63	46.17	0.010

Binary parameter: $k_{12} = 0.0267$ [36].

Solution

The calculation has to be performed iteratively. The objective of the iterative procedure is to find the pressure and vapor phase composition for which the following equilibrium condition is fulfilled:

$$x_i\varphi_i^{L} = y_i\varphi_i^{V} \tag{5.9}$$

for both components. To start with the calculation, first of all estimated values for the vapor phase composition and system pressure are required. In this case, a vapor phase mole fraction $y_1 = 0.6$ and a pressure $P = 20$ bar were chosen.

During the iterative procedure these values have to be changed until the equilibrium condition (5.9) is fulfilled. A flow diagram for this procedure is shown in Figure 5.45. For the considered example the first step of this procedure is described in detail below.

First the pure component parameters for both compounds have to be calculated with the help of Eqs. (2.162–2.164) at the given temperature (144.26 K) using the critical data P_c, T_c, and the acentric factor ω:

$$a_{11}(T) = 0.42748\frac{0.08314^2 \cdot 126.15^2}{33.94}\alpha_1(T)$$

$$= 1.3856 \cdot \alpha_1(T)(\mathrm{dm}^3)^2 \text{ bar I mol}^2$$

$$T_{r1} = \frac{144.25}{126.15} = 1.1436$$

$$\alpha_1(T) = \left[1 + (0.48 + 1.574 \cdot 0.045 - 0.176 \cdot 0.045^2)(1 - 1.1436^{0.5})\right]^2$$

$$\alpha_1(T) = 0.9251$$

$$a_{11}(T) = 1.2818\left(\mathrm{dm}^3\right)^2 \text{ bar/mol}^2$$

$$b_1 = 0.08664\frac{0.08314 \cdot 126.15}{33.94} = 0.02677 \text{ dm}^3$$

$$a_{22}(T) = 0.42748\frac{0.08314^2 \cdot 190.63^2}{46.17}\alpha_2(T) = 2.3259\,\alpha_2(T)\,(\mathrm{dm}^3)^2 \text{ bar/mol}^2$$

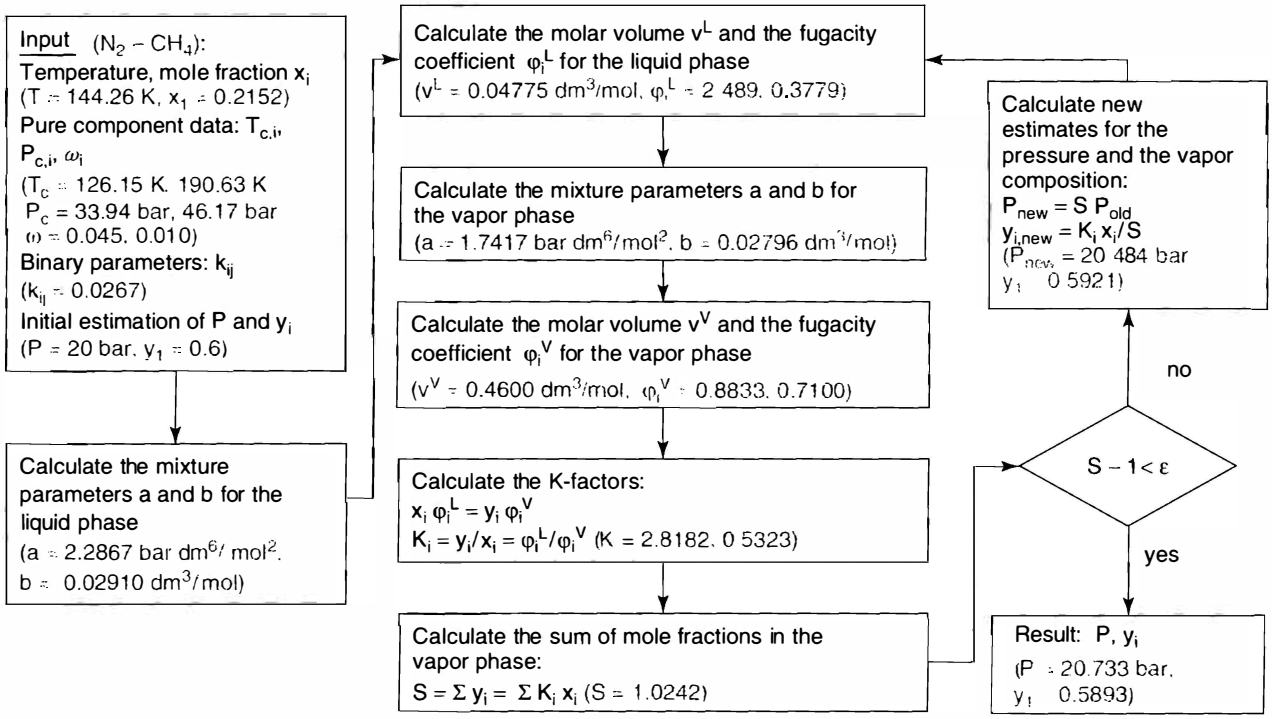

Figure 5.45 Flow diagram for the calculation of isothermal vapor–liquid equilibria using the SRK equation of state.

$$T_{r2} = \frac{144.26}{190.63} = 0.7568$$

$$\alpha_2(T) = \left[1 + (0.48 + 1.574 \cdot 0.01 - 0.176 \cdot 0.01^2)(1 - 0.7568^{0.5})\right]^2$$

$$\alpha_2(T) = 1.1331$$

$$a_{22}(T) = 2.6356(\mathrm{dm}^3)^2\ \mathrm{bar/mol}^2$$

$$b_2 = 0.08664\frac{0.08314 \cdot 190.63}{46.17} = 0.02974\ \mathrm{dm}^3/\mathrm{mol}$$

In the next step, the cross parameter a_{12} and the mixture parameters a and b for the liquid phase with the help of the mixing rules (Eqs. (4.98–4.100)) are calculated.

$$a_{12}(T) = a_{21}(T) = (1.2818 \cdot 2.6356)^{0.5}(1 - 0.0267)$$
$$= 1.7889\ (\mathrm{dm}^3)^2\ \mathrm{bar/mol}^2$$

$$a(T) = 0.2152^2 \cdot 1.2818 + 2 \cdot 0.2152 \cdot 0.7848 \cdot 1.7889 + 0.7848^2 \cdot 2.6356$$
$$= 2.2869(\mathrm{dm}^3)^2\ \mathrm{bar/mol}^2$$

$$b = 0.2152 \cdot 0.02677 + 0.7848 \cdot 0.02974 = 0.0291\ \mathrm{dm}^3/\mathrm{mol}$$

With the help of these parameters, the molar volume of the liquid has to be determined in a way that the given pressure $P = 20$ bar is obtained with the SRK equation of state.

This calculation can be performed iteratively or by solving the cubic equation of state. For the given pressure of 20 bar a molar liquid volume of 0.0477563 $\mathrm{dm}^3/\mathrm{mol}$ is obtained:

$$P = \frac{RT}{v - b} - \frac{a(T)}{v(v + b)} = \frac{0.08314 \cdot 144.26}{0.04776 - 0.0291}$$
$$- \frac{2.2869}{0.04776(0.04776 + 0.0291)} = 20\ \mathrm{bar}$$

With the help of the calculated molar volume and the various pure component and mixture parameters of the liquid phase both fugacity coefficients for the liquid phase φ_i^{L} can be calculated using Eq. (4.101). For nitrogen (1) the following value is obtained:

$$\ln \varphi_1^{\mathrm{L}} = \ln \frac{0.04776}{0.04776 - 0.0291}$$
$$- \frac{2(0.2152 \cdot 1.2818 + 0.7848 \cdot 1.7889)}{0.08314 \cdot 144.26 \cdot 0.0291} \ln \frac{0.04776 + 0.0291}{0.04776}$$
$$+ \frac{0.02677}{0.04776 - 0.0291} - \ln \frac{20 \cdot 0.04776}{0.08314 \cdot 144.26}$$
$$+ \frac{2.2869 \cdot 0.02677}{0.08314 \cdot 144.26 \cdot 0.0291^2}$$
$$\cdot \left(\ln \frac{0.04776 + 0.0291}{0.04776} - \frac{0.0291}{0.04776 + 0.0291} \right)$$

$$\varphi_1^{\mathrm{L}} = 2.4892$$

In the same way, the fugacity coefficient for methane (2) is obtained:

$$\varphi_2^{\mathrm{L}} = 0.3779$$

In the next step, the mixture parameters for the vapor phase ($y_1 = 0.6$) have to be determined:

$$a(T) = 0.6^2 \cdot 1.2818 + 2 \cdot 0.6 \cdot 0.4 \cdot 1.7889 + 0.4^2 \cdot 2.6356$$
$$= 1.7418\,(\mathrm{dm}^3)^2\,\mathrm{bar/mol}^2$$
$$b = 0.6 \cdot 0.02677 + 0.4 \cdot 0.02974 = 0.2796\,\mathrm{dm}^3/\mathrm{mol}$$

With the help of these parameters a molar volume of $0.4601\,\mathrm{dm}^3/\mathrm{mol}$ for the vapor phase is obtained for the pressure of 20 bar using the SRK equation of state. With this volume and the parameters for the vapor phase the following fugacity coefficients are obtained:

$$\varphi_1^{\mathrm{V}} = 0.8833$$

$$\varphi_2^{\mathrm{V}} = 0.7100$$

With the help of the fugacity coefficients obtained first the K-factors ($K_i = y_i/x_i$) for the two components can be calculated using Eq. (5.17):

$$K_1 = \frac{y_1}{x_1} = \frac{\varphi_1^{\mathrm{L}}}{\varphi_1^{\mathrm{V}}} = \frac{2.4892}{0.8833} = 2.8181$$

$$K_2 = \frac{y_2}{x_2} = \frac{\varphi_2^{\mathrm{L}}}{\varphi_2^{\mathrm{V}}} = \frac{0.3779}{0.7100} = 0.5323$$

Then it can be checked whether the equilibrium condition is fulfilled. In equilibrium the sum of the mole fractions in the vapor phase should be equal to 1.

$$S = \sum x_i K_i = 0.2152 \cdot 2.8181 + 0.7848 \cdot 0.5323 = 0.6065 + 0.4177 = 1.0242$$

It can be seen that with the estimated vapor phase composition and pressure the equilibrium conditions are not fulfilled. This means that new values have to be estimated for the vapor phase composition, for example, by normalizing the vapor phase mole fractions:

$$y_1 = \frac{0.6065}{1.0242} = 0.5922$$

$$y_2 = \frac{0.4177}{1.0242} = 0.4078$$

Furthermore, a new pressure is estimated using the K-factor method:

$$P_{\mathrm{new}} = P_{\mathrm{old}} \cdot S = 20.484\,\mathrm{bar}$$

The iteration can be stopped when the sum of the calculated mole fractions

$$S = \sum y_i = \sum x_i K_i,$$

only deviates by a small value for example, $\varepsilon = 10^{-5}$ from the desired value of 1.

After a few iterations the stop criterion $\varepsilon < 10^{-5}$ is fulfilled. This means that the correct equilibrium composition and pressure are obtained.

x_1	$y_{1,exp}$	$y_{1,calc}$	P_{exp} (bar)	P_{calc} (bar)
0.2152	0.5804	0.5893	20.684	20.733

At these conditions the following fugacity coefficients are obtained for the two compounds in the different phases:

φ_1^L	φ_2^L	φ_1^V	φ_2^V
2.4106	0.3655	0.8803	0.6984

In Figure 5.6, the calculated results using the SRK equation of state are shown together with the experimental data for different temperatures and the whole composition range for the system nitrogen (1)–methane (2).

The whole procedure is given in the form of a flow diagram in Figure 5.45. The same procedure shown for the binary system nitrogen–methane can be applied for multicomponent systems. For the calculation besides the critical data T_c, P_c, and the acentric factors ω_i of the compounds involved only the binary parameters k_{ij} for the quadratic mixing rule or the g^E-model parameters in the case of g^E-mixing rules are required.

For the quaternary system N_2–CO_2–H_2S–methanol calculated with the help of the SRK equation of state using binary parameters k_{ij} respectively g^E-mixing rule parameters the calculated and experimental results are shown in Figure 5.46. From the results it can be concluded that in this case only slightly improved results are obtained using g^E-model parameters.

5.6
Conditions for the Occurrence of Azeotropic Behavior

At the azeotropic point, the mole fractions of all components in the liquid phase are identical with the mole fractions in the vapor phase for homogeneous systems.

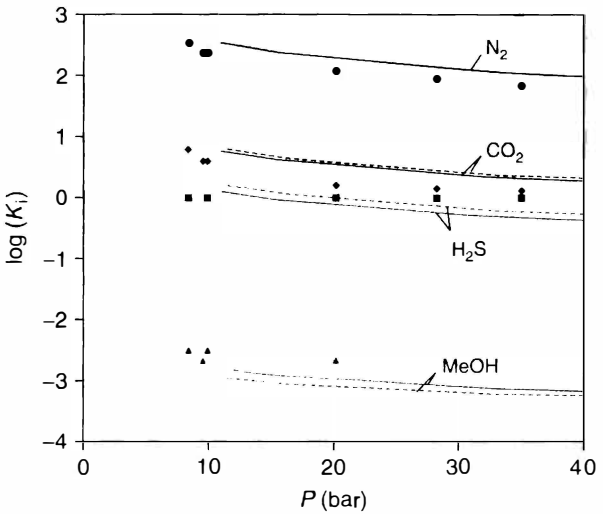

Figure 5.46 Experimental [3] and predicted K-factors for the system $N_2-CO_2-H_2S$–methanol at −15 C: ----- SRK + quadratic mixing rule; –– SRK + g^E-mixing rule

This leads to the fact that all K-factors and all relative volatilities show a value of 1 at the azeotropic point and that the system cannot be separated by ordinary distillation. A reliable knowledge of all azeotropic points for the system to be separated is of essential importance for the synthesis and design of separation processes.

For a binary system, the following relations are valid for homogeneous systems at the azeotropic point using the simplified Eq. (5.18) of Approach B:

$$\alpha_{12} = \frac{K_1}{K_2} = \frac{\gamma_1/x_1}{\gamma_2/x_2} = \frac{\gamma_1 P_1^s}{\gamma_2 P_2^s} = 1 \rightarrow \frac{\gamma_2}{\gamma_1} = \frac{P_1^s}{P_2^s} \text{ or } \frac{\gamma_1}{\gamma_2} = \frac{P_2^s}{P_1^s} \tag{5.46}$$

Using an equation of state (Approach A) the following relation is obtained for the azeotropic point:

$$\alpha_{12} = \frac{K_1}{K_2} = \frac{\gamma_1/x_1}{\gamma_2/x_2} = \frac{\varphi_1^L \varphi_2^V}{\varphi_1^V \varphi_2^L} = 1 \rightarrow \frac{\varphi_1^L}{\varphi_1^V} = \frac{\varphi_2^L}{\varphi_2^V} \tag{5.47}$$

It can be seen that starting from Eq. (5.46) azeotropic behavior always occurs if for a given composition the ratio of the pure component vapor pressures P_1^s/P_2^s is identical to the ratio of the activity coefficients γ_2/γ_1. The typical curvature of the γ_2/γ_1-ratio in logarithmic form for an azeotropic system with positive and negative deviation from Raoult's law at constant temperature is shown in Figure 5.47a,b, respectively. The azeotropic composition can directly be obtained from the intersection of the straight line for the vapor pressure ratio and the curve for the ratio of the activity coefficients γ_2/γ_1.

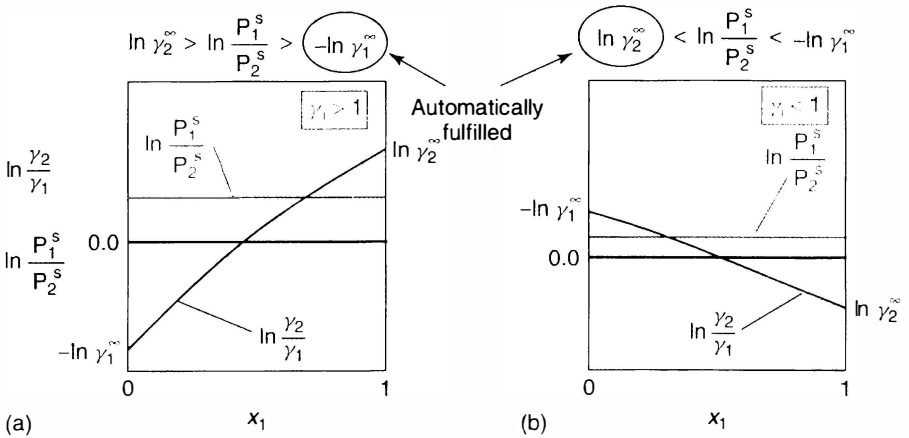

Figure 5.47 Examination of the azeotropic behavior of binary homogeneous systems at constant temperature (component 1 = low boiling compound).[15]

From Eq. (5.46), it can be seen that azeotropic behavior can easily occur in a binary system if the vapor pressures of the two components are very similar, since in this case already very small deviations from Raoult's law are sufficient to fulfill the equation and to create an azeotropic point either with positive or negative deviation from Raoult's law. If the vapor pressures are identical (e.g., at the Bancroft point), the binary system shows the azeotropic behavior.

From Figure 5.47, it can be concluded that the occurrence of azeotropic points can be calculated if besides the activity coefficients at infinite dilution the ratio of the vapor pressures is known. Azeotropic behavior occurs if the following condition for positive resp. negative deviation from Raoult's law is fulfilled (see Figure 5.47):

$$\ln \gamma_2^{\infty} > \ln \frac{P_1^s}{P_2^s} \qquad -\ln \gamma_1^{\infty} > \ln \frac{P_1^s}{P_2^s} \tag{5.48}$$

positive resp. negative deviation from Raoult's law

Since approx. 90% of the systems show positive deviation from Raoult's law, in most cases pressure maximum (temperature minimum) azeotropes are observed.

The activity coefficients at infinite dilution and the vapor pressures depend on temperature following the Gibbs–Helmholtz (Eq. 5.26) and the Clausius–Clapeyron equation (Eq. 3.64) [7], respectively. The result of the temperature dependences is that azeotropic behavior can occur or disappear with increasing or decreasing temperature (pressure). To understand if azeotropic

15) When a strange composition dependence of the activity coefficients exists also two azeotropes with pressure minimum and pressure maximum can be found in a binary system, for example, the system benzene–hexafluorobenzene shows this behavior.

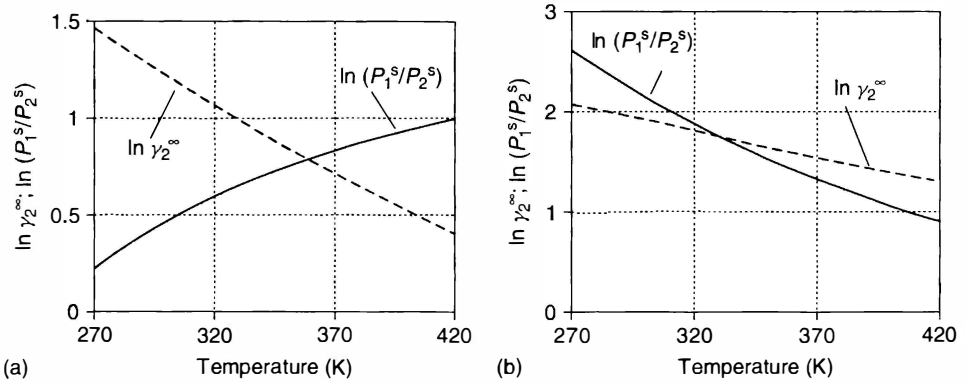

Figure 5.48 Temperature dependence of ln γ_2^∞ (- -) calculated with the help of the NRTL equation and the ratio of the vapor pressures ln P_1^s/P_2^s (—) for the system ethanol (1)–1,4-dioxane (2) (a) and acetone (1)–water (2) (b).

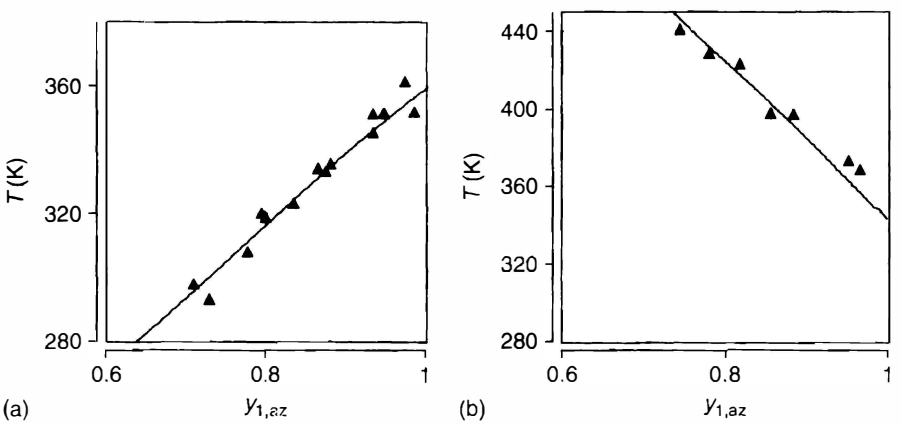

Figure 5.49 Azeotropic behavior of the system ethanol (1)–1,4-dioxane (2) (a) and acetone (1) water (2) (b). ▲ experimental [37]; — calculated using NRTL.

behavior occurs or disappears, only the knowledge of the temperature dependence of γ_2^∞ (for positive deviations from Raoult's law) and the ratio of the vapor pressures is required. For the systems ethanol–1,4-dioxane and acetone–water the experimental azeotropic data are shown in Figures 5.48 and 5.49 together with the calculated results using the NRTL equation with the parameters given in Table 5.9. While for the first system the azeotropic behavior disappears at higher temperature, the opposite is true for the second system acetone–water, where azeotropic behavior occurs at temperatures above 70 °C. As can be seen from Figure 5.49 the occurrence and disappearance of the azeotropic behavior for both systems is described reliably with the NRTL model.

Example 5.13

Determine the azeotropic points of the system acetone (1)–methanol (2) at 50, 100, and 150 °C by the ratio of the activity coefficients and vapor pressures using the Wilson equation with the interaction parameters given in the table below.

For the calculation, the following molar volumes:

$v_1 = 74.04\ \text{cm}^3\ \text{mol}^{-1}$; $v_2 = 40.73\ \text{cm}^3\ \text{mol}^{-1}$ should be used.

Parameters of the Antoine equation: $\log P_i^s(\text{mm Hg}) = A - \dfrac{B}{\vartheta(^\circ\text{C}) + C}$

Compound	A	B	C
Acetone	7.1327	1219.97	230.653
Methanol	8.08097	1582.27	239.7

Wilson parameters

i	j	a_{ij} (cal mol^{-1})	b_{ij} (cal mol^{-1} K^{-1})
1	2	−60.756	−0.06114
2	1	863.79	−1.0533

Solution

Exemplarily for the calculation of the ratio of the activity coefficients the following composition at a temperature of 100 °C is used: $x_1 = 0.2$ and $x_2 = 0.8$.

First the Wilson interaction parameters $\Delta\lambda_{ij}$ at 100 °C have to be calculated:

$$\Delta\lambda_{ij} = a_{ij} + b_{ij} \cdot T$$

$$\Delta\lambda_{12} = -60.756 - 0.06114 \cdot 373.15 = -83.57\ \text{cal mol}^{-1}$$

$$\Delta\lambda_{21} = 863.79 - 1.0533 \cdot 373.15 = 470.75\ \text{cal mol}^{-1}$$

Then the Wilson parameters Λ_{ij} can be determined:

$$\Lambda_{ij} = \frac{v_j}{v_i} \cdot \exp\left[-\frac{\Delta\lambda_{ij}}{RT}\right]$$

$$\Lambda_{12} = \frac{40.73}{74.04} \cdot \exp\left[-\frac{-83.57}{1.98721 \cdot 373.15}\right] = 0.6157$$

$$\Lambda_{21} = \frac{74.04}{40.73} \cdot \exp\left[-\frac{470.75}{1.98721 \cdot 373.15}\right] = 0.9635$$

With the help of these parameters the required activity coefficients can be calculated. Exemplarily the calculation is shown for the activity coefficient of acetone (1):

$$\ln \gamma_1 = -\ln\ (x_1 + x_2\Lambda_{12}) + x_2\left(\frac{\Lambda_{12}}{x_1 + x_2\Lambda_{12}} - \frac{\Lambda_{21}}{x_1\Lambda_{21} + x_2}\right)$$

$$\ln \gamma_1 = -\ln(0.2 + 0.8 \cdot 0.6157) + 0.8 \cdot \left(\frac{0.6157}{0.2 + 0.8 \cdot 0.6157} - \frac{0.9635}{0.2 \cdot 0.9635 + 0.8} \right) = 0.3021$$

$$\gamma_1 = 1.353$$

Similarly the following value is obtained for γ_2:

$$\gamma_2 = 1.024$$

With the help of these activity coefficients the ratio can be estimated:

$$\frac{\gamma_1}{\gamma_2} = \frac{1.353}{1.024} = 1.3213$$

Using the Antoine constants given above one obtains for the ratio of the vapor pressures P_2^s/P_1^s at 100 °C:

$$\frac{P_2^s}{P_1^s} = \frac{2649.26}{2774.1} = 0.955$$

For the whole composition range and the different temperatures selected the results are shown in Figure 5.50. From the diagram it can be seen that a strong temperature (pressure) dependence of the azeotropic composition is observed (50 °C: $x_{1,az} \approx 0.8$; 150 °C: $x_{1,az} \approx 0.2$). This is mainly caused by the different enthalpies of vaporization of the two compounds considered. While acetone shows an enthalpy of vaporization of 29.4 kJ/mol at 50 °C, the value for methanol is

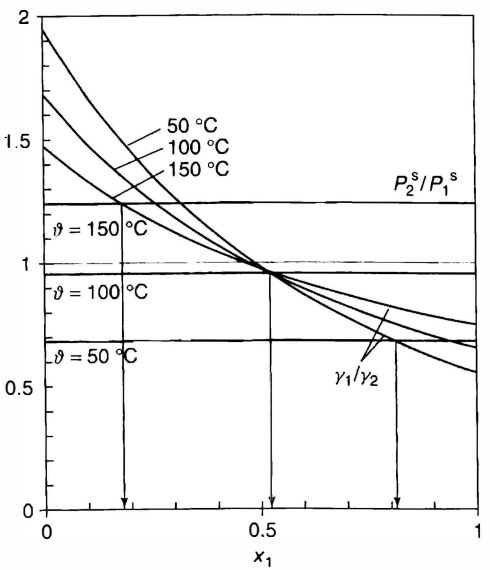

Figure 5.50 Ratio of the activity coefficients γ_1/γ_2 and ratio of the vapor pressures P_2^s/P_1^s of the system acetone (1)–methanol (2) for the determination of the azeotropic points at 50, 100, and 150 °C.

36.1 kJ/mol. The strong pressure dependence observed can be applied in practice for the separation of azeotropic systems by pressure swing distillation, this means using two distillation columns running at different pressures. Since the enthalpies of vaporization of water are higher than for organic compounds, pressure swing distillation is mostly used for the separation of water from organic compounds, as for example, the separation of tetrahydrofuran–water, acetonitrile–water, and so on.

The temperature dependence of the separation factor (see Eq. (5.18)) and of the azeotropic composition of binary systems depends on the type of azeotrope (pressure maximum, pressure minimum), the temperature dependence of the vapor pressures, and the composition and temperature dependence of the activity coefficients. These dependencies can be described with the help of the heats of vaporization and partial molar excess enthalpies following the Clausius–Clapeyron respectively the Gibbs–Helmholtz equation [38] (derivation see Appendix C, B9):

$$\left(\frac{\partial \gamma_1}{\partial T}\right)_{az} = \frac{(\gamma_1\gamma_2)_{az}\left(\Delta h_{v1} - \Delta h_{v2} + \bar{h}_2^E - \bar{h}_1^E\right)}{RT^2\left[1 - \left(\partial\gamma_1/\partial x_1\right)_{az}\right]} \tag{5.49}$$

where the expression $(\partial\gamma_1/\partial x_1)_{az}$ shows values < 1 for systems with positive deviations from Raoult's law and values > 1 for systems with negative deviations from Raoult's law. In most cases the difference of the enthalpies of vaporization is larger than the difference of the partial molar excess enthalpies.

Example 5.14

Calculate the temperature dependence of the azeotropic composition ($\gamma_{1,az} = 0.9$) of the system ethanol (1)–water (2) at 70 °C using Eq. (5.49). At 70 °C the compounds show the following enthalpies of vaporization:

$\Delta h_{v,ethanol}$: 39800 J/mol
$\Delta h_{v,water}$: 42000 J/mol

Solution

Besides the enthalpies of vaporization additionally the difference of the partial molar excess enthalpies and the slope $\partial\gamma_1/\partial x_1$ at the azeotropic point at 70 °C is required. This information can be derived from Figures 5.17 and 5.30. For the difference of the partial molar excess enthalpies $\bar{h}_2^E - \bar{h}_1^E$ approximately a value of 500 J/mol and for the slope a value of 0.9 is obtained.

Using these values the temperature dependence can be calculated:

$$\left(\frac{\partial \gamma_1}{\partial T}\right)_{az} = \frac{0.9 \cdot 0.1 \cdot (39800 - 42000 + 500)}{8.31433 \cdot 343.15^2\,(1 - 0.9)} = -1.56 \cdot 10^{-3}\ \mathrm{K}^{-1}$$

This means that the mole fraction of ethanol in the azeotrope will decrease with increasing temperature and that the azeotropic behavior should disappear at a lower temperature. This is in agreement with the experimental findings. From the enthalpies used for the calculation, it can be recognized that this is mainly caused by the higher enthalpy of vaporization of water compared to ethanol.

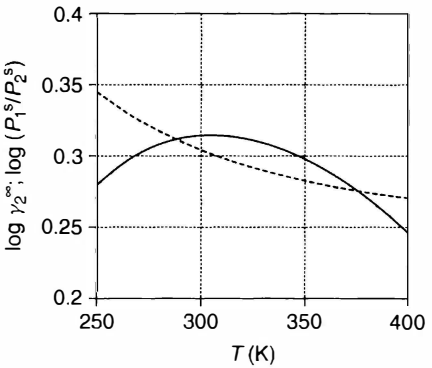

Figure 5.51 γ_2^∞ (—) and the ratio of the vapor pressures P_1^s/P_2^s in logarithmic form (- - -) as a function of temperature for the system acetone (1)–carbon tetrachloride (2).

Depending on the sign of the partial molar excess enthalpies as a function of temperature, the activity coefficient γ_2^∞ can show a maximum or a minimum in the considered temperature range following the Gibbs–Helmholtz relation. This means that the condition for azeotropic points can be fulfilled either only in a small temperature range or at low and again at high temperature. For the maximum case the condition is fulfilled for the system acetone–carbon tetrachloride. The reason is that the sign of the partial molar excess enthalpy changes because of the S-shaped heat of mixing behavior of this system. This results in a maximum for γ_2^∞, so that the condition for azeotropic behavior is fulfilled only in a limited temperature range. Figure 5.51 shows the curvature of γ_2^∞ and the ratio of the vapor pressures in logarithmic form as a function of temperature. The experimental and predicted excess enthalpies and the experimental and predicted azeotropic data using modified UNIFAC are shown in Figures 5.52 and 5.53. It can be seen that modified UNIFAC (see Section 5.9.3.1) is able to predict the occurrence and disappearance of the azeotropic behavior.

Instead of g^E-models also equations of state can be used for the determination of azeotropic behavior of binary or multicomponent systems. In Figure 5.54 the experimental and predicted azeotropic points using the group contribution equation of state VTPR (see Section 5.9.4) for the system ethane–CO_2 up to pressures of 80 bar are shown.

As mentioned before, azeotropic behavior always occurs if the compounds to be separated have identical vapor pressures (Bancroft point). Since the slope of the vapor pressure curve, following the Clausius–Clapeyron equation, depends on the value of the enthalpy of vaporization, a low boiler may become the high boiler with rising temperature, if the enthalpy of vaporization is smaller than the one for the second compound. This is shown for ethanol and benzene in Figure 5.55. While benzene is the low boiler at low temperatures, the opposite becomes true at higher temperatures, since the molar enthalpy of vaporization of the polar component ethanol is larger than the molar enthalpy of vaporization of benzene (see Appendix A).

Even the system water–deuterated water shows a Bancroft point, since deuterated water with a higher normal boiling point (101.4 °C instead of 100 °C) shows a larger enthalpy of vaporization than water. For example, at 25 °C the enthalpy

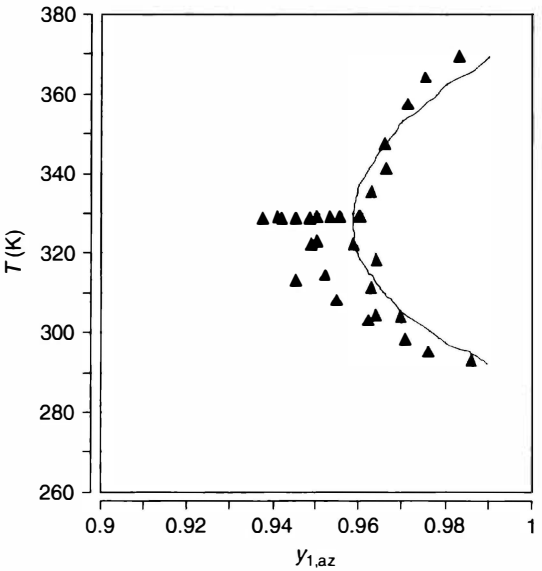

Figure 5.52 Experimental and predicted azeotropic composition of the system acetone (1)–carbon tetrachloride (2) as a function of temperature ▲ experimental [3] — predicted using modified UNIFAC.

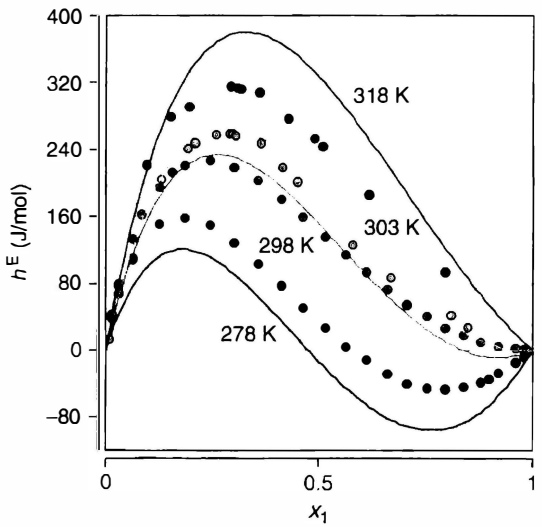

Figure 5.53 Experimental and predicted excess enthalpies of the system acetone (1)–carbon tetrachloride (2) as a function of temperature • experimental data at 5, 25, 30, 45 °C [3] — predicted using modified UNIFAC.

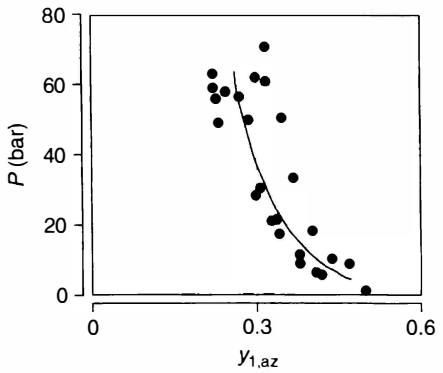

Figure 5.54 Experimental and predicted azeotropic composition of the system ethane (1)–CO_2(2) as a function of pressure. • experimental [3], — predicted using VTPR (see Section 5.9.4).

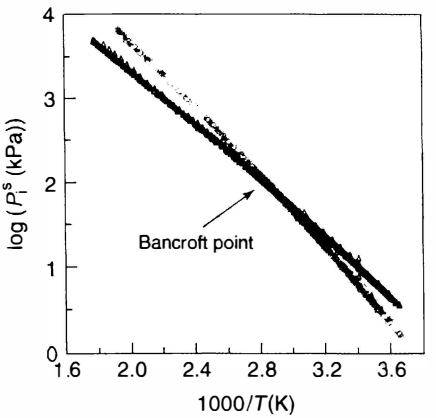

Figure 5.55 Vapor pressure of ethanol and benzene as a function of the inverse temperature experimental data [3] ethanol ▲ benzene.

of vaporization for water is 43.9 kJ/mol and for D_2O 45.35 kJ/mol. The result is that at temperatures around 220 °C the vapor pressures of water and deuterated water become identical following the Clausius–Clapeyron equation, so that even the system water–deuterated water shows azeotropic behavior in a limited temperature range (493–495 K) near the Bancroft point, as shown in Figure 5.56.

Azeotropic behavior is not limited to binary systems only. Also ternary and quaternary azeotropic points are observed. For the determination of the azeotropic points in ternary and quaternary systems, thermodynamic models (g^E-models, equations of state, group contribution methods) can again be applied [40]. Azeotropic points in homogeneous systems can be found with the help of nonlinear regression methods. At the azeotropic point all separation factors α_{ij} show a value of 1 in the case of homogeneous systems. This means that the following condition has to be fulfilled:

$$F = \sum_{i}^{n} \sum_{j>i}^{n} |\alpha_{ij} - 1| = 0 \tag{5.50}$$

For the azeotropic system acetone–chloroform–methanol, the three possible separation factor curves with a value of 1 are shown in Figure 5.57. The intersection

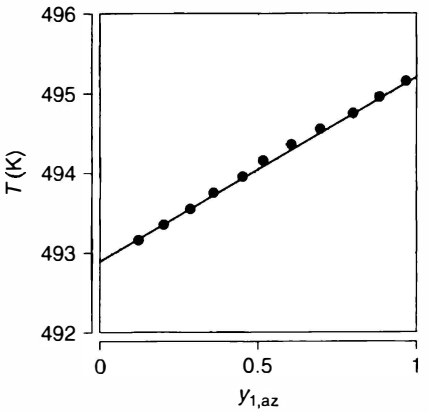

Figure 5.56 Experimental azeotropic points of water (1)–deuterated water (2) [3, 39].

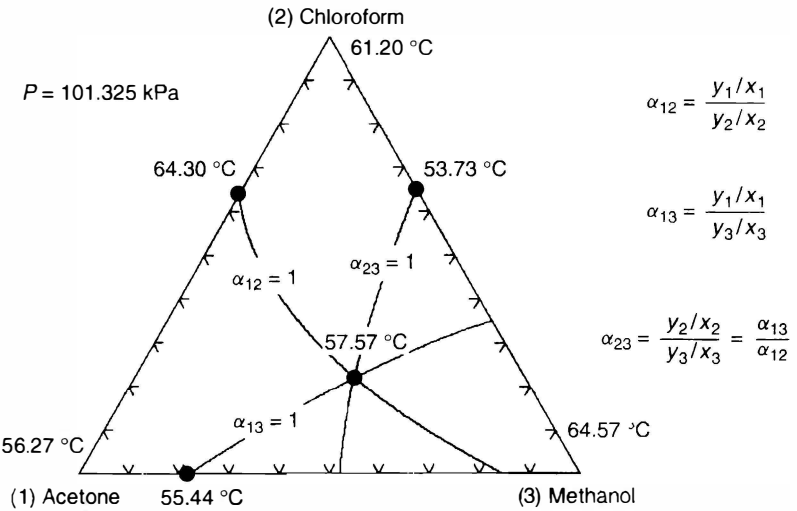

Figure 5.57 Predicted contour lines ($\alpha_{ij} = 1$) using modified UNIFAC for the ternary system acetone (1)–chloroform (2)–methanol (3) at atmospheric pressure).

of two of these curves, for example, $\alpha_{12} = 1$ and $\alpha_{13} = 1$ leads to an azeotropic point, since at the intersection point the criterion for the separation factor α_{23} is automatically fulfilled (see Figure 5.57).

In the case of heterogeneous azeotropic mixtures a different calculation procedure has to be applied. For the ternary system water–ethanol–benzene this is shown in Figure 5.58. Heterogeneous azeotropic behavior occurs if a pressure maximum can be found along the binodal curve. The required pressures can be calculated starting from the composition of the heterogeneous binary system up to the critical point. In doing so, one can start from the composition in the organic or the aqueous phase. The result is shown on Figure 5.58b. It can be seen that for both procedures a pressure maximum occurs, this means heterogeneous azeotropic

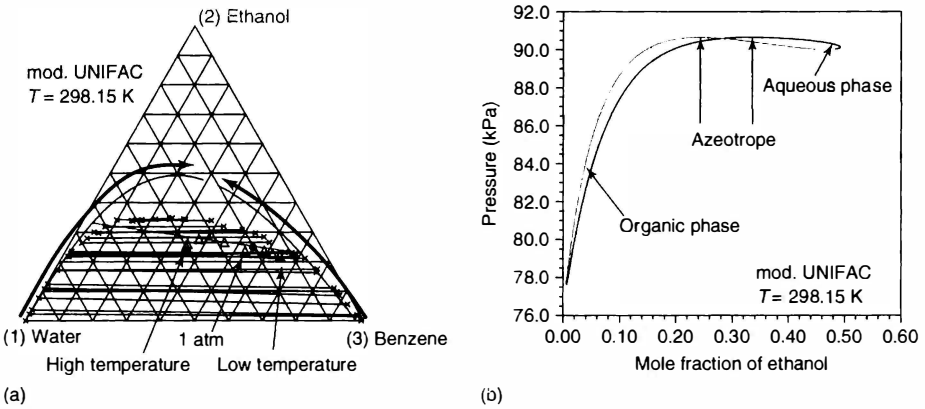

Figure 5.58 Experimental and calculated LLE behavior using modified UNIFAC for the system water–ethanol–benzene at 298.15 K (a) pressure as a function of composition of the benzene rich phase resp. water-rich phase (b).

behavior is obtained for this system. In Figure 5.58, the temperature dependence of the azeotropic composition is also shown. It can be seen that the concentration of water in the azeotrope increases with increasing temperature (pressure). The main reason for the observed temperature dependence is that the vapor pressure of water increases faster than the vapor pressures of ethanol and benzene, because of the larger enthalpy of vaporization.

Azeotropic behavior is also obtained for quaternary systems. But fortunately, azeotropic points in quinary or higher systems do not exist, since with increasing number of components it becomes more and more unlikely that for one composition all the separation factors become exactly unity.

For a large number of systems experimental (a)zeotropic information can be found in a comprehensive data compilation [37]. The knowledge of the azeotropic points is of special importance during the synthesis of separation processes and the selection of suitable solvents for azeotropic distillation.

5.7
Solubility of Gases in Liquids

The objective of absorption processes is the separation of gas mixtures or the removal of undesired compounds from gas mixtures. For the selection of the optimal solvent or solvent mixture (absorbent) and the design of absorption processes a reliable knowledge of the gas solubility as a function of temperature and pressure is of special importance.[16]

16) The reliable knowledge of gas solubilities is also required for the design of gas–liquid reactors.

Industrially important absorption processes are for example the removal of sour gases (CO_2, H_2S) from natural gas or synthesis gas, the removal of carbon dioxide in chemical plants such as ethylene oxide plants, the removal of SO_2 from flue gas, or the absorption of CO_2 in power plants (carbon capture and storage (CCS)), and so on. One has to distinguish physical and chemical absorption

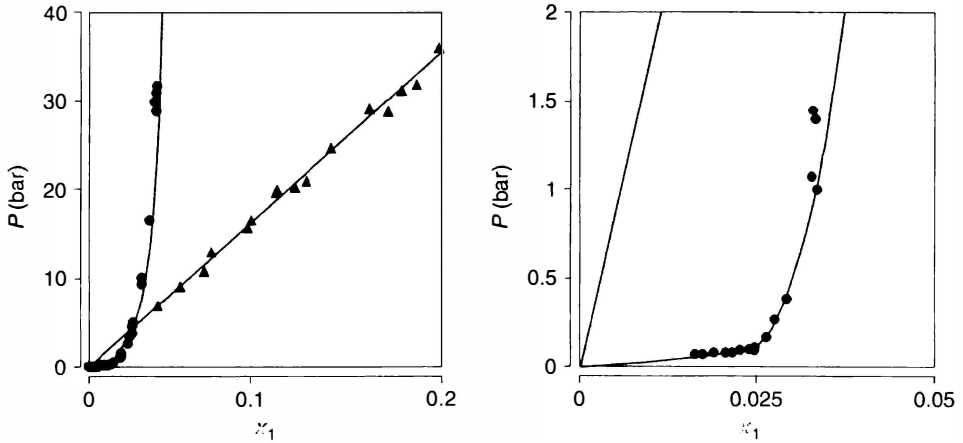

Figure 5.59 Experimental solubilities [3] of CO_2 in methanol (▲) and aqueous monoethanolamine solution (30 mass%) (●) at $T = 313.15$ K.

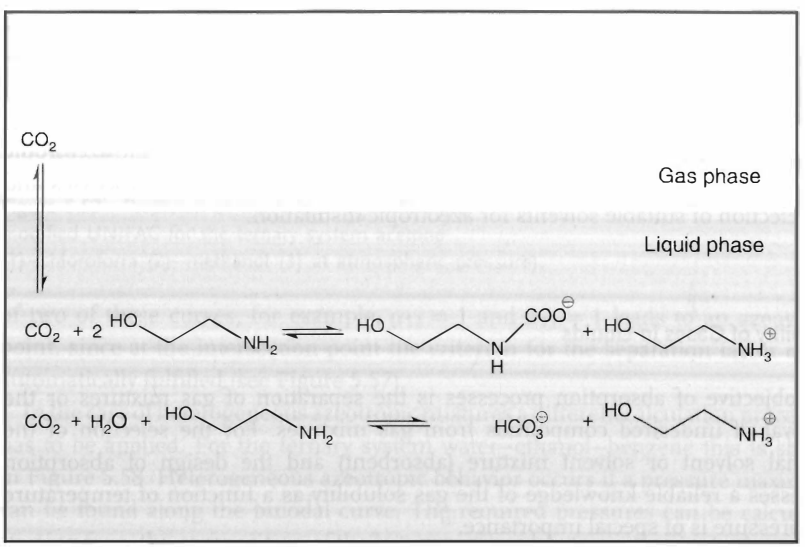

Figure 5.60 Chemical reactions which have to be considered besides the gas solubility for the absorption of CO_2 in aqueous monoethanolamine solutions.

processes. For physical absorption processes, only the knowledge of the phase equilibrium behavior is required. For chemical absorption processes, all chemical equilibria have to be taken into account in addition to the phase equilibria. Often, reaction kinetics and mass transfer has to be regarded as well. In Figure 5.59 the solubility of carbon dioxide in methanol (physical absorption) and aqueous monoethanolamine solution (chemical absorption) is shown for a temperature of 313.15 K.[17] The reactions which have to be considered for the absorption of CO_2 in monoethanolamine are shown in Figure 5.60. From Figure 5.59 it can be recognized that chemical absorption shows great advantages compared to physical absorption, when the partial pressure of the gas to be absorbed is low, as in the case of CCS-processes. Physical absorption shows advantages at high partial pressures.

For the calculation of gas solubilities for physical absorption processes both approaches discussed in Section 5.1 (Eqs. (5.9) and (5.10)) for VLE calculations can be applied.

$$x_i \varphi_i^{L} = y_i \varphi_i^{V} \tag{5.9}$$

$$x_i \gamma_i f_i^{0} = y_i \varphi_i^{V} P \tag{5.10}$$

While there is no difference for the calculation of gas solubilities in comparison to VLE in the case of the equation of state (approach A), for approach B, there is the problem that the standard state (pure liquid at system temperature and system pressure) used for VLE calculations cannot be used anymore, since supercritical compounds are not existent as liquid. This means an alternative standard fugacity is required for the $\gamma-\varphi$-approach.

5.7.1
Calculation of Gas Solubilities Using Henry Constants

An alternative is the usage of the Henry constant H_{ij} as standard fugacity f_i^0. Using the Henry constant as standard fugacity, the following expression is obtained for the calculation of gas solubilities in a binary system:

$$x_1 \gamma_1^{*} H_{12} = y_1 \varphi_1 P \tag{5.51}$$

1 = solute, 2 = solvent

The *Henry constant* is defined as

$$H_{12} = \lim_{\substack{x_1 \to 0 \\ x_2 \to 1 \\ P \to P_2^{s}}} \frac{f_1}{x_1} \tag{5.52}$$

and is exactly valid only for the case where the partial pressure of the gas is equal to zero, this means when the total pressure is identical to the vapor pressure of the solvent.

Since in the case of gas solubilities normally only a small concentration range is covered in the liquid phase, simple expressions for the description of the

17) A temperature of 313.15 K was chosen to be able to compare the solubilities. In practice methanol is used as absorbent (Rectisol process) at much lower temperatures.

concentration dependence of the activity coefficient γ_1^* like for example, Eq. (5.53) (so-called Porter equation) can be applied:

$$\ln \gamma_1^* = A\left(x_2^2 - 1\right) \tag{5.53}$$

The simple expressions used have to satisfy the asymmetric convention ($\gamma_1^* = 1$ for $x_1 \to 0, x_2 \to 1$). However, one should have in mind that equations of state have significant advantages if γ_1^* is significantly different from unity. The application of the Henry constant should be restricted to low solute concentrations $x_1 < 0.03$, so that Eq. (5.51) reduces to the usually applied form:

$$x_1 H_{12} = y_1 \varphi_1 P \tag{5.54}$$

At low pressures the fugacity coefficient also shows values close to unity, so that the following simple expression (so-called Henry's law) is obtained:

$$x_1 H_{12} = y_1 P = p_1 \tag{5.55}$$

A comparison of Eq. (5.55) with Eq. (5.16) at infinite dilution of component 1 shows that in the subcritical region the Henry constant corresponds to

$$H_{12} \approx \gamma_1^{\infty} \cdot P_1^s \tag{5.56}$$

At low pressures the following statements can be derived from Henry's law:

- the gas solubility is proportional to the partial pressure;
- the gas solubility is proportional to the reciprocal value of the Henry constant;
- the temperature dependence of the gas solubility is only determined by the temperature dependence of the Henry constant.

In comparison to the standard fugacity "pure liquid at system temperature and system pressure" used for VLE calculations, there is the great disadvantage of the Henry constant that it is not a pure component property, but has to be derived from experimental gas solubility data.

The value of the Henry constant can be very different. It strongly depends on the properties of the gas (T_c, P_c) and strength of the interactions with the solvent. In Table 5.12 Henry constants for various gases in water are listed for a temperature of 25 °C. It can be seen that these values differ by orders of magnitude. While for the light gases (He, Ar, H_2, N_2, O_2, CO, CH_4, SF_6) Henry constants greater than 40000 bar are observed, values around 1000 bar are found for CO_2, H_2S, C_2H_2 in water, where it is surprising that the Henry constant for the relatively large compound SF_6 is even greater than for helium. In Table 5.13, Henry constants for six gases in four solvents are given for a temperature of 25 °C. The values show that also the interactions between the gas and the solvent play an important role. For all the gases the values are significantly different between the polar solvent methanol and the nonpolar solvent *n*-heptane, caused by the different intermolecular forces between the compounds. Looking at the Henry constant of the sour gases (CO_2, H_2S) and methane in methanol, it seems that methanol is a highly selective absorbent for the removal of sour gases from natural gas. This effect is realized in the so-called Rectisol process [41]. Furthermore, Henry constants show strong,

Table 5.12 Henry constants of various gases in water at 25 °C [3].

Gas	H_{ij} (bar)
He	144000
Ar	40000
H_2	71000
N_2	83500
O_2	44200
H_2S	580
CO	58000
CO_2	1660
CH_4	40200
C_2H_2	1350
C_2H_4	11700
C_2H_6	30400
SF_6	236000

Table 5.13 Henry constants (bar) of various gases in different organic liquids at 25 °C [3].

	H_2	N_2	O_2	H_2S	CO_2	CH_4
Methanol	6100	3900	2200	33.5	145	1180
Acetone	3400	1850	1200	14.5	50	545
Benzene	3850	2300	1260	19.0	105	490
Heptane	1450	760	500	23.4	78	210

nonlinear temperature dependence. In Figures 5.61 and 5.62, Henry constants for various systems are shown as a function of temperature. For the three systems helium, nitrogen, and oxygen in water shown in Figure 5.61 even a maximum of the Henry constant is observed. This means that the gas solubility for a given partial pressure can increase as well as decrease with increasing temperature depending on the temperature range considered. In Figure 5.62 it is shown that for the systems with hydrogen the Henry constant decreases with increasing temperature, while the opposite behavior is observed for methane in methanol and carbon dioxide in toluene.

In process simulators, the temperature dependence of the Henry constants is often described by the following expression:

$$\ln \frac{H_{12}(T)}{\text{bar}} = A_{12} + \frac{B_{12}}{T} + C_{12} \ln \frac{T}{K} + D_{12} T + \frac{E_{12}}{T^2} \tag{5.57}$$

Usually the data situation does not justify adjusting all parameters. In most cases only two of them (A, B or A, D) can be fitted. The value of the constant A depends on the chosen unit for the pressure.

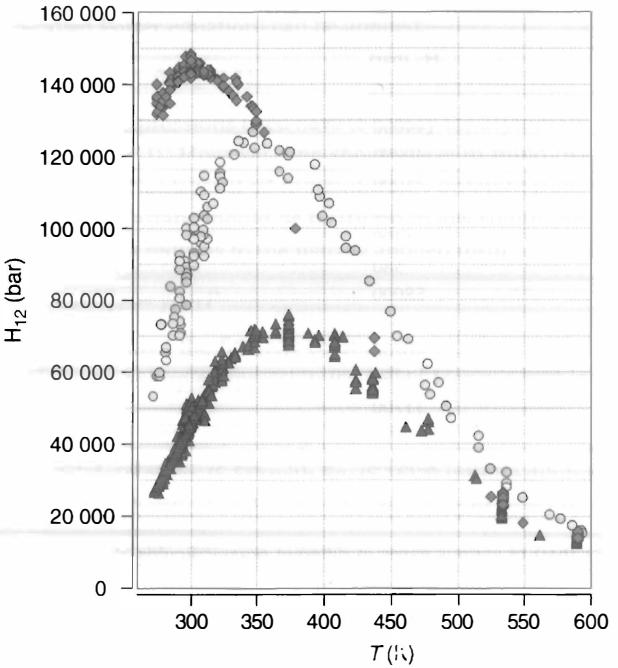

Figure 5.61 Henry constants of He, N_2, and O_2 in water as a function of temperature experimental [3] ♦ helium, ● nitrogen, ▲ oxygen.

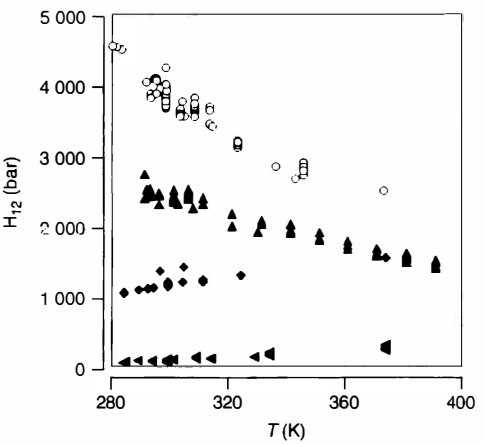

Figure 5.62 Henry constants of various gases in organic solvents as a function of temperature. Experimental data from [3]. ● hydrogen in benzene, ▲ hydrogen in cyclohexane, ♦ methane in methanol, ◄ carbon dioxide in toluene.

Example 5.15

Determine the Henry constant for carbon dioxide (1) in water (2) with the help of the following phase equilibrium data at 50 °C:

$x_1 \cdot 10^3$	p_1 (kPa)
0.342	101.33
0.683	202.65
1.354	405.3
2.02	607.95
2.66	810.6
3.3	1013.3
3.93	1216
4.55	1419
5.15	1621
5.75	1824

$P^s_{H_2O}$ = 12.3 kPa at 50 °C, virial coefficients: $B_{11} = -102\ cm^3/mol$, $B_{12} = -198\ cm^3/mol$, $B_{22} = -812\ cm^3/mol$.

Solution

For the calculation of the fugacity coefficients the total pressure has to be determined first. Since the partial pressure of water is approximately identical with the vapor pressure at 50 °C (12.3 kPa), the total pressure can directly be calculated, for example, for $p_1 = 405.3$ kPa (data point 3):

$$P = 405.3 + 12.3 = 417.6\ kPa$$

With these values the vapor phase composition is obtained:

$$y_1 = \frac{405.3}{417.6} = 0.9705$$

With this information, the second virial coefficient B and the fugacity coefficient for carbon dioxide can be calculated using Eq. (4.89):

$$B = 0.9705^2\,(-102) + 2 \cdot 0.9705 \cdot 0.0295\,(-198) + 0.0295^2\,(-812) = -108\ cm^3/mol$$

With Eq. (4.87) follows for the fugacity coefficient:

$$\ln\varphi_1 = \{2\,[0.9705\,(-102) + 0.0295\,(-198)] + 108\}\,\frac{417.6}{8314.33 \cdot 323.15}$$

$$\varphi_1 = 0.9843$$

In the next step the fugacity f_1 and the ratio f_1/x_1 can be calculated:

$$f_1 = y_1\varphi_1 P = \varphi_1 p_1 = 0.9843 \cdot 405.3 = 398.94\ kPa$$

$$f_1/x_1 = 398.94/0.001354 = 294600\ kPa = 2946\ bar$$

Table 5.14 Experimental gas solubility data, fugacities, fugacity coefficients and the ratio f_1/x_1 for the system CO_2–water at 50 °C.

$x_1 \cdot 10^3$	p_1 (kPa)	φ_1	f_1 (kPa)	f_1/x_1 (bar)
0.342	101.33	0.9960	100.92	2951
0.683	202.65	0.9920	201.01	2943
1.354	405.3	0.9843	398.94	2946
2.02	607.95	0.9768	593.83	2940
2.66	810.6	0.9693	785.7	2954
3.3	1013.3	0.9618	974.63	2953
3.93	1216	0.9545	1160.6	2953
4.55	1419	0.9471	1344.0	2954
5.15	1621	0.9399	1523.6	2958
5.75	1824	0.9327	1701.2	2959

For the other data points the fugacity coefficients φ_1, fugacities f_1 and ratios f_1/x_1 are given in Table 5.14.

From a diagram (see Figure 5.63a) where the ratio f_1/x_1 is plotted against the liquid mole fraction of carbon dioxide, the Henry constant can be determined at the mole fraction $x_1 = 0$. Besides the ratio f_1/x_1, additionally the ratio p_1/x_1 is shown in Figure 5.63. While the ratio f_1/x_1 stays nearly constant, the values for the ratio p_1/x_1 are distinctly different already at low partial pressures. But the extrapolation to $x_1 = 0$ ($p_1 \to 0$) leads to the same value for the Henry constant ($H_{1,2} \approx 2950$ bar).

Another option to determine the Henry constant is the plot of the fugacity f_1 over the mole fraction x_1. That is shown in Figure 5.63b. In this diagram the Henry

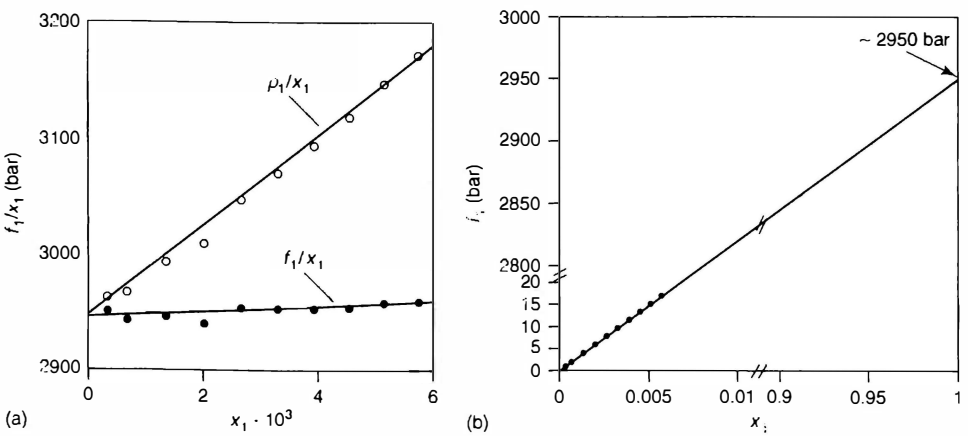

Figure 5.63 $f_1/x_1 (p_1/x_1)$ resp. f_1 as a function of x_1 for the system CO_2(1) water (2) at 50 °C.

constant is obtained from the straight line through the experimental data at the intersection at $x_1 = 1$. Both procedures lead to the same value.

Henry's law is valid exactly only for $P = P_2^s$. However, the pressure dependence of the Henry constant is relatively low, but it can be taken into account by

$$\left(\frac{\partial \ln H_{12}}{\partial P}\right)_T = \frac{\bar{v}_1^\infty}{RT} \tag{5.58}$$

where $\bar{v}_1^{\infty}$[18] is the partial molar volume of the dissolved gas (1) in the solvent (2) at infinite dilution. Assuming that the partial molar volume is constant, the Henry constant at the pressure P can directly be calculated using Eq. (5.59), which is known as *Krichevsky–Kasarnovsky equation.*

$$\ln H_{12}(P) = \ln H_{12}(P_2^s) + \frac{\bar{v}_1^\infty (P - P_2^s)}{RT} \tag{5.59}$$

For mixed solvents, an empirical logarithmic mixing rule

$$\ln \frac{H_{i,\text{mix}}}{\text{bar}} = \frac{\sum_j x_j \ln \frac{H_{ij}}{\text{bar}}}{\sum_j x_j} \tag{5.60}$$

can be applied, where the summation is only carried out for solvents for which the Henry constant is known.

This mixing rule makes sense only in cases where the Henry constants for the gases in the highly concentrated compounds of the solvent are known.

Example 5.16

Calculate the Henry constant of CO_2 in a liquid mixture of methanol, water and trioxane at 25 °C. The concentrations and the Henry constants of CO_2 in the pure solvents are given in the following table:

	x	$H_{CO_2,i}$ (bar) at $\vartheta = 25\,°C$
Methanol	0.39	145
Water	0.6	1660
Trioxane	0.01	unknown

Solution

Using Eq. (5.60), one has to take into account that only the concentrations of methanol and water are counted, as the Henry constant of CO_2 in trioxane is not

18) The partial molar volumes at infinite dilution can be obtained from the observed volume change during absorption.

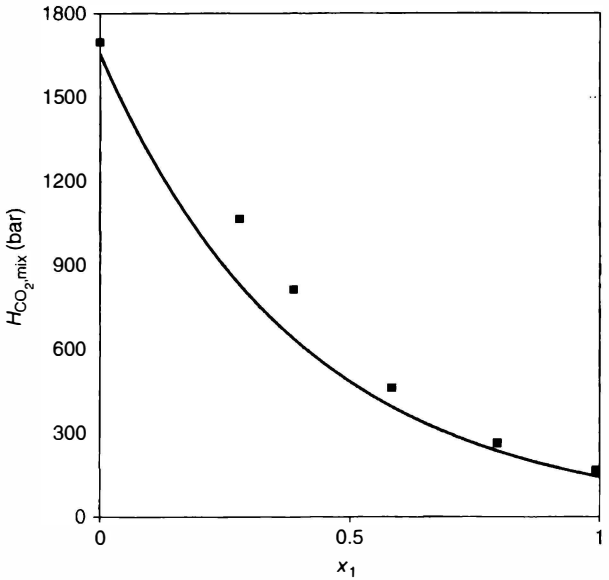

Figure 5.64 Henry constant of CO_2 in the system methanol (1)–water (2) at 25 °C — correlation; ■ experimental data from [42].

known:

$$\ln\frac{H_{CO_2,mix}}{\text{bar}} = \frac{\sum_j x_j \ln\frac{H_{CO_2,j}}{\text{bar}}}{\sum_j x_j} = \frac{0.39\cdot \ln 145 + 0.6\cdot \ln 1660}{0.39+0.6}$$

$$= 6.4545 \Rightarrow H_{CO_2,mix} = 635\ \text{bar}$$

There is an experimental value for $x_{methanol} = 0.3885$ and $x_{water} = 0.6115$ at $\vartheta = 25\,°C$, giving $H_{CO_2,mix} = 749\,\text{bar}$ [42]. Clearly, the simple mixing rule can by far not be taken as exact; however, at least the correct order of magnitude is met, which is usually sufficient in process simulation. Figure 5.64 shows the relationship of the Henry constant H_{CO_2} at $\vartheta = 25\,°C$ as a function of the methanol concentration. It can be seen that in this case the mixing rule works in a qualitatively correct way.

When dissolving a gas in the liquid phase the enthalpy of the gas changes similarly to the enthalpy change of vaporization. The enthalpy of solution at infinite dilution $\Delta h_i^{\infty L}$ – the enthalpy difference between the gaseous and the dissolved solute – can be expressed with the help of the Henry constant as derived below.

Starting from the phase equilibrium condition

$$\mu_i^V = \mu_i^L \tag{5.61}$$

and

$$\mu_i^V = \mu_i^{0V} + RT\ln\frac{f_i^V}{f_i^{0V}} \tag{5.62}$$

where the standard fugacity is based on the pure component, and

$$\mu_i^L = \mu_i^{\infty L} + RT \ln (x_i \gamma_i^*) \tag{5.63}$$

where the standard fugacity is based on the state of infinite dilution, one obtains

$$\frac{\mu_i^{0V} - \mu_i^{\infty L}}{RT} = \ln \frac{x_i f_i^{0V}}{f_i^V} \tag{5.64}$$

as γ_i^* becomes unity at infinite dilution. Considering

$$H_{i,mix} = \lim_{x_1 \to 0} \frac{f_i^L}{x_i} \qquad \text{and} \qquad f_i^L = f_i^V$$

one obtains

$$\frac{\mu_i^{0V} - \mu_i^{\infty L}}{RT} = -\ln \frac{H_{i,mix}}{f_i^{0V}} \tag{5.65}$$

Using the van't Hoff equation (see Appendix C, A7), differentiation of both sides with respect to temperature yields

$$-\frac{h_i^{0V} - h_i^{\infty L}}{RT^2} = -\frac{d \ln \frac{H_{i,mix}}{f_i^{0V}}}{dT} = -\frac{f_i^{0V}}{H_{i,mix} f_i^{0V}} \frac{1}{} \frac{dH_{i,mix}}{dT} = -\frac{1}{H_{i,mix}} \frac{dH_{i,mix}}{dT} \tag{5.66}$$

and therefore

$$\Delta h_i^{\infty L} = h_i^{0V} - h_i^{\infty L} = \frac{RT^2}{H_{i,mix}} \frac{dH_{i,mix}}{dT} \tag{5.67}$$

The application of Henry's law is recommended especially for systems with a single solvent, such as the solubility of nitrogen in water or, as shown below, the solubility of methane in benzene. In multicomponent mixtures with one or more

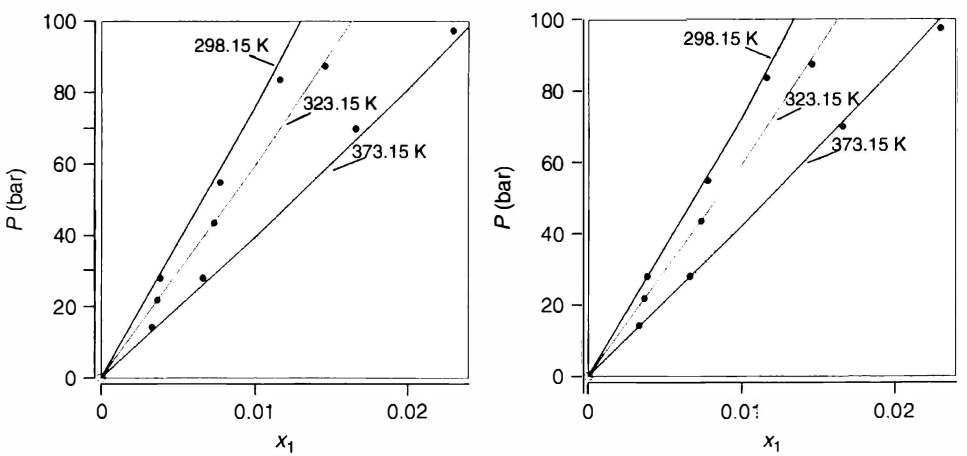

Figure 5.65 Experimental and calculated *Px*-data using the SRK equation of state with quadratic mixing rules for the system nitrogen (1)–NMP (2) at different temperatures. (a) $k_{12} = 0.3403$, (b) $k_{12} = -0.07938 - 0.001297\,T$.

supercritical compounds the use of Henry constants must be examined carefully. In this case the use of an equation of state should be preferred.

5.7.2 Calculation of Gas Solubilities Using Equations of State

As mentioned before, the great advantage of the equation of state approach is that for the calculation of VLE no standard fugacity (vapor pressure, Henry constant) is required. This means that there is no difference in the calculation procedure for VLE and gas solubilities. In Figure 5.65 typical results are shown for the system nitrogen–NMP (N-Methylpyrrolidone) at different temperatures. For the correlation the SRK equation of state with quadratic mixing rules was used. It can be seen that the results can be slightly improved when a binary parameter k_{12} with a linear temperature dependence is used for the temperature range covered.

Example 5.17

Calculate the Henry constant for methane in benzene at 60 °C with the help of the SRK equation of state ($k_{12} = 0.08$ [36]).

Pure component properties

Component	T_c (K)	P_c (bar)	ω
Methane	190.63	46.17	0.010
Benzene	562.6	49.24	0.212

Solution

The calculation can be carried out in the same way as shown in Example 5.12 for the system nitrogen–methane. For the calculation only initial values for the pressure and vapor phase mole fraction are required. With the calculated fugacity coefficients new values for the pressure and vapor phase mole fractions can be calculated. This iterative procedure is stopped at a given convergence criterion. For a mole fraction of $x_1 = 0.01$ in the liquid phase in equilibrium the following values are obtained:

$$y_1 = 0.9014$$
$$P = 5.666 \text{ bar}$$

$$\varphi_1^L = 89.70 \quad \varphi_2^L = 0.0915$$
$$\varphi_1^V = 0.9951 \quad \varphi_2^V = 0.9193$$

Using these values the Henry constant can be calculated:

$$H_{12} = \frac{f_1}{x_1} = \frac{y_1 \varphi_1^V P}{x_1} = \frac{0.9014 \cdot 0.9951 \cdot 5.666}{0.01} = 508.2 \text{ bar}$$

or

$$H_{12} = \frac{f_1}{x_1} = \frac{x_1 \varphi_1^L P}{x_1} = \varphi_1^L P = 89.70 \cdot 5.666 = 508.2 \text{ bar}$$

In fact the Henry constant should be calculated for $x_1 \rightarrow 0$. But when the interaction energies are not too strong as in this case, the Henry constant can be used up to a few mole-%.

5.7.3 Prediction of Gas Solubilities

If no experimental data are available gas solubilities can be predicted today with the help of group contribution equations of state, such as Predictive Soave–Redlich–Kwong (PSRK) [43] or VTPR [44]. These models are introduced in Sections 5.9.4 and 5.9.5.

Up to the 1970s, methods based on the regular solution theory and the fugacity of a hypothetical liquid were suggested for the prediction of gas solubilities. This procedure can lead to reasonable results as long as only nonpolar components are regarded. According to the method of Prausnitz and Shair [45], the reduced standard fugacity of the solute (hypothetical liquid) is described by the following expression:

$$\ln \frac{f_1^0 (1.013 \text{ bar})}{P_{c1}} = 7.81 - \frac{8.06}{T_{r1}} - 2.94 \ln T_{r1} \tag{5.68}$$

which is valid in the temperature range $0.7 < T_{r1} < 2.5$. Figure 5.66 shows the temperature dependence of the reduced standard fugacity of the hypothetical liquid.

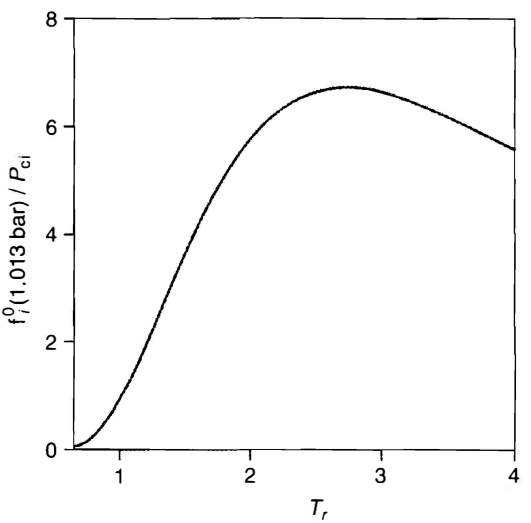

Figure 5.66 Temperature dependence of the reduced standard fugacity of the solute (hypothetical liquid).

Table 5.15 Hypothetical liquid molar volumes and solubility parameters at $\vartheta = 25$ °C.

Gas	v_i (10^{-6} m³/mol)	δ_i (J/m³)$^{0.5}$	T_c (K)	P_c (bar)
N_2	32.4	5279	126.2	33.9
CO	32.1	6405	132.9	35
O_2	33	8185	154.6	50.4
Ar	57.1	10906	150.8	48.7
CH_4	52	11622	190.4	46
CO_2	55	12277	304.1	73.8
Kr	65	13095	209.4	55
C_2H_4	65	13505	282.4	50.4
C_2H_6	70	13505	305.4	48.8
Rn	70	18068	377	62.8
Cl_2	74	17802	416.9	79.8

According to the regular solution theory, the corresponding activity coefficient at infinite dilution can be expressed as

$$\ln \gamma_1^{\infty} = \frac{v_1}{RT} (\delta_1 - \delta_2)^2 \tag{5.69}$$

with the solubility parameter

$$\delta_i(T) = \left(\frac{\Delta h_{Vi}(T) - RT}{v_i} \right)^{0.5} \tag{5.70}$$

For supercritical gases no liquid phase and thus no values for v_i and Δh_{Vi} exist. In Table 5.15 hypothetical values for the molar liquid volume and the solubility parameter for some well-known light gases at $\vartheta = 25$°C are listed. As nothing better is available, these values are also applied at other temperatures as well. The Henry constant can finally be calculated using Eq. (5.56), where instead of the vapor pressure the fugacity of the hypothetical liquid is used.

Example 5.18

Estimate the Henry constant of methane (1) in benzene (2) at $\vartheta = 60$ °C using the method of Prausnitz and Shair.

Solution

The values for the solute from Table 5.15 are

$$v_1 = 52 \cdot 10^{-6} \text{ m}^3/\text{mol}$$
$$\delta_1 = 11622 \text{ (J/m}^3)^{0.5}$$

$$T_{c1} = 190.4 \text{ K}$$
$$P_{c1} = 46.0 \text{ bar}$$

For benzene, the solubility parameter can be determined using the following information:

$$M = 78.114 \text{ g/mol}$$

$$\Delta h_{v2}(60^\circ\text{C}) = 408.7 \text{ J/g}$$

$$\rho_2(60^\circ\text{C}) = 837.9 \text{ kg/m}^3 \Rightarrow v_2 = 93.22 \cdot 10^{-6} \text{ m}^3/\text{mol}$$

leading to

$$\delta_2 = \left(\frac{408.7 \cdot 78.114 - 8.31433 \cdot 333.15}{93.22 \cdot 10^{-6}} \right)^{0.5} = 17685 \text{ (J/m}^3)^{0.5}$$

Thus, the activity coefficient of the solute at infinite dilution is calculated via

$$\ln \gamma_1^\infty = \frac{v_1}{RT} (\delta_1 - \delta_2)^2 = \frac{52 \cdot 10^{-6}}{8.3143 \cdot 333.15} (11622 - 17685)^2$$

$$= 0.6901 \Rightarrow \gamma_1^\infty = 1.994$$

The standard fugacity can be determined with Eq. (5.68) for $T_{r1} = 333.15/190.4 = 1.75$:

$$f_1^0 = 46.0 \exp\left(7.81 - \frac{8.06}{1.75} - 2.94 \ln 1.75\right) = 218.7 \text{ bar}$$

The result for the Henry constant at $\vartheta = 60^\circ\text{C}$ is

$$H_{12}(60^\circ\text{C}) = 218.7 \text{ bar} \cdot 1.994 = 436.1 \text{ bar}$$

The experimental value is approx. 513 bar [46].

5.8 Liquid–Liquid Equilibria

In Section 5.2 it was shown that strongly real behavior leads to the formation of two liquid phases with different compositions. The concentration differences of the compounds in the different phases can be used, for example, for the separation by extraction. As in the case of other phase equilibria, the fugacities in the different liquid phases are identical in the case of LLE:

$$f_i' = f_i'' \qquad i = 1, 2, \ldots, n \tag{5.71}$$

As shown before, the fugacities can either be described using activity coefficients or fugacity coefficients. Using activity coefficients the following relation is obtained:

$$\left(x_i \gamma_i f_i^0\right)' = \left(x_i \gamma_i f_i^0\right)'' \tag{5.72}$$

Since the standard fugacity f_i^0 is the same for the two liquid phases, the following simple equation results from Eq. (5.72):

$$x_i' \gamma_i' = x_i'' \gamma_i'' \tag{5.73}$$

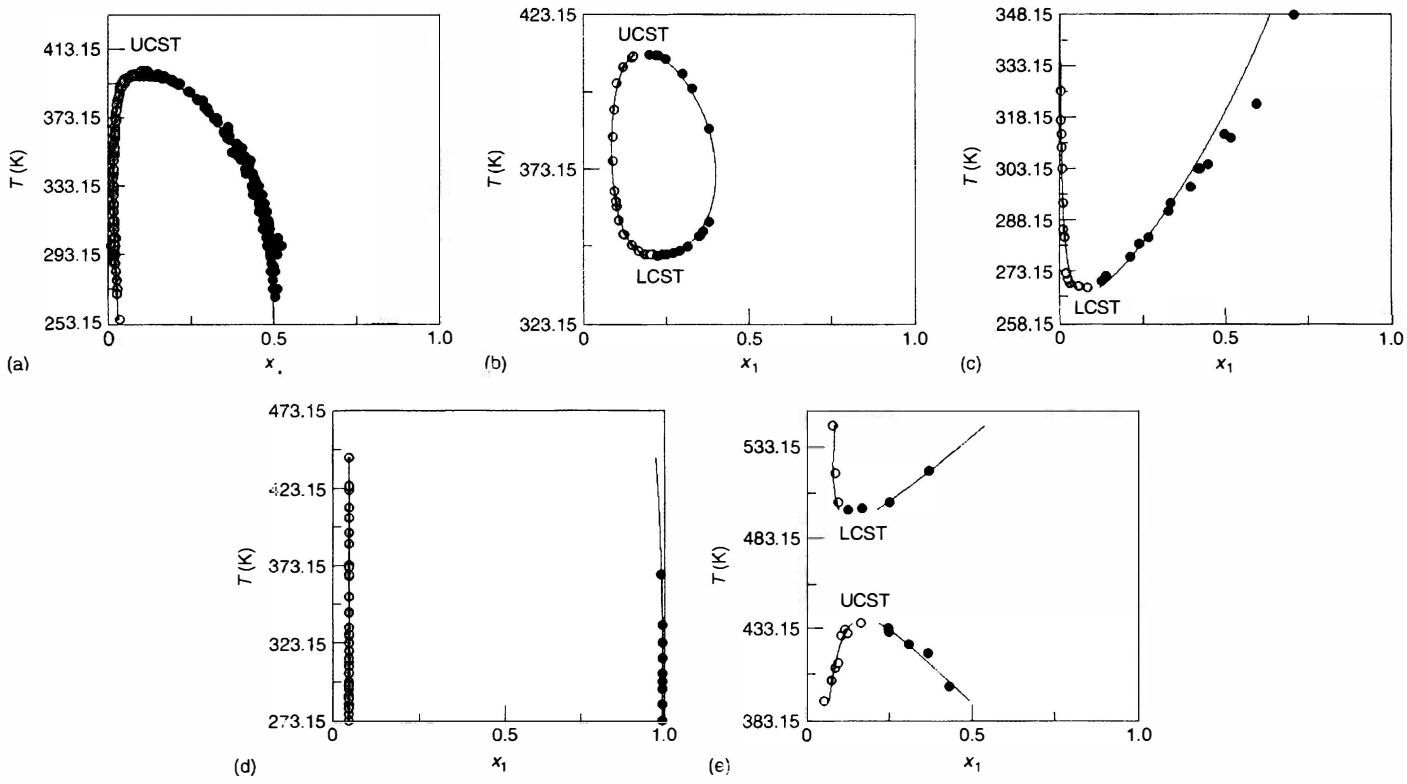

Figure 5.67 Observed temperature dependences of binary LLE [3] (a) 1-butanol (1)–water (2), (b) tetrahydrofuran (1)–water (2), (c) dipropylamine (1)–water (2), (d) *n*-hexane (1)–water (2), (e) benzene (1)–sulfur (2).

The product $x_i\gamma_i$ is also called *activity* a_i (see section 4.8). This means that the so-called isoactivity criterion has to be fulfilled in the case of LLE.

Using fugacity coefficients, a similar relation results:

$$(x_i\varphi_i^L)' = (x_i\varphi_i^L)'' \tag{5.74}$$

Two liquid phases always occur in the case of strong positive deviation from Raoult's law. The LLE behavior as a function of temperature only depends on the temperature dependence of the activity coefficients. The possible temperature dependencies for binary systems at constant pressure[19] are shown in Figure 5.67 in the form of the temperature-concentration-diagrams, the so-called binodal curves.

In most cases the mutual solubility rises with increasing temperature until the system becomes homogeneous above the upper critical solution temperature (UCST). This behavior is shown in Figure 5.67a. The other cases shown in Figure 5.67 occur more rarely than this behavior. In case (c) the mutual solubility increases with decreasing temperature until the two-phase region completely disappears below the lower critical solution temperature (LCST). Sometimes, even both critical solution temperatures occur (case (b)). Finally, there are systems with a miscibility gap over the entire temperature range. Cases (a), (c), and (d) can be regarded as special cases of (b), as in many cases the binodal line is interrupted by the melting curve, the boiling curve, or both. A very complex behavior is found for sulfur with aromatic compounds, for example, benzene–sulfur. For this system the LLE behavior disappears at the UCST. But at higher temperatures again a miscibility gap occurs.

For the ternary case, the most frequently observed curve shapes are shown in the form of triangular diagrams in Figure 5.68. Like in binary systems, the two-phase region is limited by the binodal curve. The two liquid phases in equilibrium are connected by so-called tie lines. From the tie line end points the distribution coefficient K_i between the two phases ' and '' can be calculated.

$$K_i = \frac{x_i''}{x_i'} \tag{5.75}$$

In so-called closed systems (case (a)), which are observed for about 75% of the systems, only one binary pair shows a miscibility gap. For these systems, a critical point C arises, where both liquid phases show the same concentration. Case (b) presents a system where two binary pairs show partial miscibility (open system). This behavior occurs in about 20% of all cases. Besides these most important cases, however, there are a large number of other possibilities [47]. For example, there are systems where all binary subsystems are homogeneous, but a miscibility gap (island) is found in the ternary system (see Figure 5.76). Additionally, there is the chance that three liquid phases are formed.

19) For not too large pressure differences, for example a few bar, the pressure influence can usually be neglected for condensed phases. But as shown in Sections 5.8.2 and 8.1.4, high pressures can have a significant influence on the LLE and SLE behavior.

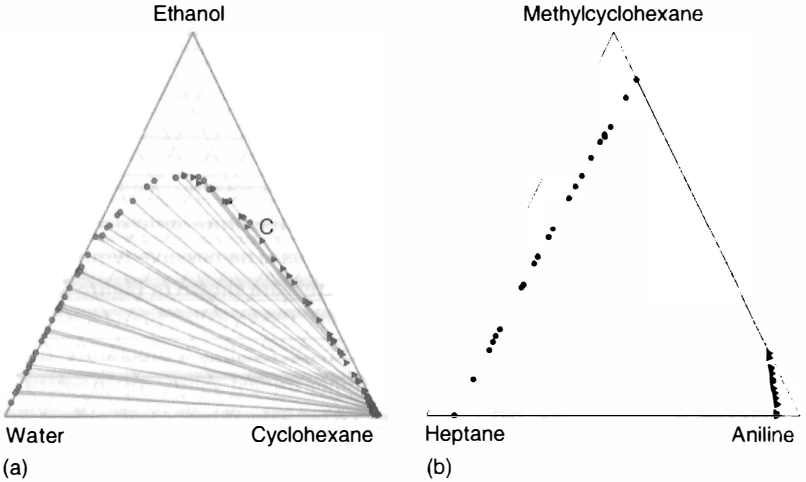

Figure 5.68 The most important types of ternary LLE [3] at a temperature of 25 C.

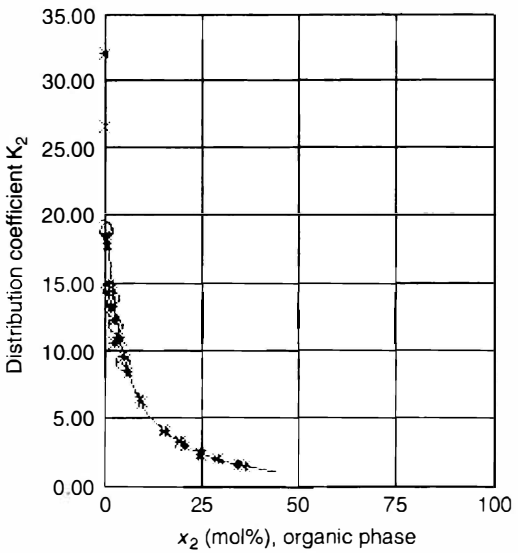

Figure 5.69 Experimental [3] and calculated partition coefficients of ethanol in the system water(1)–ethanol(2)–cyclohexane(3) at 298.15 K using UNIQUAC.

The distribution coefficients are not constant. They strongly depend on the concentration. For the system water–ethanol–cyclohexane the distribution coefficients for ethanol are shown in Figure 5.69. It can be seen that the largest distribution coefficients are obtained at infinite dilution. These values at infinite dilution are called *Nernst distribution coefficients.*

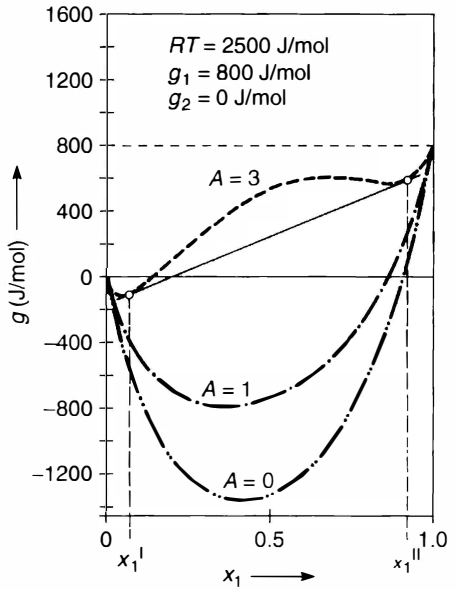

Figure 5.70 Concentration dependence of the molar Gibbs energy for systems with different strong real behavior A = coefficient of the Porter equation (Eq. (5.19)).

Equation (5.73) forms the basis for the calculation of LLE. As can be learned from this equation, the concentration and the temperature dependence of LLE is described via the activity coefficients. However, the occurrence of two liquid phases and critical solution temperatures cannot be understood alone by this equation (isoactivity criterion).

Looking at the concentration dependence of the Gibbs energy, it is easier to understand the formation of two liquid phases. For an ideal binary system, the molar Gibbs energy at a given composition (see Chapter 4) can be calculated by

$$g_{\text{ideal}} = x_1 g_1 + x_2 g_2 + RT(x_1 \ln x_1 + x_2 \ln x_2) \tag{5.76}$$

Since the mole fractions are always smaller than 1, the last term is negative and zero for $x_1 = 1$ and $x_2 = 1$. Therefore, the molar Gibbs energy as a function of composition shows a minimum (see Figure 5.70 with A = 0). However, in case of a real system the excess Gibbs energy has to be added:

$$g_{\text{real}} = g_{\text{ideal}} + g^{\text{E}} \tag{5.77}$$

$$g_{\text{real}} = g_{\text{ideal}} + RT(x_1 \ln \gamma_1 + x_2 \ln \gamma_2) \tag{5.78}$$

With increasing positive deviation from Raoult's law the positive contribution of the excess Gibbs energy is enlarged and, consequently, the molar Gibbs energy at the composition considered. This is shown in Figure 5.70. For example, it is assumed that the contribution of the excess Gibbs energy can be taken into account by Porter's approach ($g^{\text{E}}/RT = Ax_1x_2$). The resulting curve shape of the molar

Gibbs energy for different values of the parameter A is shown in Figure 5.70. With increasing g^E-values, this means increasing values of the parameter A, the molar Gibbs energy becomes larger. Because of the equilibrium criterion (minimum of Gibbs energy), in the case of strongly real behavior (i.e., in Figure 5.70 for $A = 3$) two liquid phases with the concentration x_1' and x_1'' are formed. At these concentrations the molar Gibbs energy of the two phases shows a lower value than a homogeneous mixture. For the Gibbs energy for a mole fraction of $x_1 = 0.5$, an approximate value of 540 J/mol is obtained for the homogeneous composition, while for the heterogeneous composition an approximate value of 250 J/mol results. In Figure 5.70 the values of the molar Gibbs energy for the composition of the coexisting liquid phases ' and '' are shown by the tangent and for the homogeneous composition by the dashed line.

According to this, the formation of two liquid phases can only occur if the curve shape of the Gibbs energy as a function of the composition shows an inflexion point, that is, there must be a region where the following condition is valid:

$$\left(\frac{\partial^2 g}{\partial x^2}\right)_{T,P} < 0 \tag{5.79}$$

The same criterion can be applied for the Gibbs energy of mixing:

$$\left(\frac{\partial^2 \Delta g}{\partial x^2}\right)_{T,P} < 0 \tag{5.80}$$

In turn, the different g^E-models can be used to describe the contribution of the excess Gibbs energy or activity coefficients. An exception is the Wilson model. No miscibility gap can be represented by this equation because the Wilson equation describes a monotone behavior of the composition for each parameter combination, that is, $(\partial^2 \Delta g/\partial x^2 > 0)$ (see Appendix C, E3).

It is more complicated to calculate LLE in multicomponent systems accurately than to describe vapor-liquid or solid-liquid equilibria. The reason is that in the case of LLE the activity coefficients have to describe not only the concentration dependence but also the temperature dependence correctly, whereas in the case of the other phase equilibria (VLE, SLE) the activity coefficients primarily have to describe the deviation from ideal behavior (Raoult's law resp. ideal solid solubility), and the temperature dependence is mainly described by the standard fugacities (vapor pressure resp. melting temperature and heat of fusion).

This is the main reason why up to now no reliable prediction of the LLE behavior is possible. Even the calculation of the LLE behavior of ternary systems using binary parameters can lead to poor results for the distribution coefficients and the binodal curve. Fortunately, it is quite easy to measure LLE data of ternary and higher systems up to atmospheric pressure.

Example 5.19

Calculate the miscibility gap for the system *n*-butanol (1)–water (2) at 50 °C and additionally the corresponding pressure and vapor phase composition using the

UNIQUAC equation with the help of the UNIQUAC parameters fitted to VLE data [6]:

$$\Delta u_{12} = 129.7 \text{ cal/mol}, \quad \Delta u_{21} = 489.6 \text{ cal/mol}$$

Pure component properties:

Component	r_i	q_i	P_i^s (kPa)
n-Butanol	3.4543	3.052	4.61
Water	0.92	1.4	12.36

Solution

For the calculation of the miscibility gap the procedure shown in Figure 5.73 can be applied. However, for a binary system the miscibility gap can also be determined graphically. For the graphical approach the activity coefficients are evaluated for different concentrations. For illustration, the activity coefficient γ_1 is calculated for a mole fraction $x_1 = 0.05$. Using the UNIQUAC equation, the values for τ_{12} and τ_{21} are determined (see Table 5.6):

$$\tau_{12} = \exp\frac{-\Delta u_{12}}{RT} = \exp\frac{-129.7}{1.98721 \cdot 323.15} = 0.8171 \qquad \tau_{21} = 0.4685$$

Furthermore for the calculation of the combinatorial part the values for V_1 and F_1 are required:

$$V_1 = \frac{r_1}{r_1 x_1 + r_2 x_2} = \frac{3.4543}{3.4543 \cdot 0.05 + 0.92 \cdot 0.95} = 3.3$$

$$F_1 = \frac{q_1}{q_1 x_1 + q_2 x_2} = \frac{3.052}{3.052 \cdot 0.05 + 1.4 \cdot 0.95} = 2.0585$$

Then the combinatorial part of the activity coefficient can be calculated

$$\ln \gamma_1^C = 1 - V_1 + \ln V_1 - 5q_1\left(1 - \frac{V_1}{F_1} + \ln \frac{V_1}{F_1}\right)$$

$$\ln \gamma_1^C = 1 - 3.3 + \ln (3.3) - 5 \cdot 3.052\left(1 - \frac{3.3}{2.0585} + \ln \frac{3.3}{2.0585}\right) = 0.8956$$

In the next step the contribution of the residual part is determined:

$$\ln \gamma_1^R = -q_1 \ln\frac{q_1 x_1 + q_2 x_2 \tau_{21}}{q_1 x_1 + q_2 x_2} + q_1 q_2 x_2\left[\frac{\tau_{21}}{q_1 x_1 + q_2 x_2 \tau_{21}} - \frac{\tau_{12}}{q_1 x_1 \tau_{12} + q_2 x_2}\right]$$

$$\ln \gamma_1^R = -3.052 \cdot \ln \frac{3.052 \cdot 0.05 + 1.4 \cdot 0.95 \cdot 0.4685}{3.052 \cdot 0.05 + 1.4 \cdot 0.95} + 3.052 \cdot 1.4 \cdot 0.95 \cdot \left[\frac{0.4685}{3.052 \cdot 0.05 + 1.4 \cdot 0.95 \cdot 0.4685} - \frac{0.8171}{3.052 \cdot 0.05 \cdot 0.8171 + 1.4 \cdot 0.95} \right]$$

$$\ln \gamma_1^R = -3.052 \ln \frac{0.7757}{1.4826} + 4.0592 \left(\frac{0.4685}{0.7757} - \frac{0.8171}{1.45469} \right)$$

$$= 1.977 + 0.1716 = 2.1486$$

$$\ln \gamma_1 = \ln \gamma_1^R + \ln \gamma_1^C = 2.1486 + 0.8956 = 3.0442$$

$$\gamma_1 = 20.99$$

In the same way, the activity coefficient of component 2 and the activities for component 1 and 2 can be calculated:

$x_1 = 0.05 \quad \gamma_1 = 20.99 \quad a_1 = 1.0495 \quad x_2 = 0.95 \quad \gamma_2 = 1.028 \quad a_2 = 0.9766$

For other mole fractions x_1 the following activities are calculated:

x_1	0.005	0.01	0.0015	0.02	0.05	0.1	0.2	0.4	0.6
a_1	0.2824	0.4972	0.6598	0.9801	1.0495	0.9605	0.7253	0.6141	0.6802
a_2	0.9953	0.9913	0.9878	0.9848	0.9762	0.9842	1.0332	1.0951	0.9766

In the case of a miscibility gap, an intersection is obtained when the activity of component 2 is plotted against the activity of component 1 for different mole fractions x_1 as in the example considered (see Figure 5.71). At the intersection the

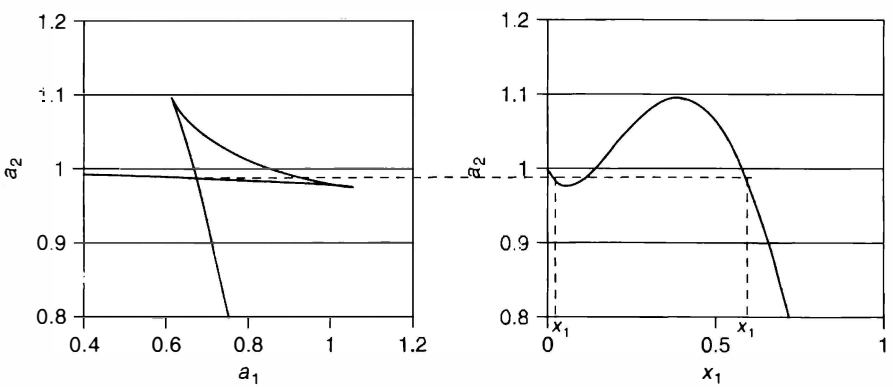

Figure 5.71 Graphical determination of LLE for binary systems exemplary shown for the system butanol (1)–water (2) at 50 °C.

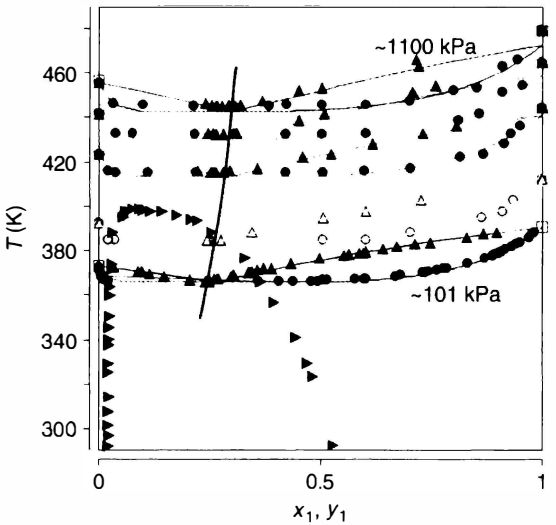

Figure 5.72 Experimental and calculated VLE and azeotropic data using the UNIQUAC parameters given in Example 5.19 together with experimental LLE data [3] — azeotropic composition.

equilibrium condition (Eq. (5.73)) is fulfilled. This means that the same activities are obtained for two different compositions. As can be seen, the intersection is obtained at approx. $x_1 = 0.015$ and $x_1 = 0.59$, when the activity of component 2 is plotted against the mole fraction x_1 (Figure 5.72).

For the system *n*-butanol (1)–water (2) at 50 °C the following values are obtained in equilibrium:

$x_1' = 0.01556$	$\gamma_1' = 43.40$	$a_1' = 0.6753$	$x_1'' = 0.5906$	$\gamma_1'' = 1.143$	$a_1'' = 0.6751$
$x_2' = 0.9844$	$\gamma_2' = 1.003$	$a_2' = 0.9873$	$x_2'' = 0.4094$	$\gamma_2'' = 2.412$	$a_2'' = 0.9875$

Using these values obtained for phase ' or phase " directly the corresponding pressure and mole fraction in the vapor phase can be calculated.

$$P = x_1\gamma_1 P_1^s + x_2\gamma_2 P_2^s$$

$$P = 0.01556 \cdot 43.4 \cdot 4.61 + 0.9844 \cdot 1.003 \cdot 12.36)$$

$$= 3.113 + 12.204 = 15.317\ \text{kPa}$$

$$y_1 = \frac{p_1}{P} = \frac{3.113}{15.317} = 0.2032$$

Because the activities in phase ' and " are identical, the same results are obtained starting from the composition in phase ", this means for $x_1 = 0.5906$.

For the entire composition range, the VLLE results are shown in Figure 5.72, together with the calculated and experimental data for a few isobaric VLE data, the calculated azeotropic composition as $f(T)$ and experimental LLE data.[20] It can be recognized that at atmospheric pressure the system *n*-butanol(1)–water(2) shows a heterogeneous azeotrope with a mole fraction of approximately $y_{1,az} = 0.25$ and a temperature of 366 K. At other pressures, the azeotropic composition will change. The change of the azeotropic composition depends not only on the temperature dependence of the vapor pressures, but also on the temperature dependence of the activity coefficients. In Figure 5.72 the typical temperature dependence is shown in the form of isobaric *Txy*-diagrams. While at atmospheric pressure a heterogeneous azeotropic point occurs, homogeneous azeotropic behavior is observed at higher pressures (temperatures). The temperature dependence of the azeotropic behavior is discussed in detail in Section 5.6.

While the calculation of binary LLE can be performed graphically, the calculation of LLE for ternary and higher systems has to be performed iteratively. One possible procedure for a multicomponent system is shown in Figure 5.73 in the form of a flow diagram. The method takes into account the isoactivity conditions (Eq. (5.73)) and the material balance.

Starting from the mole numbers n_i (initial feed stream to the equilibrium stage) with a composition in the two phase region, mole numbers n_i' (composition) are estimated for the liquid phase. From the difference $n_i - n_i'$, the mole numbers n_i'' (composition) in the second liquid phase can be calculated. Then the activity coefficients of the components in the two liquid phases are determined. In the next step it is checked if the isoactivity condition is fulfilled. Of course, after the first step the isoactivity condition will not be fulfilled. Therefore, the estimated mole numbers n_i' have to be changed in the right way. Using the *K*-factor method, the following equation is obtained for the variation of the mole numbers starting from Eq. (5.73) and the material balance:

$$x_i' \gamma_i' = x_i'' \gamma_i'' \qquad \text{resp.} \qquad \frac{n_i'}{n_T'} \gamma_i' = \frac{n_i''}{n_T''} \gamma_i''$$

with

$$n_T' = \Sigma n_i' \quad \text{and} \quad n_T'' = \Sigma n_i''$$

one obtains

$$n_i'' = n_i' \frac{n_T'' \gamma_i'}{n_T' \gamma_i''}$$

Taking into account the material balance $n_i'' = n_i - n_i'$

$$n_i - n_i' = n_i' \frac{n_T'' \gamma_i'}{n_T' \gamma_i''} \rightarrow n_i = n_i' + n_i' \frac{n_T'' \gamma_i'}{n_T' \gamma_i''} = n_i' \cdot \left[1 + \frac{n_T'' \gamma_i'}{n_T' \gamma_i''} \right]$$

new mole numbers in phase ' can be calculated using the following relation:

20) A comparison of the calculated LLE in Example 5.19 at 50 °C with the experimental findings shows a disagreement. While 59 mol% butanol were determined for the butanol rich phase, experimentally less than 50 mol% was found. The reason is that parameters fitted to VLE data do not describe the LLE behavior correctly.

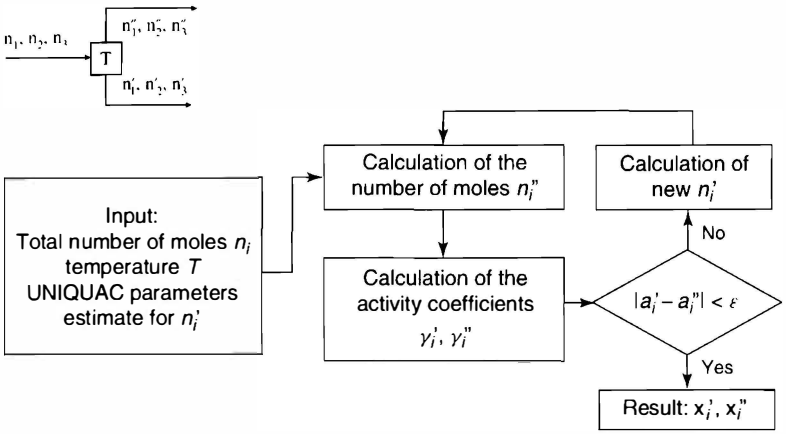

Figure 5.73 Flow diagram for the calculation of LLE using the *K*-factor method.

$$n'_{i,\text{new}} = \frac{n_i}{1 + \gamma_i' n_T''/\gamma_i'' n_T'}$$

The iteration is stopped when the activities in the different phases are identical within a small value ε. If the feed composition is outside the two-phase region, the solution will lead to the trivial solution, where the composition of the two liquid phases is identical.

Example 5.20

Calculate the LLE composition for the system water (1)–ethanol (2)–benzene (3) for the following feed stream: $n_1 = 1$ mol, $n_2 = 0.3$ mol, and $n_3 = 1$ mol at 25 °C with the help of the UNIQUAC model.

UNIQUAC parameters $\Delta u_{ij}(K)$ fitted to LLE data at 25 °C:

Compound	1	2	3
1	0	526.02	309.64
2	−318.06	0	−91.532
3	1325.1	302.57	0

Relative van der Waals properties:

Compound	r_i	q_i
Water	0.9200	1.400
Ethanol	2.1055	1.972
Benzene	3.1878	2.400

Solution

To start the calculation, first the mole numbers in phase ' have to be estimated. Let us assume that $n_1' = 0.8$ mol, $n_2' = 0.1$ mol, and $n_3' = 0.2$ mol are in phase ', for the given feed $n_1'' = 0.2$ mol, $n_2'' = 0.2$ mol, and $n_3'' = 0.8$ mol remain for phase ''. Then for these phases in the next step the activity coefficients can be calculated with the help of the UNIQUAC equation.

UNIQUAC parameters τ_{ij}

Compound	1	2	3
1	1	0.1713	0.35397
2	2.9060	1	1.3593
3	0.01174	0.36247	1

The following composition is obtained for phase ' : $x_1' = 0.8/1.1 = 0.7273$, $x_2' = 0.0909$, $x_3' = 0.1818$.

For this composition the activity coefficients have to be calculated. That is exemplarily shown for component 1:

$$V_1 = \frac{r_1}{r_1x_1 + r_2x_2 + r_3x_3}$$

$$= \frac{0.92}{0.92 \cdot 0.7273 + 2.1055 \cdot 0.0909 + 3.1878 \cdot 0.1818} = 0.6389$$

$$F_1 = \frac{q_1}{q_1x_1 + q_2x_2 + q_3x_3} = \frac{1.4}{1.4 \cdot 0.7273 + 1.972 \cdot 0.0909 + 2.4 \cdot 0.1818}$$

$$= 0.8569$$

$$\ln \gamma_1^C = 1 - V_1 + \ln V_1 - 5q_1\left(1 - \frac{V_1}{F_1} + \ln \frac{V_1}{F_1}\right)$$

$$\ln \gamma_1^C = 1 - 0.6389 + \ln (0.6389) - 5 \cdot 1.4\left(1 - \frac{0.6389}{0.8569} + \ln \frac{0.6389}{0.8569}\right)$$

$$= 0.1873$$

$$\ln \gamma_1^R = q_1\left(1 - \ln \frac{q_1x_1 + q_2x_2\tau_{21} + q_3x_3\tau_{31}}{q_1x_1 + q_2x_2 + q_3x_3} - \frac{q_1x_1}{q_1x_1 + q_2x_2\tau_{21} + q_3x_3\tau_{31}}\right.$$

$$\left. - \frac{q_2x_2\tau_{12}}{q_1x_1\tau_{12} + q_2x_3\tau_{32}} - \frac{q_3x_3\tau_{13}}{q_1x_1\tau_{13} + q_2x_2\tau_{23} + q_3x_3}\right)$$

$$\ln \gamma_1^R = 1.4 \cdot \left(1 - \ln \frac{1.4 \cdot 0.7273 + 1.972 \cdot 0.0909 \cdot 2.906 + 2.4 \cdot 0.1818 \cdot 0.01174}{1.4 \cdot 0.7273 + 1.972 \cdot 0.0909 + 2.4 \cdot 0.1818}\right.$$

$$- \frac{1.4 \cdot 0.7273}{1.4 \cdot 0.7273 + 1.972 \cdot 0.0909 \cdot 2.906 + 2.4 \cdot 0.1818 \cdot 0.01174}$$

$$- \frac{1.972 \cdot 0.0909 \cdot 0.1713}{1.4 \cdot 0.7273 \cdot 0.1713 + 1.972 \cdot 0.0909 + 2.4 \cdot 0.1818 \cdot 0.36247}$$

$$\left. - \frac{2.4 \cdot 0.1818 \cdot 0.35397}{1.4 \cdot 0.7273 \cdot 0.35397 + 1.972 \cdot 0.0909 \cdot 1.3593 + 2.4 \cdot 0.1818}\right)$$

$$= 0.2640$$

$$\ln \gamma_1 = \ln \gamma_1^C + \ln \gamma_1^R = 0.1873 + 0.2640 = 0.4513$$

$$\gamma_1 = 1.570$$

The activity coefficients for all components in both phases are given in the following table:

Phase '			Phase "		
n_i	x_i	γ_i	n_i	x_i	γ_i
0.8	0.7273	1.570	0.2	0.1667	8.856
0.1	0.0909	0.2948	0.2	0.1667	0.860
0.2	0.1818	18.11	0.8	0.6667	1.425

Using these data improved mole numbers are calculated for phase ' with the help of the *K*-factor method. Then the mole numbers in phase ", the compositions and the activity coefficients are calculated again. For n_1' one obtains

$$n_1' = \frac{1}{1 + \frac{1.57 \cdot 1.2}{8.856 \cdot 1.1}} = 0.8379$$

and for all other values:

Phase '			Phase "		
n_i	x_i	γ_i	n_i	x_i	γ_i
0.8379	0.7458	1.181	0.1621	0.1378	20.99
0.2183	0.1943	0.7311	0.0817	0.0694	0.5809
0.0673	0.0600	36.77	0.9327	0.7928	1.258

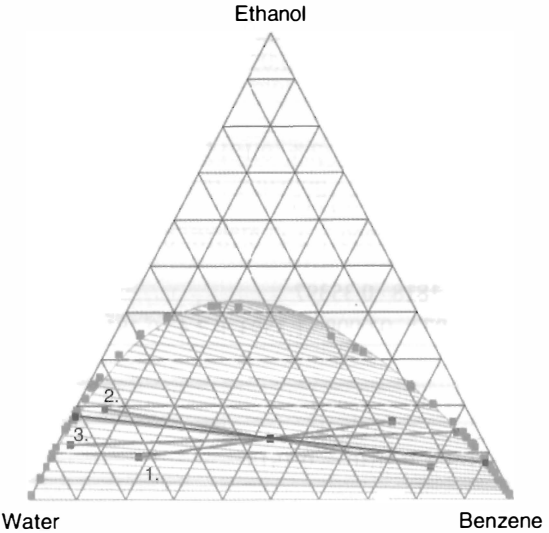

Figure 5.74 The first three steps of the *K*-factor method together with the experimental and calculated LLE behavior of the ternary system water–ethanol–benzene at 25 °C using UNIQUAC.

After a few steps, convergence – this means LLE – is obtained, since the changes of the calculated mole numbers are below a small value ε. The final values are:

Phase '			**Phase "**		
n_i	x_i	γ_i	n_i	x_i	γ_i
0.9799	0.8112	1.053	0.0201	0.0184	46.35
0.2153	0.1782	1.006	0.0847	0.0776	2.310
0.0128	0.0106	88.49	0.9872	0.9040	1.039

The results of the first three steps and the final LLE results for the system water–ethanol–benzene at 25 °C are shown in Figure 5.74. It can be seen that after three steps the equilibrium composition is nearly reached, also for poor initial estimates.

5.8.1 Temperature Dependence of Ternary LLE

The temperature dependence of LLE of ternary systems can be very different, as shown for binary systems in Figure 5.67. In most cases, the miscibility gap

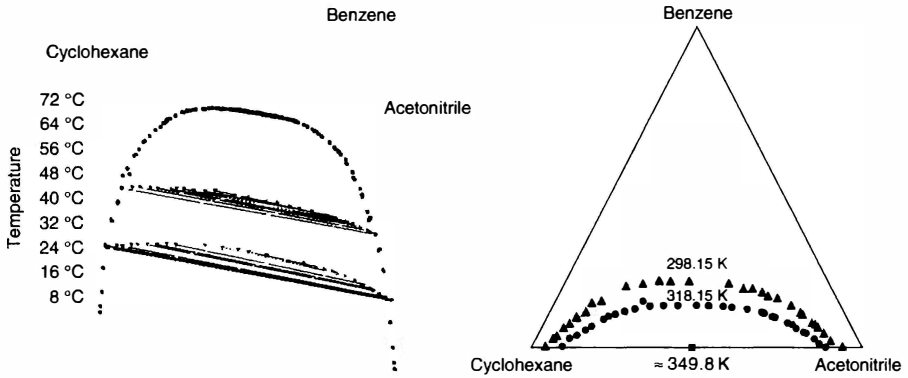

Figure 5.75 Qualitative progress of the temperature dependence of ternary liquid–liquid equilibria.

becomes smaller with increasing temperature. For a closed system this behavior is shown in Figure 5.75. In the case presented, the mutual solubility increases with increasing temperature, this means, the range of concentration where two liquid phases coexist decreases more and more until the heterogeneous region disappears above the UCST of the binary system AB.

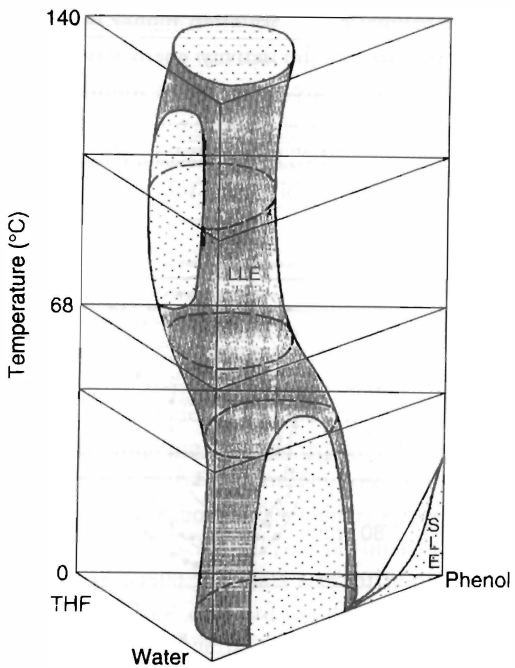

Figure 5.76 LLE behavior of the ternary system tetrahydrofuran–water–phenol as a function of temperature.

But as mentioned above, the temperature dependence can be much more complex. For the system tetrahydrofuran–water–phenol this is shown in Figure 5.76. At temperatures below 66 °C, only the system phenol–water shows a miscibility gap, whereas the other two binaries are homogeneous in this temperature range. The binary miscibility gap extends into the ternary area. Above the UCST of the system phenol–water, the formation of an island curve is observed, where all binary systems are homogeneous while the ternary system is heterogeneous. At approx. 72 °C, the LCST of the system tetrahydrofuran–water is reached. The binary system shows a miscibility gap up to a temperature of about 137 °C. Above the UCST of the system tetrahydrofuran–water again an island curve is formed in the ternary system. Up to now this complex LLE behavior can not be described with the help of a g^E-model, even with linear or quadratic temperature-dependent model parameters. Since phenol has a melting point at approx. 41 °C, in Figure 5.76 additionally the SLE behavior for the system phenol–water is shown.

5.8.2
Pressure Dependence of LLE

Although it was mentioned at the beginning of Section 5.8 that pressure differences of a few bar only have a negligible influence on the LLE behavior, in practice often higher pressures are realized. Already a slight volume compression of a liquid can lead to very high pressures. In centrifugal extractors often higher pressures are observed. The influence of the pressure on the activity coefficients (LLE) can be taken into account if the excess volumes are known. The influence can directly be calculated using Eq. (5.27). The activity coefficients will decrease with increasing pressure in the case of negative partial molar excess volumes, as shown in Example 5.7. This means that the miscibility gap becomes smaller with

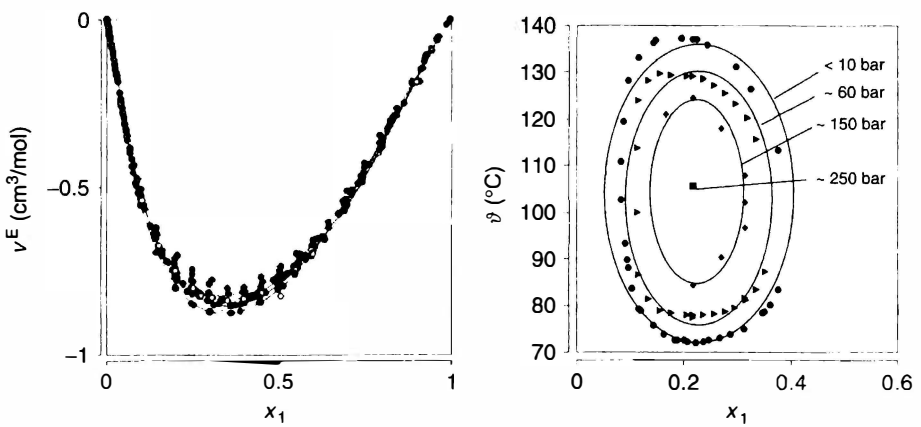

Figure 5.77 Excess volumes and LLE behavior of the system tetrahydrofuran (1)–water (2) [3] as a function of pressure.

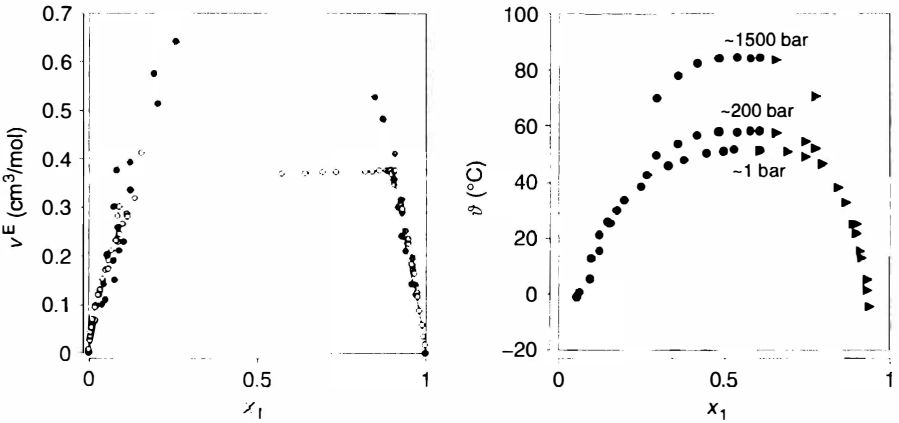

Figure 5.78 Excess volumes and LLE behavior of the system methanol (1)–*n*-heptane (2) [3] as a function of pressure.

increasing pressure. The opposite is true in the case of positive partial molar excess volumes. The influence of the sign of the excess volumes on the LLE behavior is exemplarily shown in Figures 5.77 and 5.78 for the systems tetrahydrofuran–water and methanol–heptane.

For the system tetrahydrofuran–water, negative excess volumes are observed. This results in the fact that the system becomes homogeneous at pressures around 250 bar.

In contrast, the miscibility gap becomes larger with increasing pressure for the system methanol–heptane (see Figure 5.78) because of the positive partial molar excess volumes for this system.

5.9 Predictive Models

Both approaches (g^E-models ($\gamma-\varphi$ approach), equations of state ($\varphi-\varphi$ approach)) allow the calculation of multicomponent systems using binary information alone. However, often the required experimental binary data are missing.

Assuming that 1000 compounds are of technical interest, phase equilibrium information for about 500000 binary systems are required to fit the required binary parameters to describe all possible binary and multicomponent systems. Although more than 64500 VLE data sets for nonelectrolyte systems have been published up to now, VLE data are available for only 10300 binary systems, since for a few systems a large number of data sets were published, for example, for the systems ethanol–water, ammonia–water, water–carbon dioxide, methanol–water, methane–nitrogen more than 150 data sets are available. This means that only for ~2% of the required systems at least one VLE data set is available. If only

consistent VLE data are accepted or if more than one VLE data set is desired, the percentage even decreases to ~1.2%. If also information about the dilute range and the temperature dependence in the form of γ^{∞} and h^E should be used to fit the required model parameters, the percentage of the available systems is less than 0.2%, although approximately 62500 γ^{∞}-values and 21000 h^E-data sets have been published, which are stored in the Dortmund Data Bank [3].

Since the assumption of ideal behavior can lead to very erroneous results and measurements are very time consuming, reliable predictive models with a large range of applicability would be desirable.

Because of the importance of distillation processes, first it was the objective to develop models only for the prediction of VLE. The first predictive model with a wide range of applicability was developed by Hildebrand and Scatchard [48]. The so-called regular solution theory is based on considerations of van Laar, who was a student of van der Waals and used the van der Waals equation of state to derive an expression for the excess Gibbs energy [49]. Since the two parameters a and b of the van der Waals equation of state can be obtained from critical data, it should be possible to calculate the required activity coefficients using critical data. However, the results were strongly dependent on the mixing rules applied.

5.9.1
Regular Solution Theory

Hildebrand and Scatchard [48] showed that better results are obtained, if instead of the van der Waals constants a and b molar volumes v_i and so-called solubility parameters δ_i are used instead. For binary systems the following relations are obtained for the activity coefficients:

$$\ln \gamma_1 = \frac{v_1 \Phi_2^2 (\delta_1 - \delta_2)^2}{RT}$$
$$\ln \gamma_2 = \frac{v_2 \Phi_1^2 (\delta_1 - \delta_2)^2}{RT} \tag{5.81}$$

Φ_i volume fraction of component $i = (x_i v_i)/\Sigma x_j v_j$
δ_i solubility parameter of component i.

The solubility parameter δ_i can be calculated using values for the enthalpy of vaporization and the molar volume v_i at 298.15 K:

$$\delta_i = \left(\frac{\Delta h_{vi} - RT}{v_i} \right)^{0.5} \tag{5.82}$$

Δh_{vi} molar heat of vaporization of component i (cal/mol).

For regular solutions the solubility parameters δ_i and molar volumes v_i can be assumed to be constant for a larger temperature range. For a few compounds the parameters are given in Table 5.16.

Table 5.16 Molar volumes and solubility parameters for selected compounds.

Compound	v_i (cm³/mol)	δ_i (cal/cm³)$^{0.5}$
Carbon tetrachloride	97	8.6
Carbon disulfide	61	10.0
n-Pentane	116	7.1
Benzene	89	9.2
Cyclohexane	109	8.2
Hexene-1	126	7.3
n-Hexane	132	7.3
Toluene	107	8.9
n-Heptane	148	7.4
n-Octane	164	7.5

The regular solution theory is not limited to binary systems. It can directly be applied for the calculation of activity coefficients in multicomponent systems:

$$\ln \gamma_i = \frac{v_i}{RT} (\delta_i - \bar{\delta})^2 \tag{5.83}$$

where the mean solubility parameter:

$$\bar{\delta} = \sum_i \Phi_i \delta_i = \frac{\sum_i x_i v_i \delta_i}{\sum_i x_i v_i} \tag{5.84}$$

can be obtained by summation over all compounds.

However, the regular solution theory can only be applied for nonpolar systems and systems with positive deviations from Raoult's law.

Example 5.21

Estimate the activity coefficients at infinite dilution for the system benzene (1)–cyclohexane (2) at 353.15 K.

Solution

With the values given in Table 5.16 the values at infinite dilution ($\Phi_2 = 1, \Phi_1 = 1$) can directly be estimated:

$$\ln\gamma_1^\infty = \frac{89\,(9.2 - 8.2)^2}{1.98721 \cdot 353.15} = 0.1268 \qquad \ln\gamma_2^\infty = \frac{109\,(9.2 - 8.2)^2}{1.98721 \cdot 353.15} = 0.1553$$
$$\gamma_1^\infty = 1.135 \qquad \gamma_2^\infty = 1.168$$

Experimentally, higher values were measured ($\gamma_1^\infty \approx 1.35, \gamma_2^\infty \approx 1.44$) [3].

5.9.2
Group Contribution Methods

Group contribution methods do not show these weaknesses discussed for the regular solution theory.

In group contribution methods it is assumed that the mixture does not consist of molecules but of functional groups. In Figure 5.79 this is shown for the systems ethanol–*n*-hexane. Ethanol can be subdivided in a methyl-, methylene- and alcohol-group and *n*-hexane in two methyl- and four methylene-groups. It can be shown that the required activity coefficients can be calculated if only the interaction parameters between the functional groups are known. For example, if the group interaction parameters between the alkane and the alcohol group are known, not only the activity coefficients (VLE behavior) of the system ethanol–*n*-hexane, but also for all other alkane–alcohol or alcohol–alcohol systems can be predicted. The great advantage of group contribution methods is that the number of functional groups is much smaller than the number of possible molecules.

The required equation of the solution of groups concept can be derived from the excess Gibbs energy of the groups in the mixture and the excess Gibbs energy in the pure compound.

For the pure compound i built up by functional groups one can derive the following expression for the molar (g^E) and total Gibbs energy (G^E):

$$\frac{g^{E(i)}}{RT} = \sum_k X_k^{(i)} \ln \Gamma_k^{(i)}$$

$$\frac{G^{E(i)}}{RT} = n^{(i)} \sum_k \nu_k^{(i)} \ln \Gamma_k^{(i)} \qquad \sum_i \frac{G^{E(i)}}{RT} = \sum_i \sum_k n^{(i)} \nu_k^{(i)} \ln \Gamma_k^{(i)}$$

For a mixture built up by functional groups one can write

$$\frac{g^{E(m)}}{RT} = \sum_k X_k \ln \Gamma_k$$

$$\frac{G^{E(m)}}{RT} = \sum_i \left(n^{(i)} \nu^i\right) \sum_k X_k \ln \Gamma_k \qquad \frac{G^{E(m)}}{RT} = \sum_i \sum_k n^{(i)} \nu_k^i \ln \Gamma_k$$

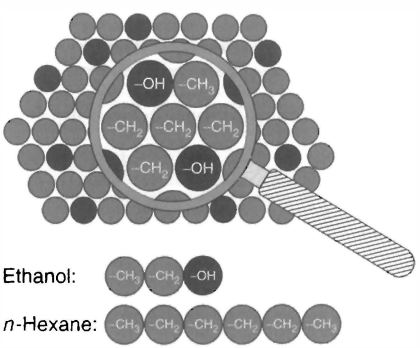

Figure 5.79 Group contribution concept.

From the difference of the excess Gibbs energies for the groups in the mixture and in the pure compound (standard state) one can derive an expression for the required activity coefficient γ_i:

$$\frac{G^E}{RT} = \sum_i n^{(i)} \ln \gamma_i = \frac{G^{E(m)}}{RT} - \sum_i \frac{G^{E(i)}}{RT}$$

$$= \sum_i \sum_k n^{(i)} \nu_k^{(i)} \ln \Gamma_k - \sum_i \sum_k n^{(i)} \nu_k^{(i)} \ln \Gamma_k^{(i)}$$

$$= \sum_i n^{(i)} \left[\sum_k \nu_k^{(i)} \left(\ln \Gamma_k - \ln \Gamma_k^{(i)} \right) \right]$$

which leads to the equation for the solution of groups concept:

$$\ln \gamma_i = \sum_k \nu_k^{(i)} \left(\ln \Gamma_k - \ln \Gamma_k^{(i)} \right)$$

with

$\Gamma_k^{(i)}$	group activity coefficient of group k in pure component i
Γ_k	group activity coefficient of group k in the mixture
$\nu_k^{(i)}$	number of groups k in component i
$\nu^{(i)}$	number of groups in component i

$$\nu^{(i)} = \sum_i \nu_k^{(i)} = \nu_1^{(i)} + \nu_2^{(i)} + \ldots + \nu_m^{(i)}$$

$n^{(i)}$	number of moles of component i
$n_T = \sum_i n^{(i)}$	total number of moles in the mixture
$n^{(i)} \nu^{(i)}$	total number of moles of groups of component i
$\sum_i n^{(i)} \nu^{(i)}$	total number of moles of groups in the mixture
$X_k^{(i)} = \frac{\nu_k^{(i)}}{\nu^{(i)}}$	group mole fraction of group k in compound i
$X_k = \frac{\sum_i n^{(i)} \nu_k^{(i)}}{\sum_i n^{(i)} \nu^{(i)}}$	group mole fraction of group k in the mixture

5.9.3 UNIFAC Method

The first group contribution method for the prediction of VLE (activity coefficients) was the so-called analytical solution of groups (ASOG) method [50, 51], developed within Shell. The ASOG method uses the Wilson model to describe the concentration dependence of the group activity coefficients required in the solution of groups concept.

In 1975, the UNIFAC group contribution method was published by Fredenslund *et al.* [27, 52, 53]. Like the ASOG method, the UNIFAC method is based on the

solution of groups concept. But in the UNIFAC method, the activity coefficients are calculated from a combinatorial and a residual part exactly like in the UNIQUAC model (see Eq. (5.85)). While the temperature-independent combinatorial part takes into account the size and form of the molecules, that is, the entropic contribution, the residual part considers the enthalpic interactions:

$$\ln \gamma_i = \ln \gamma_i^C + \ln \gamma_i^R \tag{5.85}$$

The combinatorial part $\ln \gamma_i^C$ can be calculated using the following equation, which is identical to the UNIQUAC model:

$$\ln \gamma_i^C = 1 - V_i + \ln V_i - 5q_i \left(1 - \frac{V_i}{F_i} + \ln \frac{V_i}{F_i}\right) \tag{5.86}$$

where V_i (volume/mole fraction ratio) and F_i (surface area/mole fraction ratio) can be calculated for a given composition using the relative van der Waals volumes r_i and van der Waals surface areas q_i of the molecules:

$$V_i = \frac{r_i}{\sum_j r_j x_j} \tag{5.87}$$

$$F_i = \frac{q_i}{\sum_j q_j x_j} \tag{5.88}$$

For the UNIFAC group contribution method the relative van der Waals properties r_i and q_i can be obtained using the relative van der Waals group volumes R_k and relative van der Waals group surface areas Q_k, which can be derived from x-ray data. Tabulated values for R_k and Q_k can be found by Hansen *et al.* [53]. They can also be derived from the tabulated van der Waals properties published by Bondi [54]. For selected groups the R_k and Q_k values are given in the Appendix H:

$$r_i = \sum_k \nu_k^{(i)} R_k \tag{5.89}$$

$$q_i = \sum_k \nu_k^{(i)} Q_k \tag{5.90}$$

where $\nu_k^{(i)}$ is the number of functional groups of type k in compound i.

The temperature-dependent residual part $\ln \gamma_i^R$ takes into account the interactions between the different compounds. In group contribution methods, this part is calculated via the solution of groups concept using group activity coefficients Γ_k and $\Gamma_k^{(i)}$:

$$\ln \gamma_i^R = \sum_k \nu_k^{(i)} \left(\ln \Gamma_k - \ln \Gamma_k^{(i)}\right) \tag{5.91}$$

Γ_k and $\Gamma_k^{(i)}$ are the group activity coefficients for group k in the mixture, respectively, for the pure compound i. For the description of the concentration dependence of the group activity coefficients the UNIQUAC equation is used:

$$\ln \Gamma_k = Q_k \left[1 - \ln\left(\sum_m \Theta_m \Psi_{mk}\right) - \sum_m \frac{\Theta_m \Psi_{km}}{\sum_n \Theta_n \Psi_{nm}}\right] \tag{5.92}$$

The surface area fractions Θ_m and the group mole fractions X_m of group m can be calculated using the following relations:

$$\Theta_m = \frac{Q_m X_m}{\sum_n Q_n X_n} \tag{5.93}$$

$$X_m = \frac{\sum_j \nu_m^{(j)} x_j}{\sum_j \sum_n \nu_n^{(j)} x_j} \tag{5.94}$$

The parameter Ψ_{nm} contains the group interaction parameter a_{nm} between the functional groups n and m, for example, between alkanes and ketones:

$$\Psi_{nm} = \exp\left(-\frac{a_{nm}}{T}\right) \tag{5.95}$$

These functional groups are called *main groups*. They often consist of more than one subgroup. For example, in the case of alkanes one has to distinguish between CH_3-, CH_2-, CH–, and C-groups. The different alkane subgroups all have different values for the van der Waals properties. The same is true for the ketone group, where one has to distinguish between the CH_3CO-, CH_2CO-, and CHCO–group. In the UNIFAC method, for every main group combination two temperature-independent group interaction parameters (a_{nm}, a_{mn}) are required, which were fitted almost exclusively to consistent experimental vapor–liquid equilibrium data stored in the Dortmund Data Bank [3]. Since the interactions are defined per area, depending on the subgroup different strong interactions are calculated for e.g. CH_3-CH_2CO and CH_2-CH_2CO pairs. By definition, the group interaction parameters between identical main groups (a_{nn}, a_{mm}) are equal to 0. This means that the parameters $\Psi_{nn}$and Ψ_{mm}become unity. The van der Waals properties and the published group interaction parameters can be found in the internet (see Appendix H).

Example 5.22

Calculate the VLE of the system *n*-hexane (1)–2-butanone (2) at 60 °C for a mole fraction of $x_1 = 0.5$ with the help of the UNIFAC method assuming ideal behavior of the vapor phase.

Vapor pressures and structural information:

Component	P_i^s at 60 °C (kPa)	CH_3	CH_2	CH_3CO
n-Hexane	75.85	2	4	–
2-Butanone	51.90	1	1	1

van der Waals properties:

Group	R_k	Q_k
CH_3	0.9011	0.848
CH_2	0.6744	0.540
CH_3CO	1.6724	1.488

Group interaction parameters a_{nm} between the main group alkanes (CH_2) and ketones (CH_2CO):

a_{nm}(K)	CH_2	CH_2CO
CH_2	0.0	476.4
CH_2CO	26.76	0.0

Solution

First of all the van der Waals properties of the two compounds can be calculated with the help of the van der Waals properties of the groups:

$$r_1 = 2 \cdot 0.9011 + 4 \cdot 0.6744 = 4.4998$$
$$q_1 = 2 \cdot 0.848 + 4 \cdot 0.54 = 3.856$$
$$r_2 = 1 \cdot 0.9011 + 1 \cdot 0.6744 + 1 \cdot 1.6724 = 3.2479$$
$$q_2 = 1 \cdot 0.848 + 1 \cdot 0.54 + 1 \cdot 1.488 = 2.876$$

Using these van der Waals properties for $x_1 = 0.5$ the following values are obtained for V_i and F_i:

$$V_1 = \frac{4.4998}{0.5\,(4.4998 + 3.2479)} = 1.1616$$
$$V_2 = \frac{3.2479}{0.5\,(4.4998 + 3.2479)} = 0.8384$$
$$F_1 = \frac{3.856}{0.5\,(3.856 + 2.876)} = 1.1456$$
$$F_2 = \frac{2.876}{0.5\,(3.856 + 2.876)} = 0.8544$$

With the help of these values the combinatorial part can be calculated. For *n*-hexane (1)

$$\ln \gamma_1^C = 1 - 1.1616 + \ln 1.1616 - 5 \cdot 3.856 \left(1 - \frac{1.1616}{1.1456} + \ln \frac{1.1616}{1.1456}\right)$$
$$= -0.00994$$

For 2-butanone (2) the following value is obtained:

$$\ln \gamma_2^C = -0.001210$$

For the calculation of the group activity coefficients in the mixture first of all the parameters Ψ_{nm}, the group mole fractions and surface area fractions have to be determined. For the parameters Ψ_{nm} the following values are obtained:

$$\Psi_{CH_3,CH_3CO} = \Psi_{CH_2,CH_3CO} = \exp\frac{-476.4}{333.15} = 0.2393$$
$$\Psi_{CH_3CO,CH_3} = \Psi_{CH_3CO,CH_2} = \exp\frac{-26.76}{333.15} = 0.9228$$
$$\Psi_{CH_3,CH_3} = \Psi_{CH_2,CH_2} = \Psi_{CH_3CO,CH_3CO} = \Psi_{CH_2,CH_3} = \Psi_{CH_3,CH_2} = 1$$

The following group mole fractions and surface area fractions are obtained for the considered binary system at $x_1 = 0.5$:

$$X_{CH_3} = \frac{(2+1)\,0.5}{(6+3)\,0.5} = 0.3333$$
$$X_{CH_2} = \frac{(4+1)\,0.5}{(6+3)\,0.5} = 0.5556$$
$$X_{CH_3CO} = \frac{0.5}{(6+3)\,0.5} = 0.1111$$

$$\Theta_{CH_3} = \frac{0.848 \cdot 0.3333}{0.848 \cdot 0.3333 + 0.54 \cdot 0.5556 + 1.488 \cdot 0.1111} = 0.3779$$
$$\Theta_{CH_2} = 0.4011$$
$$\Theta_{CH_3CO} = 0.2210$$

Now all values are available to calculate the group activity coefficients in the binary system:

$$\ln \Gamma_{CH_3} = 0.848\left[1 - \ln(0.3779 + 0.4011 + 0.221 \cdot 0.9228) - \frac{0.3779 + 0.4011}{0.3779 + 0.4011 + 0.221 \cdot 0.9228} - \frac{0.221 \cdot 0.2393}{(0.3779 + 0.4011)\,0.2393 + 0.221}\right]$$
$$\ln \Gamma_{CH_3} = 0.080458$$
$$\ln \Gamma_{CH_2} = 0.051235$$
$$\ln \Gamma_{CH_3CO} = 0.92872$$

For the pure compounds the following group mole fractions and surface area fractions are obtained:

For *n*-hexane (1):

$$X^{(1)}_{CH_3} = 0.3333 \qquad X^{(1)}_{CH_2} = 0.6667$$

$$\Theta_{CH_3} = \frac{0.848 \cdot 0.3333}{0.848 \cdot 0.3333 + 0.54 \cdot 0.6667} = 0.4398$$
$$\Theta_{CH_2} = 0.5602$$

For 2-butanone (2):

$$X^{(1)}_{CH_3} = 0.3333 \quad X^{(1)}_{CH_2} = 0.3333 \quad X^{(1)}_{CH_3CO} = 0.3333$$

$$\Theta_{CH_3} = \frac{0.848 \cdot 0.3333}{0.848 \cdot 0.3333 + 0.54 \cdot 0.3333 + 1.488 \cdot 0.3333} = 0.2949$$

$$\Theta_{CH_2} = 0.1878$$

$$\Theta_{CH_3CO} = 0.5173$$

With these values the group activity coefficients in the pure compounds can be calculated. For pure *n*-hexane (1) one obtains

$$\ln \Gamma^{(1)}_{CH_3} = 0.0 \qquad \ln \Gamma^{(1)}_{CH_2} = 0.0$$

and for 2-butanone (2)

$$\ln \Gamma^{(2)}_{CH_3} = 0.848 \left[1 - \ln (0.2949 + 0.1878 + 0.5173 \cdot 0.9228) - \frac{0.2949 + 0.1878}{0.2949 + 0.1878 + 0.5173 \cdot 0.9228} - \frac{0.5173 \cdot 0.2393}{(0.2949 + 0.1878)\,0.2393 + 0.5173} \right]$$

$$\ln \Gamma^{(2)}_{CH_3} = 0.29038$$

$$\ln \Gamma^{(2)}_{CH_2} = 0.18491$$

$$\ln \Gamma^{(2)}_{CH_3CO} = 0.262$$

Herewith all values are available to calculate the residual part of the activity coefficients following the solution of groups concept and finally to calculate the required activity coefficients:

$$\ln \gamma_1^R = 2\,(0.80458 - 0) + 4\,(0.051235 - 0) = 0.365856$$

$$\ln \gamma_1 = \ln \gamma_1^R + \ln \gamma_1^C = 0.365856 - 0.00994 = 0.35592$$

$$\gamma_1 = 1.4275$$

$$\ln \gamma_2^R = (0.080458 - 0.29038) + (0.051235 - 0.18491) + (0.92872 - 0.262) = 0.32312$$

$$\ln \gamma_2 = \ln \gamma_2^R + \ln \gamma_2^C = 0.32312 - 0.01210 = 0.31102$$

$$\gamma_2 = 1.3648$$

Assuming ideal vapor phase behavior the knowledge of the activity coefficients allows calculating the partial pressures, total pressure, and the vapor phase mole fraction:

$$P = p_1 + p_2 = 0.5 \cdot 1.4275 \cdot 75.85 + 0.5 \cdot 1.3648 \cdot 51.9 = 89.55\ \text{kPa}$$

$$y_1 = \frac{p_1}{P} = \frac{0.5 \cdot 1.4275 \cdot 75.85}{89.55} = 0.6045$$

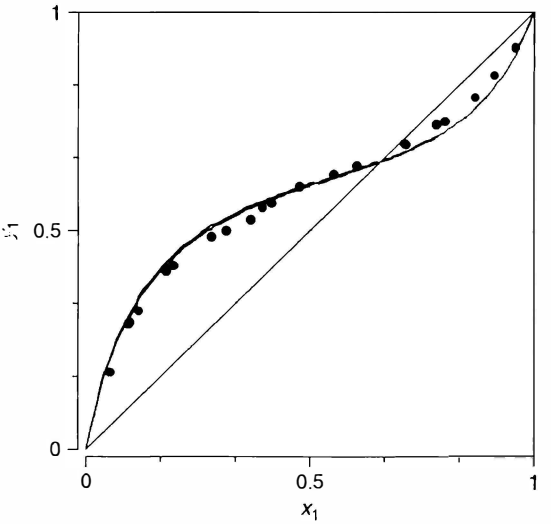

Figure 5.80 Experimental and predicted y–x-data for the system *n*-hexane (1)-2-butanone (2) at 60 °C.

The results for the whole composition range are shown in Figure 5.80. It can be seen that good agreement between experimental and predicted VLE is observed. In Figure 5.81 it is shown that good results are obtained not only for the system *n*-hexane–2-butanone, but also for all the other alkane–ketone systems. It can be seen that even the azeotropic points are predicted accurately. It is worth mentioning that for all systems shown the same two group interaction parameters were used, which describe the interaction between the alkane and ketone group.

Because of the reliable results obtained for VLE and the large range of applicability, the method was directly integrated into the different process simulators. However, in spite of the reliable results for VLE, UNIFAC also shows a few weaknesses, for example, unsatisfying results are obtained:

- for the activity coefficients at infinite dilution,
- for the excess enthalpies, this means the temperature dependence of the activity coefficients following the Gibbs–Helmholtz relation, and
- for strongly asymmetric systems, this means for compounds very different in size.

For the system 2-butanone–*n*-hexane the predicted results of the excess enthalpy using UNIFAC are shown in Figure 5.82 together with the experimental data. It can be seen that the predicted excess enthalpies are not in agreement with the experimental values. This means that an extrapolation to high or low temperatures will produce incorrect results. The same is true for all other alkane–ketone systems, as shown in Figure 5.86.

All these weaknesses are not surprising, since with the VLE data used to fit the required temperature-independent group interaction parameters no information

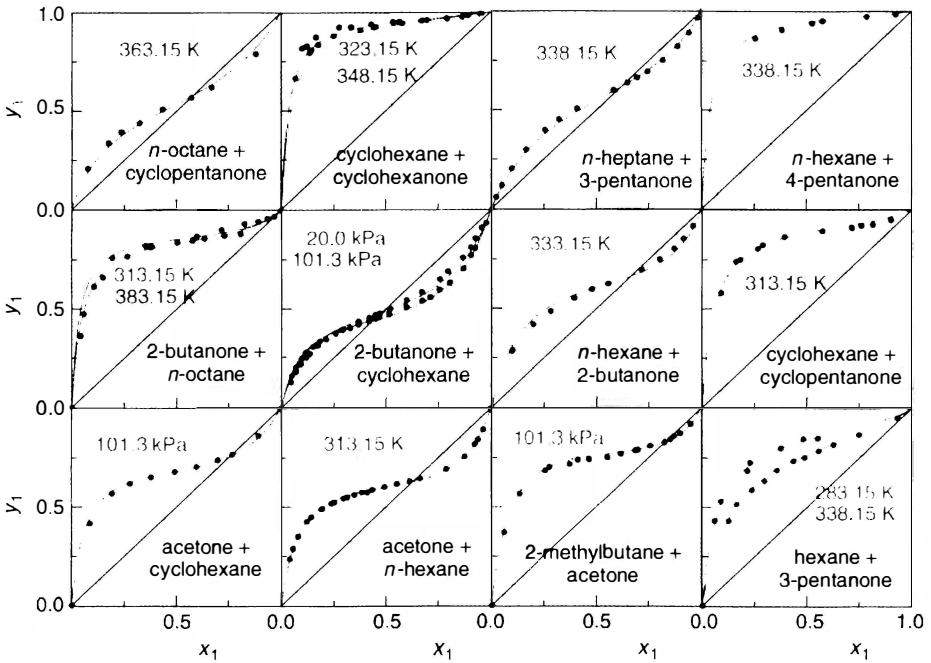

Figure 5.81 Experimental [3] and predicted VLE data for alkane–ketone systems using UNIFAC.

about the temperature dependence (excess enthalpies), very asymmetric systems and the very dilute region is used, since VLE data are usually only measured between 5 and 95 mol% for symmetric or slightly asymmetric systems. An extrapolation to infinite dilution can be very dangerous. However, activity coefficients at infinite dilution measured with special techniques (gas stripping or dilutor technique, ebulliometry, gas–liquid chromatography) provide the required information for the dilute composition range. At the same time systems investigated by gas-liquid chromatography are very asymmetric, since the compounds involved (stationary phase, solutes) show very different volatility. VLE data measured at different temperatures (pressures) deliver an idea about the temperature dependence, but measurements are time consuming. The most accurate information about the temperature dependence is obtained from excess enthalpies measured by isothermal flow calorimetry.

5.9.3.1 Modified UNIFAC (Dortmund)

To reduce the weaknesses of UNIFAC, the modified UNIFAC method was developed [55]. The main differences compared to original UNIFAC are:

- an empirically modified combinatorial part was introduced to improve the results for asymmetric systems;
- temperature-dependent group interaction parameters are used;

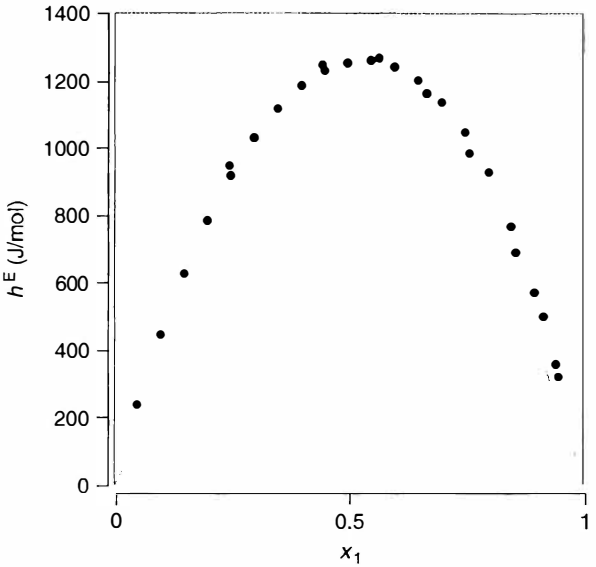

Figure 5.82 Experimental [3] and predicted excess enthalpies using UNIFAC of the system 2-butanone (1)–*n*-hexane (2) at 25 °C.

- additional main groups, for example, for cyclic alkanes, formic acid, and so on, were added.

For fitting the temperature-dependent group interaction parameters of modified UNIFAC, in contrast to original UNIFAC, besides VLE data the following data are also used:

- activity coefficients at infinite dilution,
- excess enthalpy data,
- excess heat capacity data,
- LLE data,
- SLE data of simple eutectic systems, and
- azeotropic data.

The various thermodynamic properties deliver different important information for fitting reliable temperature-dependent parameters. The contributions can be summarized as follows:

- VLE (azeotropic data) provide the information about the activity coefficients for a wide composition range (5–95 mol%);
- the required data for the dilute range are delivered by the activity coefficients at infinite dilution;
- at the same time, γ^{∞}-values measured by gas–liquid chromatography provide reliable information about the real behavior of asymmetric systems.

- excess enthalpies (excess heat capacities) deliver the required information about the temperature dependence;
- h^E-values at high temperature (often at 140 °C) together with SLE data of simple eutectic systems at low temperature are important supporting data for fitting reliable temperature-dependent group interaction parameters.

For fitting the parameters simultaneously to the different types of data, weighting factors are used for the different contributions to the objective function:

$$F = w_{VLE} \sum \Delta VLE + w_{\gamma^\infty} \sum \Delta \gamma^\infty + w_{h^E} \sum \Delta h^E + w_{c_p^E} \sum \Delta c_p^E + w_{LLE} \sum \Delta LLE + w_{SLE} \sum \Delta SLE + w_{AZD} \sum \Delta AZD \quad (5.96)$$

The modifications of modified UNIFAC compared to original UNIFAC are summarized below. The combinatorial part is calculated using the following slightly modified empirical equation:

$$\ln \gamma_i^C = 1 - V_i' + \ln V_i' - 5q_i \left(1 - \frac{V_i}{F_i} + \ln \frac{V_i}{F_i}\right) \quad (5.97)$$

for which besides V_i the following volume/mole fraction ratio V_i' is used:

$$V_i' = \frac{r_i^{3/4}}{\sum_j r_j^{3/4} x_j} \quad (5.98)$$

To describe the temperature dependence, linear or quadratic temperature-dependent parameters were introduced in Eq. (5.95):

$$\Psi_{nm} = \exp\left(-\frac{a_{nm} + b_{nm}T + c_{nm}T^2}{T}\right) \quad (5.99)$$

While linear temperature-dependent group interaction parameters are already required to describe the VLE behavior and excess enthalpies simultaneously, quadratic temperature-dependent parameters are used when the system shows a strong temperature dependence of the excess enthalpies.

Most important for the application of group contribution methods for the synthesis and design of separation processes is a comprehensive and reliable parameter matrix with reliable parameters. The present status of modified UNIFAC is shown in Figure 5.84. Today parameters are available for 91 main groups. In the recent years new main groups were introduced for the different types of amides, isocyanates, epoxides, anhydrides, peroxides, carbonates, various sulfur compounds, and so on. In the last year the range of applicability was even extended to systems with ionic liquids [56].

Because of the importance of modified UNIFAC for process development the range of applicability is continuously extended by filling the gaps in the parameter table and revising some of the existing parameters with the help of systematically measured data and by using new experimental data published and stored in the Dortmund Data Bank [3]. For fitting temperature-dependent parameters, in particular excess enthalpy data covering a wide temperature range are desirable. These data can be measured using for example isothermal flow

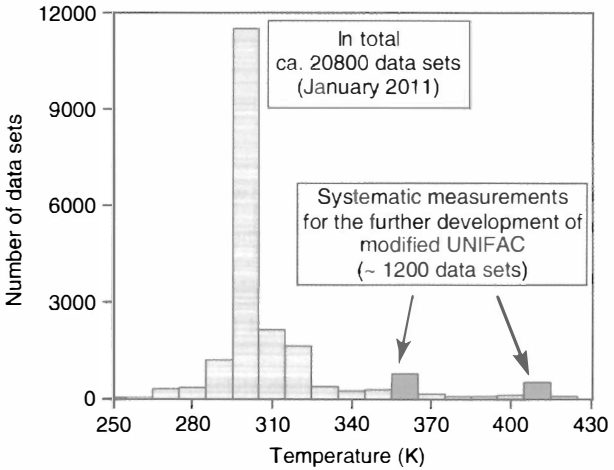

Figure 5.83 Available excess enthalpy data as a function of temperature.

calorimetry. But unfortunately most of the published data were measured near room temperature (see Figure 5.83). To complete the data base and in particular to get the required supporting data at high temperature for fitting the temperature-dependent group interaction parameters of modified UNIFAC, nearly 1200 data sets were systematically measured by isothermal flow calorimetry. Additionally, a large number of VLE data, SLE of eutectic systems, and activity coefficients at infinite dilution were measured systematically in our laboratory.

Since 1996, further extension (i.e., revision of the existing parameters, filling of gaps in the parameter matrix or the introduction of new main groups) was carried out within the UNIFAC consortium. The current status of the complete parameter matrix is always available via internet [57]. A great part of the modified UNIFAC parameters was published by Gmehling *et al.* [58]. The published van der Waals properties and modified UNIFAC group interaction parameters are given in the internet (see Appendix I). But a great part of the group interaction parameters were revised using a larger database to fit the parameters. The revised and the new fitted parameters are only available for the sponsors of the company consortium [57].

Modified UNIFAC is an ideal thermodynamic model for process development. With the help of this predictive model easily various process alternatives can be compared, suitable solvents for separation processes like azeotropic distillation, extractive distillation, extraction can be selected, the influence of solvents on chemical equilibrium conversion can be predicted, and so on.

Modified UNIFAC can also be applied to provide artificial data for fitting the missing binary parameters of the parameter matrix of a g^E-model. But if the key components of a separation step are considered, for the final design an experimental examination of the results is recommended.

The progress achieved when going from UNIFAC to modified UNIFAC can be recognized from a comparison of the results for 2200 consistent binary VLE data sets. Using the UNIQUAC equation for the correlation of the 2200 VLE data sets

Figure 5.84 Present status of the modified UNIFAC method.

a mean absolute deviation of 0.0058 for the vapor phase mole fraction is obtained. While for original UNIFAC method a mean deviation of 0.0141 results, a mean deviation of 0.0088 of the vapor phase mole fractions is achieved with modified UNIFAC (see Figure 5.85). This means that the deviation with UNIFAC compared to a correlation of the VLE data using the UNIQUAC model was improved by nearly a factor of 3 from 0.0083 (0.0141-0.0058) to 0.0030 (0.0088-0.0058). As can be seen from Figure 5.85, similar improvements are also obtained for the predicted temperatures and pressures.

Not only the results for VLE, but also for SLE, LLE, excess enthalpies, excess heat capacities, activity coefficients at infinite dilution were distinctly improved when going from UNIFAC to modified UNIFAC. For excess enthalpies this is shown in Figure 5.86. It can be seen that in all cases the predicted results are in good agreement with the experimental findings in the case of modified UNIFAC, while

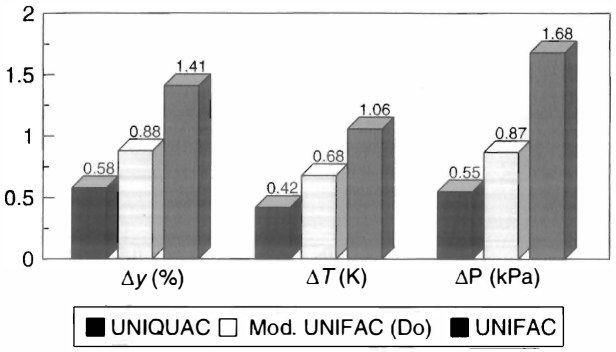

Figure 5.85 Mean absolute deviation in vapor phase mole fraction, temperature, and pressure for the correlation, respectively, prediction of 2200 binary consistent VLE data.

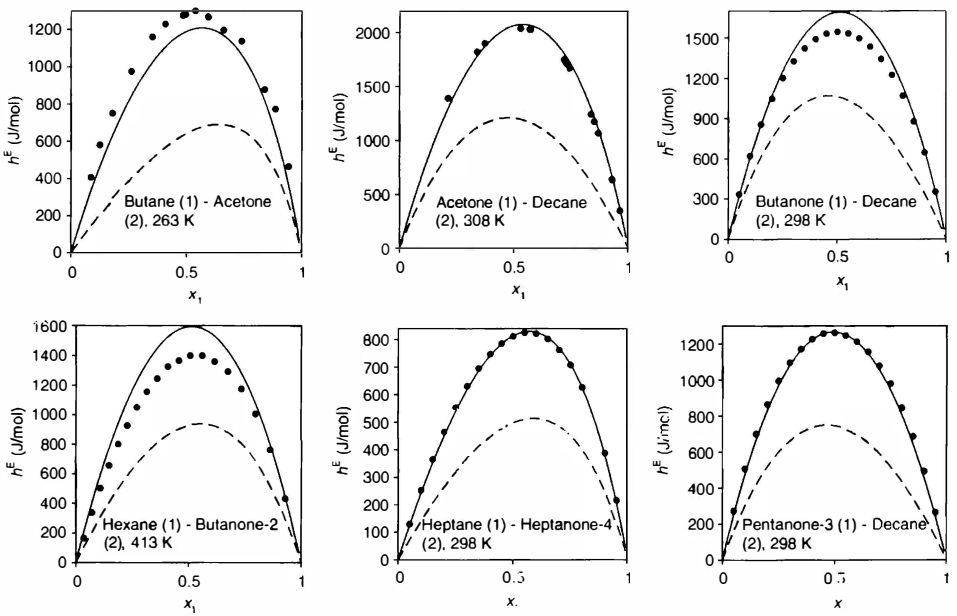

Figure 5.86 Experimental [3] and predicted excess enthalpies for different binary alkane – ketone systems:
– – – original UNIFAC; — modified UNIFAC.

the results of original UNIFAC show strong deviations as already discussed in Section 5.9.3.

Typical results for VLE, excess enthalpies, SLE, activity coefficients at infinite dilution, excess heat capacities, and azeotropic data for systems of alkanes with ketones are shown in Figures 5.87 and 5.88. While in Figure 5.87 results are

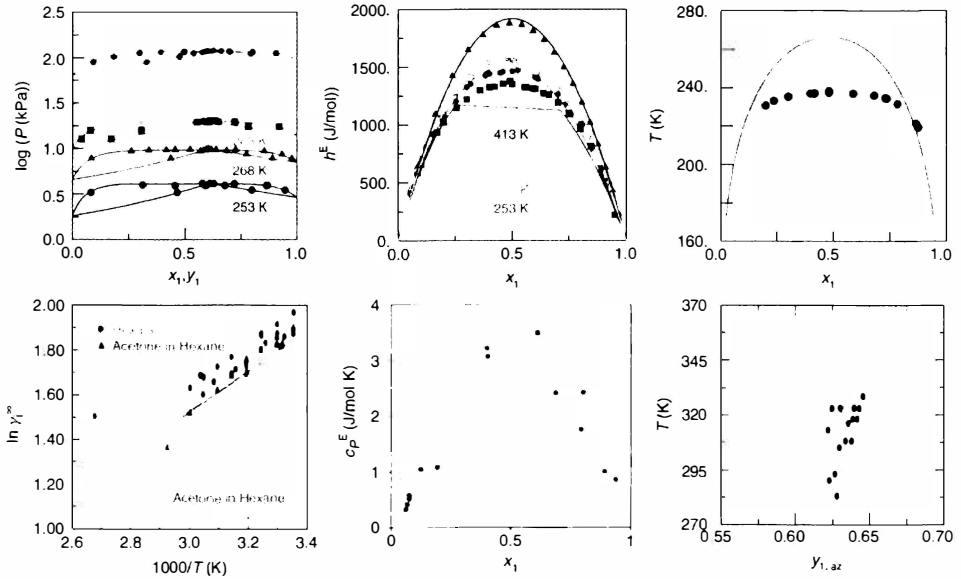

Figure 5.87 Experimental and predicted results for the system acetone (1) – hexane (2) — modified UNIFAC; ▲ ● ■ experimental [3].

presented for the system acetone–*n*-hexane, in Figure 5.88 a comparison of the predicted and experimental results for VLE, h^E, SLE, azeotropic data, LLE and γ^∞ for different ketones with various alkanes is presented. In the case of SLE, additionally the curvature assuming ideal behavior is shown by the dashed lines. The improvements obtained when taking into account the real behavior is obvious. Of course, the same group interaction parameters are applied for all the predictions. As can be seen in all cases, good agreement is obtained for the different phase equilibria and excess properties, although a wide temperature range (−100 to 160 °C) is covered. The correct description of the temperature dependence is achieved by the reliable prediction of the excess enthalpies in the temperature range covered.

In the meantime the range of applicability of modified UNIFAC was even extended to systems with ionic liquids [56]. In Figure 5.89 the experimental and predicted activity coefficients at infinite dilution of various *n*-alkanes in different alkyl-methyl-imidazolium bistrifluoromethylsulfonylimides are shown as a function of temperature. It can be seen that not only the temperature dependence, but also the dependence of the activity coefficients from the number of C-atoms of the alkanes and the alkyl rests is properly described.

Besides the prediction of phase equilibria the group contribution methods UNIFAC or modified UNIFAC can be applied for other applications of great practical interest, for example, the calculation of octanol–water partition coefficients

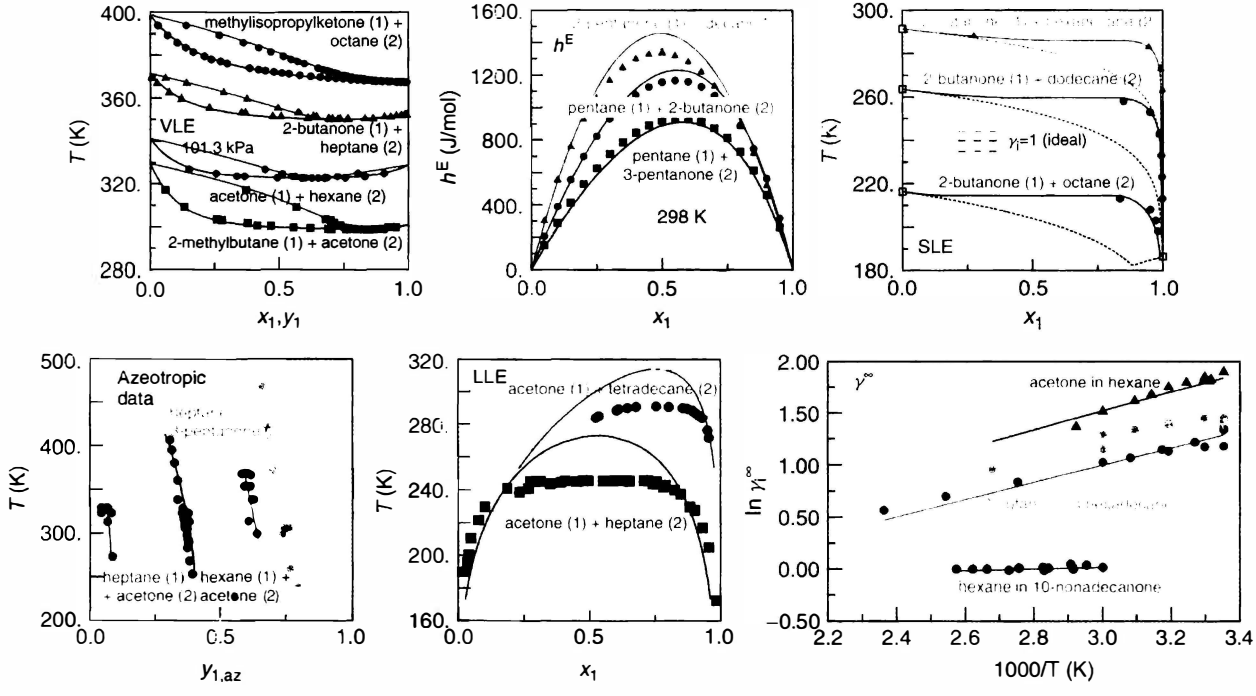

Figure 5.88 Experimental and predicted results for different phase equilibria for alkane-ketone systems — modified UNIFAC; ▲ ● ■ experimental [3].

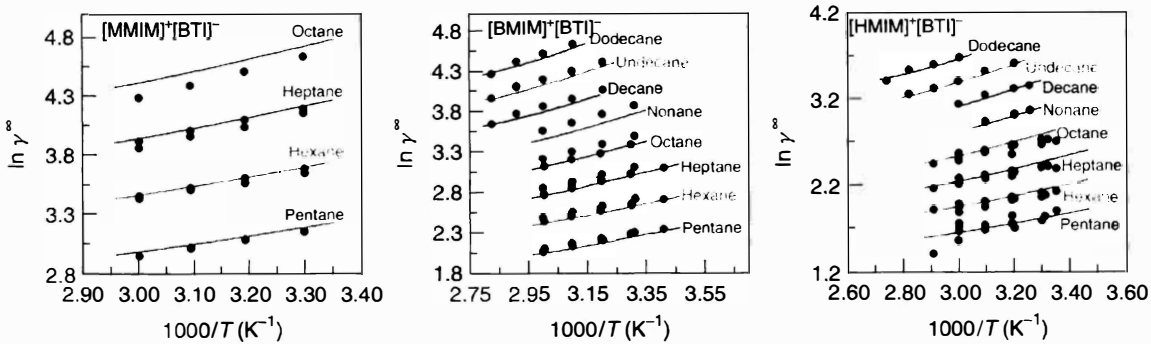

Figure 5.89 Experimental [3] and predicted activity coefficients at infinite dilution of various *n*-alkanes in three alkyl (methyl, butyl, hexyl)-methyl-imidazolium bis-trifluoromethylsulfonylimides as a function of temperature.

of persistent chemicals [59] to decide about their fate in the environment, or the flash points of flammable liquid mixtures [60].

5.9.3.2 Weaknesses of the Group Contribution Methods UNIFAC and Modified UNIFAC

As shown before the group contribution method modified UNIFAC is a powerful and reliable predictive g^E-model. It was continuously further developed in the last 20 years so that the method provides reliable results and a large range of applicability. But in spite of the great advantages compared to original UNIFAC (better results for excess enthalpies, activity coefficients at infinite dilution, asymmetric systems) it shows the typical weaknesses of a group contribution approach. Hence, for example

- Isomer effects cannot be predicted. This means the same activity coefficients are obtained, for example, for *o*-/*m*-/*p*-xylene or phenanthrene/anthracene with the different solvents. But at least in the case of VLE or SLE calculation this is not a great problem, since the required standard fugacities, that is, vapor pressure, melting point, and heat of fusion are of much greater importance than small differences of the activity coefficients. Similar problems are also observed for other predictive models, for example, the quantum chemical approach.
- Unreliable results are obtained for group contribution methods in the case, if a large number of functional groups have to be taken into account, as in the case of pharmaceuticals or when the molecule shows groups such as, –C(Cl)(F)(Br) as for example, in refrigerants. But also in these cases similar problems are observed for other approaches, for example, the quantum-chemical methods.
- Furthermore, poor results are obtained for the solubilities and activity coefficients at infinite dilution of alkanes or naphthenes in water. This was accepted by the developers of modified UNIFAC to achieve reliable VLE results, for example, for alcohol/water systems. The reason was that starting from experimental γ^{∞}-values of approx. 250000 for *n*-hexane in water at room temperature it was not possible to fit alcohol–water parameters which deliver γ^{∞}-values for hexanol in water of 800 and at the same time describe the azeotropic composition of ethanol and higher alcohols with water properly and obtain homogeneous behavior for alcohol–water systems up to C_3-alcohols and heterogeneous behavior starting from C_4-alcohols. To allow for a prediction of hydrocarbon solubilities in water an empirical relation was developed [61, 62], which allows the estimation of the solubilities of hydrocarbons in water and of water in hydrocarbons (see below).
- For the system *tert*-butanol–water a miscibility gap is predicted, although tertiary butanol in contrast to 1-butanol, 2-butanol, and isobutanol forms a homogeneous mixture with water.

As mentioned before, unsatisfying results of modified UNIFAC are obtained for the activity coefficients at infinite dilution and the solubilities of hydrocarbons in water. Typical results are given in Table 5.17. From the listed solubilities it can be

Table 5.17 Experimental [3] and predicted solubilities of *n*-hexane and cyclohexane in water at 25 °C using modified UNIFAC.

Hydrocarbon	Solubility in water x_{exp}	Solubility in water x_{calc}
n-Hexane	$2.5 \cdot 10^{-6}$	$1.5 \cdot 10^{-4}$
Cyclohexane	$1.3 \cdot 10^{-5}$	$1.7 \cdot 10^{-3}$

Table 5.18 Parameters for the empirical estimation of hydrocarbon solubilities in water.

Hydrocarbon	A	B	C
Alkanes [62]	1.104	0.0042	−2.817
Naphthenes	1.3326	0.006427	−3.676
Alkenes	1.523	0.00603	−3.0418

seen that the solubilities and therewith the activity coefficients at infinite dilution are approximately a factor 100 off.

To obtain satisfying results for the solubility of alkanes the following empirical relation was suggested by Banerjee [61] for the temperature range 273–373 K:

$$\log \frac{c_{\text{hydrocarbon in water}}}{\text{mol l}^{-1}} = A \cdot \log \left(\frac{55.56}{\gamma^{\infty}_{\text{hydrocarbon in water at 298.15K}^*}} \right) + B \cdot T + C$$

*predicted using modified UNIFAC (5.100)

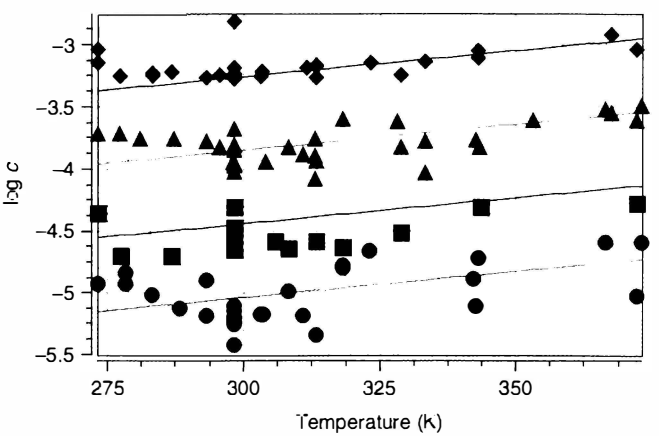

Figure 5.90 Experimental [3] and predicted solubilities c (mol/l) of alkanes in water as a function of temperature using Eq. (5.100) [62]: ♦ *n*-pentane; ▲ *n*-hexane; ■ *n*-heptane; ● *n*-octane.

Table 5.19 Parameters for the empirical estimation of water solubilities in hydrocarbons.

Hydrocarbon	A	B	C
Alkanes	2.3171	0.01796	−3.672
Naphthenes	0.1806	0.01532	−7.172
Alkenes	−1.1104	0.011	−8.332

For the different hydrocarbons the parameters A, B, and C were fitted to solubility data stored in the Dortmund Data Bank and are given in Table 5.18. For the calculation of the hydrocarbon solubilities only the activity coefficient of the hydrocarbon in water at 25 °C predicted using modified UNIFAC is required.

Typical results for different alkanes are shown in Figure 5.90. It can be seen that the predicted results are in good agreement with the experimental findings.

For the calculation of the solubility of water in alkanes a similar equation can be applied. Also in this case the required parameters A, B, and C were fitted to solubility data stored in the Dortmund Data Bank:

$$\log x_{\text{water in hydrocarbon}} = A \cdot \log\left(\frac{1}{\gamma^{\infty}_{\text{water in hydrocarbon at 298.15 K*}}}\right) + B \cdot T + C$$

*predicted using modified UNIFAC (5.101)

The parameters A, B and C for Eq. (5.101) are given in Table 5.19

Example 5.23

Calculate the solubilities of *n*-hexane in water and water in *n*-hexane at 298.15 K with the help of the empirical relations given above.

Solution

First the activity coefficients at infinite dilution of *n*-hexane in water and water in *n*-hexane at 25 °C have to be calculated. Using the modified UNIFAC parameters given in Appendix I an activity coefficient at infinite dilution of 6618 for *n*-hexane in water and a value of 135.9 for water in *n*-hexane is obtained. With these values directly the solubilities can be calculated:

$$\log \frac{c_{n\text{-hexane in water}}}{\text{mol l}^{-1}} = 1.104 \cdot \log\left(\frac{55.56}{6618}\right) + 0.0042 \cdot 298.15 - 2.817$$

$$= -3.8566$$

$$c_{n\text{-hexane in water}} = 1.39 \cdot 10^{-4} \text{ mol/l}$$

$$x_{n\text{-hexane in water}} \approx 2.53 \cdot 10^{-6}$$

$$\log x_{\text{water in } n\text{-hexane}} = 2.3171 \cdot \log\left(\frac{1}{135.9}\right) + 0.01796 \cdot 298.15 - 3.672$$

$$= -3.260$$

$$x_{\text{water in } n\text{-hexane}} = 0.000549$$

Experimentally *n*-hexane solubilities between $9.44 \cdot 10^{-5}$ and $1.55 \cdot 10^{-4}$ mol/l are reported (see Figure 5.90). As well the water solubility is in very good agreement with the experimental values.

5.9.4
Predictive Soave–Redlich–Kwong (PSRK) Equation of State

As can be recognized from the results shown before, modified UNIFAC is a very powerful predictive model for the development and design of chemical processes, in particular separation processes. However, modified UNIFAC is a g^E-model. This means that it cannot handle supercritical compounds. For supercritical compounds either Henry constants have to be introduced or Approach A has to be used. In the latter case, an equation of state is required, which is able to describe the *PvT* behavior of both the vapor (gas) and the liquid phase.

As mentioned in Section 2.5 the first equation of state which was able to describe the *PvT* behavior of the liquid and the vapor phase was developed by van der Waals. With only two parameters *a* and *b*, the van der Waals equation of state is able to describe the different observed phenomena, such as condensation, evaporation, the two phase region and the critical behavior. But the calculated densities, vapor

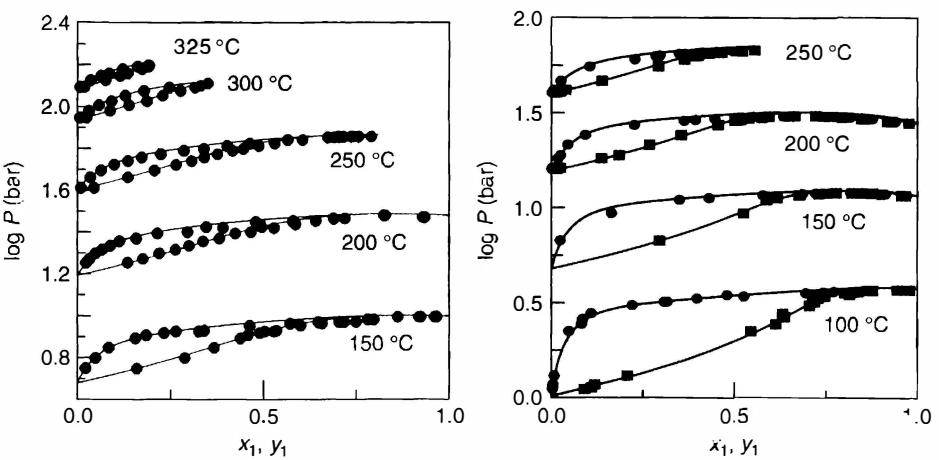

Figure 5.91 Experimental and predicted VLE data using PSRK for the systems ethanol (1)–water (2) (left hand side) and acetone (1)–water (2) (right hand side) at subcritical and supercritical conditions.

pressures, etc. using the van der Waals equation of state were only in qualitative agreement with the experimental findings.

Therefore today improved cubic equations of state like the SRK [63] or the PR equation [64] are used. But up to 1979 the application of the equations of state approach was limited to nonpolar or slightly polar compounds in particular because of the empirical quadratic mixing rules used. Huron and Vidal [35] combined the advantages of g^E-models and equations of state by introducing more sophisticated so-called g^E-mixing rules (see Section 4.9.2). With the application of original UNIFAC for the prediction of the required g^E-values in the mixing rule predictive group contribution equations of state were developed [43]. While in the approach of Huron and Vidal infinite pressure is taken as reference state, in the group contribution equation of state PSRK (predictive SRK) atmospheric pressure is used. The great advantage of this approach is that in the PSRK method the already available UNIFAC parameters can directly be used. But now the UNIFAC parameters can be applied at supercritical conditions. For the systems

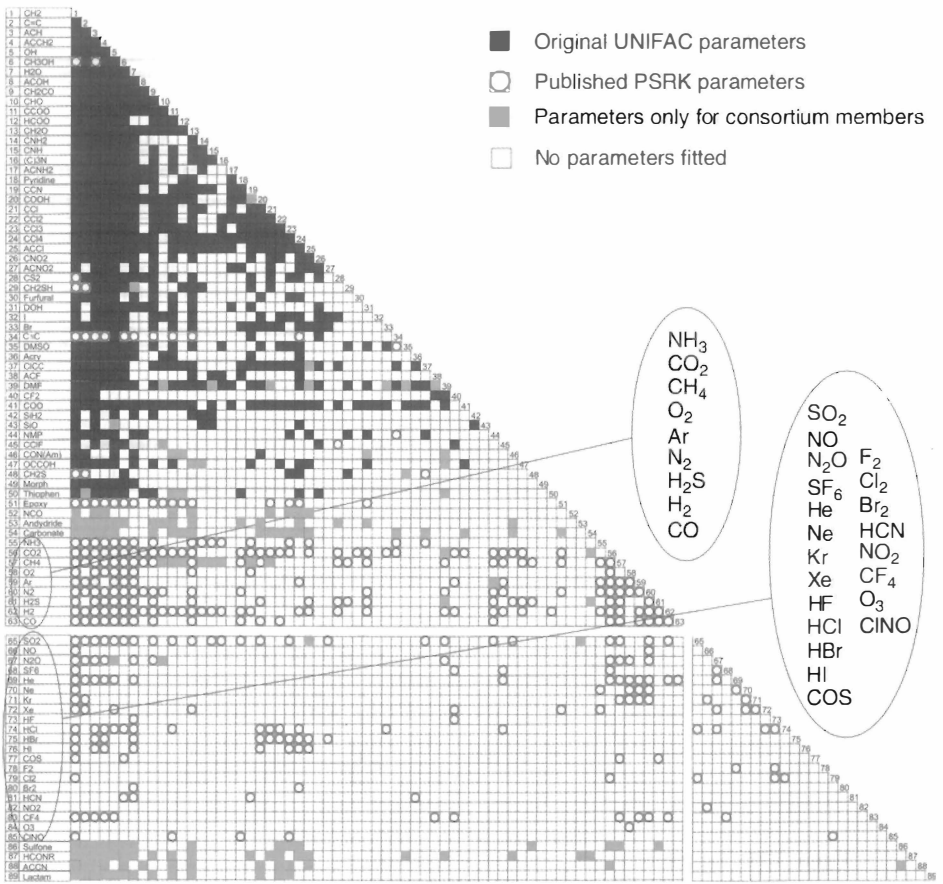

Figure 5.92 Current parameter matrix of the group contribution equation of state PSRK

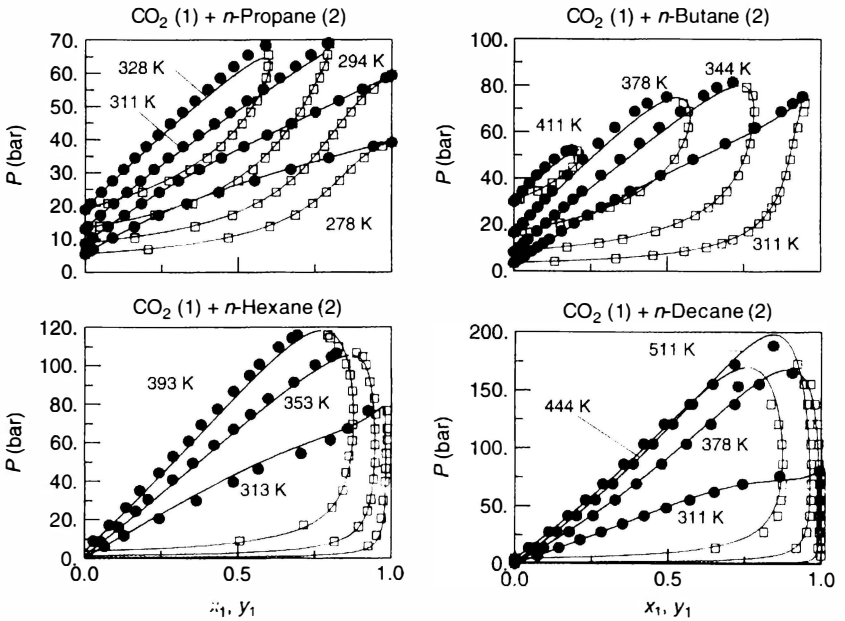

Figure 5.93 Experimental and predicted VLE data using PSRK for various CO_2–alkane systems at subcritical and supercritical conditions.

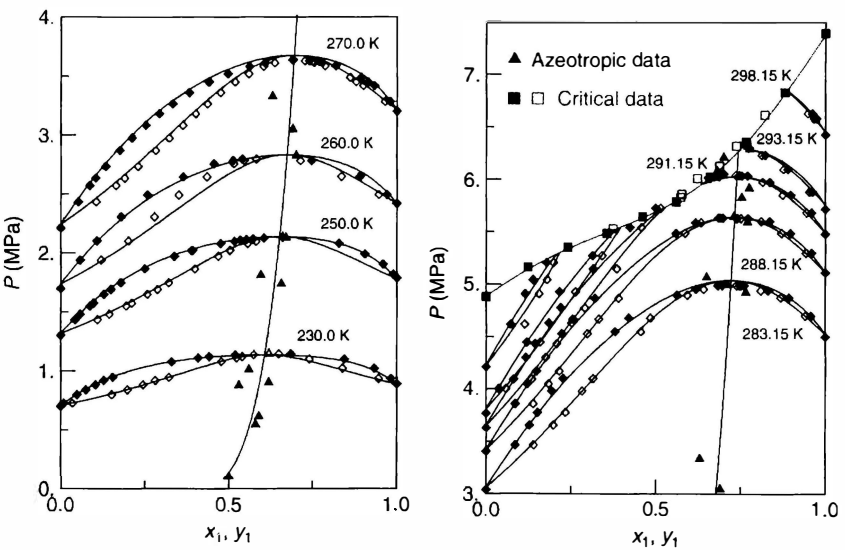

Figure 5.94 Experimental and predicted VLE, azeotropic and critical data of the system CO_2 (1) -ethane (2) using PSRK as a function of temperature.

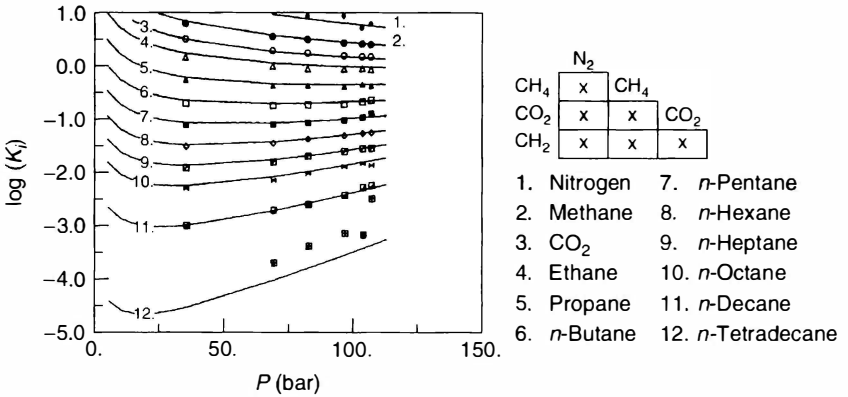

Figure 5.95 Experimental [65] and predicted K-factors for a 12-component system using PSRK at a temperature of 322 K as a function of pressure and the required parameter matrix for the group contribution equation of state PSRK.

ethanol–water and acetone–water this is shown in Figure 5.91. It can be seen that the results are very satisfying.

To use PSRK for process synthesis and design a large matrix with reliable parameters is desirable. The possibility to handle systems at supercritical conditions all of a sudden allowed including also gases like CO_2, CH_4, H_2S, H_2, and so on, as new functional groups in the parameter matrix. In total, 30 different gases were added as new main groups. The required parameters for the gases were fitted to VLE data of low boiling substances and gas solubilities stored in the Dortmund Data Bank [3]. The current PSRK parameter matrix is given in Figure 5.92.

Typical VLE results for different CO_2–alkane systems are shown in Figures 5.93 and 5.94. While in Figure 5.93 only VLE data for four different CO_2-alkane (propane, butane, hexane, decane) are shown, for the system ethane[21]–CO_2 additionally the experimental and predicted azeotropic and critical data are shown. As can be seen, excellent results are obtained for all systems considered. This means that the group contribution concept can also be applied for the gases included in the PSRK matrix.

Predicted results using PSRK for a 12 component system at 322 K are shown in Figure 5.95 in the form of the K-factors ($K_i = y_i/x_i$) as a function of pressure. Using classical mixing rules 66 binary parameters would be required. In the case of a group contribution equation of state the number of required parameters in this case goes down to 6, since all alkanes are described with the same group interaction parameters. This is a great advantage of group contribution equations of state in comparison to the typical equation of state approach, in particular for processes such as the gas-to-liquid process, where a large number of alkanes, alkenes, alcohols besides a few gases have to be handled.

21) In PSRK, ethane is built up by two methyl groups.

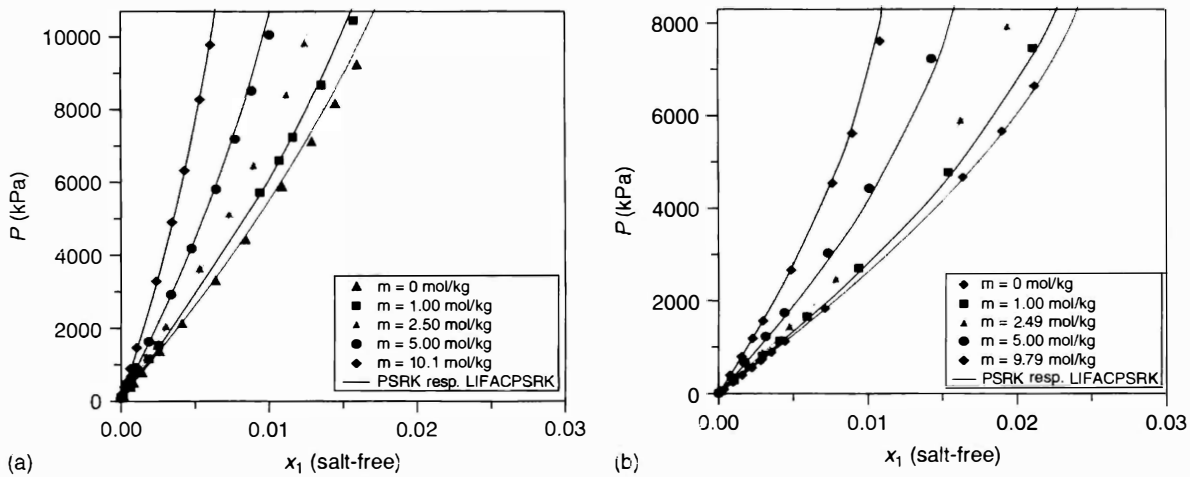

Figure 5.96 Experimental and predicted (PSRK + LIFAC) results for the system CO_2 (1)–H_2O (2)–$NaNO_3$ (3) at 40 °C (a) and 100 °C (b).

PSRK was even extended to systems with strong electrolytes by using the electrolyte model LIFAC [66] instead of the original UNIFAC method for calculating the excess Gibbs energy. The LIFAC method takes into account the middle range and long range interactions of the electrolytes by the Debye–Hückel and a modified *Pitzer* term (see Section 7.3.5). The PSRK model in combination with the LIFAC model allows the prediction of salting in and salting out effect of strong electrolytes on VLE and gas solubilities. In Figure 5.96 the influence of sodium nitrate on the solubility of carbon dioxide in water for different salt concentrations at 40 °C and 100 °C is shown. As can be seen not only the salt effect but also the temperature dependence for this ternary system is described with the required accuracy.

5.9.5 VTPR Group Contribution Equation of State

The PSRK model [43] provides reliable predictions of VLE and gas solubilities. Therefore, PSRK was implemented in most process simulators and is well accepted as a predictive thermodynamic model for the synthesis and design of the different processes in chemical, gas processing, and petroleum industry. But also PSRK shows all the weaknesses of UNIFAC and the SRK equation of state. Since the SRK equation of state is used in the group contribution equation of state PSRK, poor results are obtained for liquid densities of the pure compounds and the mixtures. Furthermore, poor results are obtained for activity coefficients at infinite dilution, heats of mixing and very asymmetric systems because of the use of original UNIFAC. Ahlers and Gmehling [44] developed a generalized group contribution

Table 5.20 Main differences between the new group contribution equation of state VTPR and the PSRK model.

Module	PSRK	VTPR
Equation of state	Soave–Redlich–Kwong	Volume-translated Peng–Robinson
α-Function	Generalized Mathias–Copeman	Generalized Twu
Mixing rule for the parameter a	$\frac{a}{bRT} = \sum_i x_i \frac{a_{ii}}{b_i RT} + \frac{1}{A}\left(\frac{g^E}{RT} + \sum_i x_i \ln \frac{b}{b_i}\right)$ $A = -0.64663$	$\frac{a}{b} = \sum_i x_i \frac{a_{ii}}{b_i} + \frac{g^{E,R}}{A}$ $A = -0.53087$
Mixing rule for the parameter b	$b = \Sigma x_i b_i$	$b_{ij}^{3/4} = \left(b_{ii}^{3/4} + b_{jj}^{3/4}\right)/2$ $b = \sum_i \sum_j x_i x_j b_{ij}$
g^E information	(a) original UNIFAC (b) temp-depend. PSRK parameters	Temp-depend. VTPR parameters
Database	VLE, GLE	VLE, GLE, h^E, SLE, γ^∞

equation of state called *VTPR*, where most of the weaknesses of PSRK were removed (see also Sections 2.5.5 and 4.9.2). The main differences between PSRK and VTPR are summarized in Table 5.20.

A better description of liquid densities is achieved, by using the volume translated PR (Peneloux *et al.* [33]) instead of the SRK equation of state, which is used in the PSRK model. Based on the ideas of Chen *et al.* [67] an improved g^E-mixing-rule is used. The prediction of asymmetric systems is improved by using a quadratic b mixing-rule with a modified combination rule [67]. The improvements obtained when going from the group contribution equation of state PSRK to VTPR can be recognized from the predicted results using these models for symmetric alkane–alkane systems shown in Figure 5.97 and asymmetric alkane–alkane

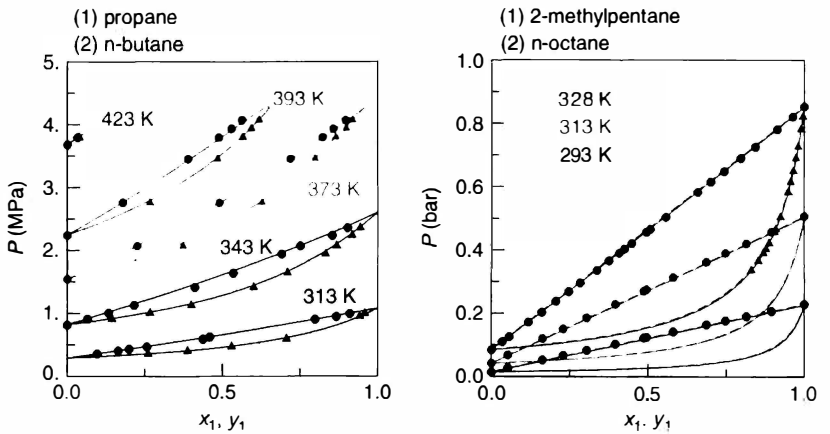

Figure 5.97 Experimental and predicted VLE data for symmetric alkane–alkane systems ---- PSRK — VTPR.

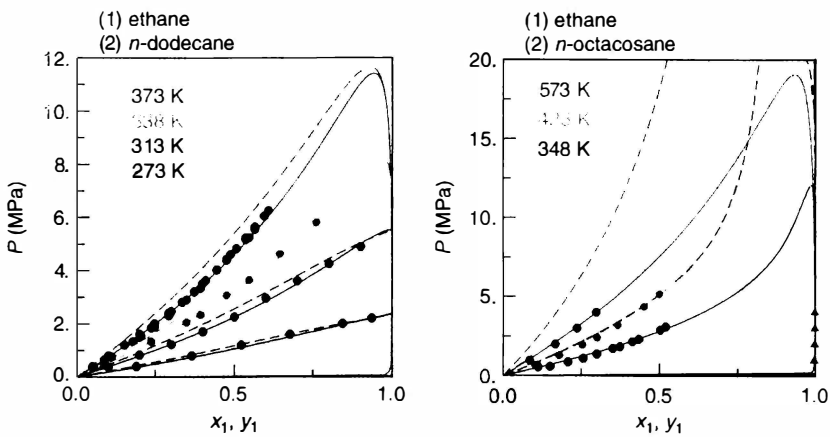

Figure 5.98 Experimental and predicted VLE data for asymmetric alkane–alkane systems ---- PSRK — VTPR.

systems shown in Figure 5.98. For the prediction of alkane–alkane systems no interaction parameters are required for both models. This means that the results mainly depend on the mixing rules used. As can be seen from the *Pxy*-diagrams much better results are predicted using VTPR instead of PSRK in the case of the asymmetric systems ethane–dodecane and ethane–octacosane, while nearly the same results are obtained for the symmetric systems propane–butane and 2-methylpentane–*n*-octane.

In the case of the group contribution equation of state VTPR, instead of temperature-independent group interaction parameters from original UNIFAC, temperature-dependent group interaction parameters as in modified UNIFAC are used. As for modified UNIFAC, the required temperature-dependent group interaction parameters of VTPR are fitted simultaneously to a comprehensive data base. Besides VLE data for systems with sub and supercritical compounds, gas

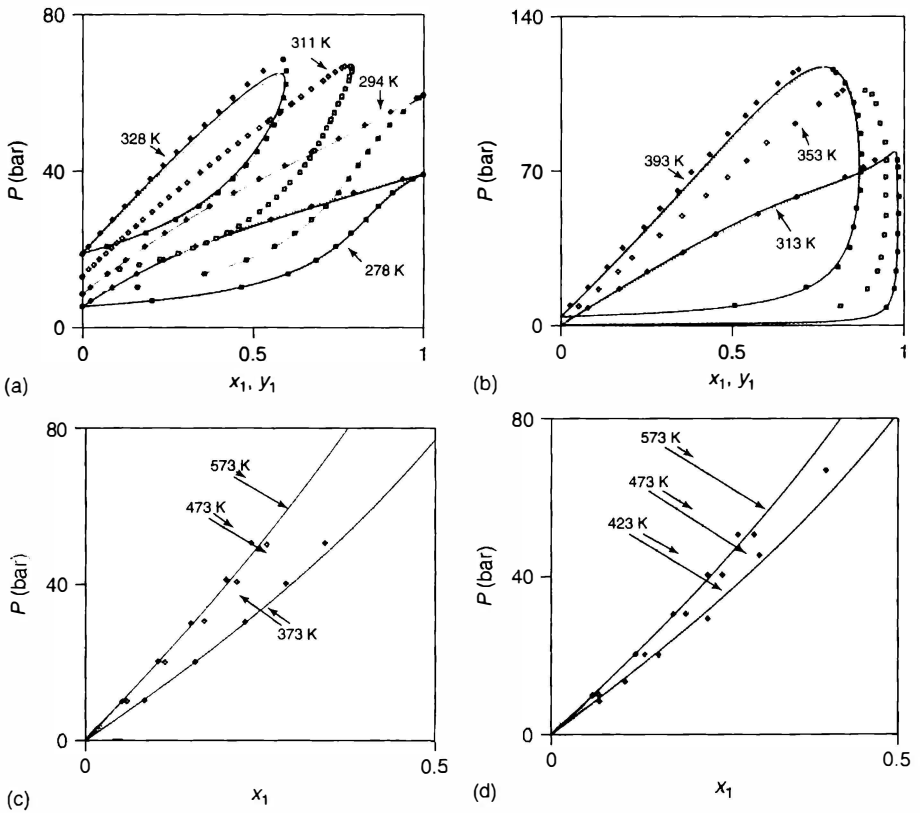

Figure 5.99 Experimental and predicted VLE data for different CO_2–alkane systems (a) CO_2(1) – propane(2) (b) CO_2(1) – *n*-hexane(2) (c) CO_2(1) – *n*-eicosane(2) (d) CO_2(1) – *n*-octacosane(2) PSRK — VTPR group contribution equation of state.

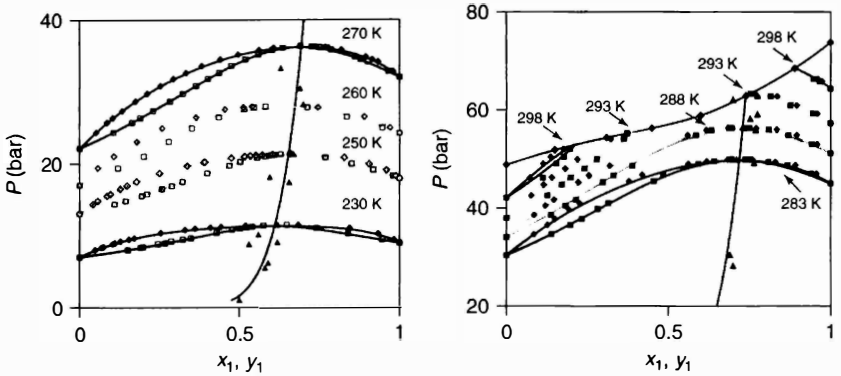

Figure 5.100 Experimental and predicted VLE data, azeotropic points and critical data for the system CO_2 (1)–ethane (2) using VTPR.

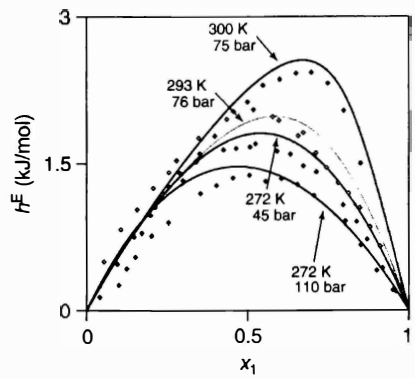

Figure 5.101 Experimental and predicted excess enthalpy data for the system CO_2(1)–ethane (2).

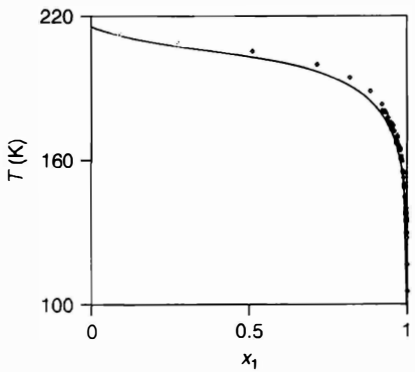

Figure 5.102 Experimental and predicted SLE data for the system ethane (1)–CO_2 (2) • experimental [3, 68] —- group contribution equation of state VTPR.

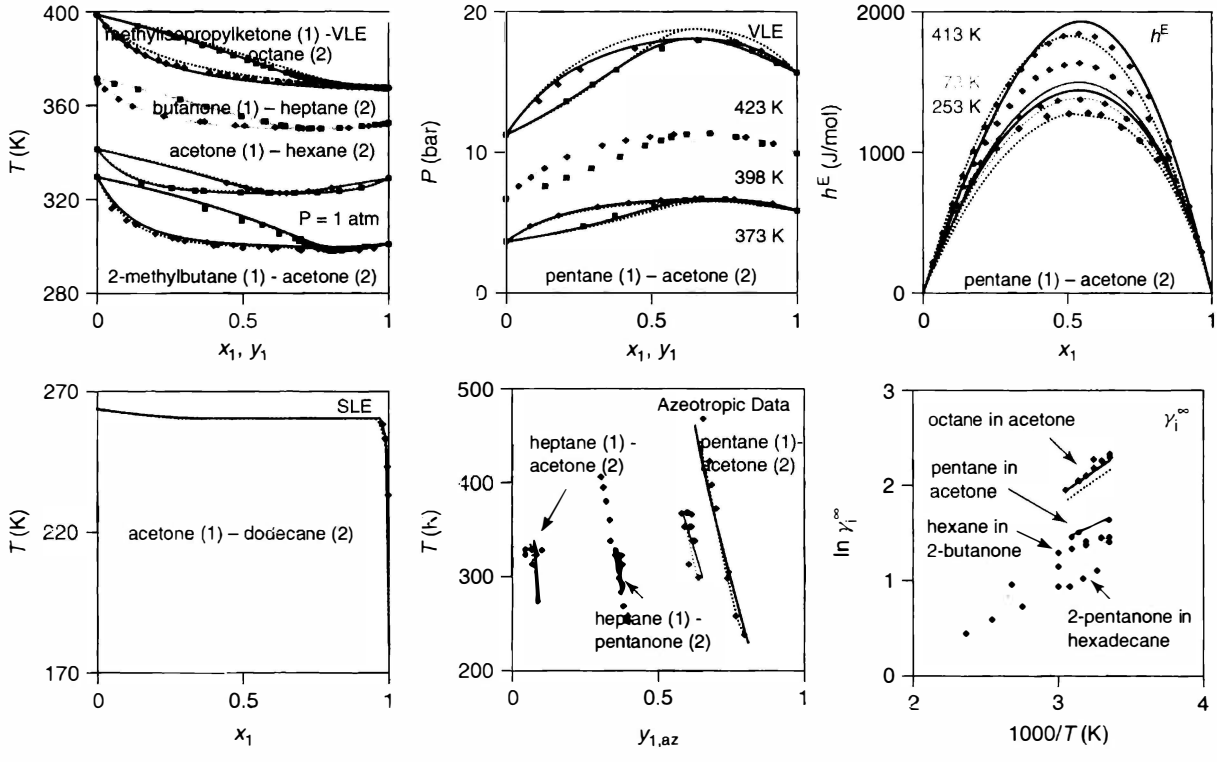

Figure 5.103 Experimental and predicted phase equilibrium data and excess enthalpies for alkanes with ketones predicted using modified UNIFAC respectively the group contribution equation of state VTPR; ·· modified UNIFAC, — group contribution equation of state VTPR.

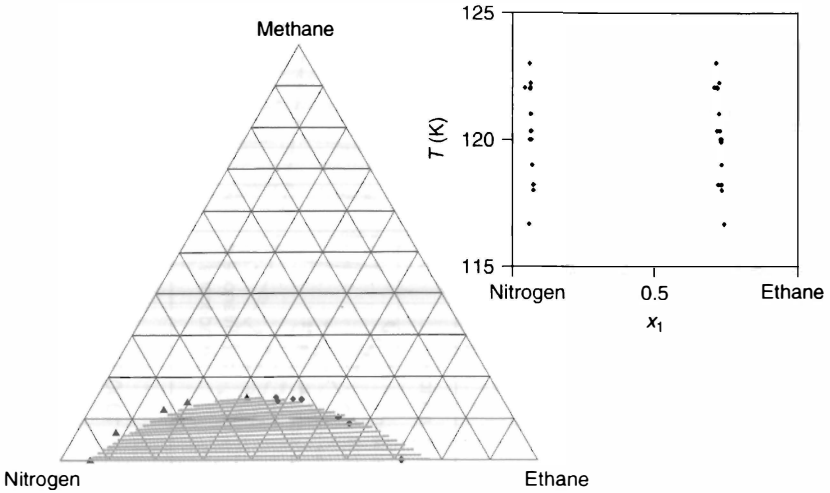

Figure 5.104 Experimental and predicted LLE data using VTPR for the ternary system nitrogen–ethane–methane at 122 K and the binary system ethane–nitrogen [3].

solubilities, SLE of eutectic systems, activity coefficients at infinite dilution and excess enthalpies covering a large temperature and pressure range are used.

The results obtained for the different pure component properties and various phase equilibria of the new group contribution equation of state are very promising [44]. In Figure 5.99 the predicted VLE results for different alkane–CO_2-systems using PSRK and the group contribution equation of state VTPR are presented. While both methods show similar results for the slightly asymmetric system CO_2–propane and CO_2–*n*-hexane, again much better results are achieved for the strongly asymmetric system CO_2–eicosane and CO_2–octacosane with the group contribution equation of state VTPR because of the improved mixing rules.

Using the same parameters, VLE, azeotropic data, critical data and excess enthalpies for the system CO_2–ethane were predicted. A comparison of the predicted and experimental results is shown in Figures 5.100 and 5.101. It can be seen that as in the case of PSRK (see Figure 5.94) excellent agreement between the predicted results and the experimental findings is obtained. In Figure 5.101 the experimental and predicted excess enthalpies for the systems CO_2–ethane using the group contribution equation of state VTPR are shown. It can be seen that nearly a perfect description of the VLE, azeotropic, and the critical line is obtained. Furthermore, not only the temperature, but also the pressure dependence of the excess enthalpies is described correctly with the group contribution equation of state VTPR. Perhaps it has to be mentioned again that for all the predictions (VLE, azeotropic data, critical line, h^E) shown in Figures 5.99–5.101 the same parameters were used to describe the interactions between CO_2 and alkanes.

Using the same group interaction parameters, other phase equilibria can be predicted as well. The predicted SLE behavior of the binary system ethane–CO_2

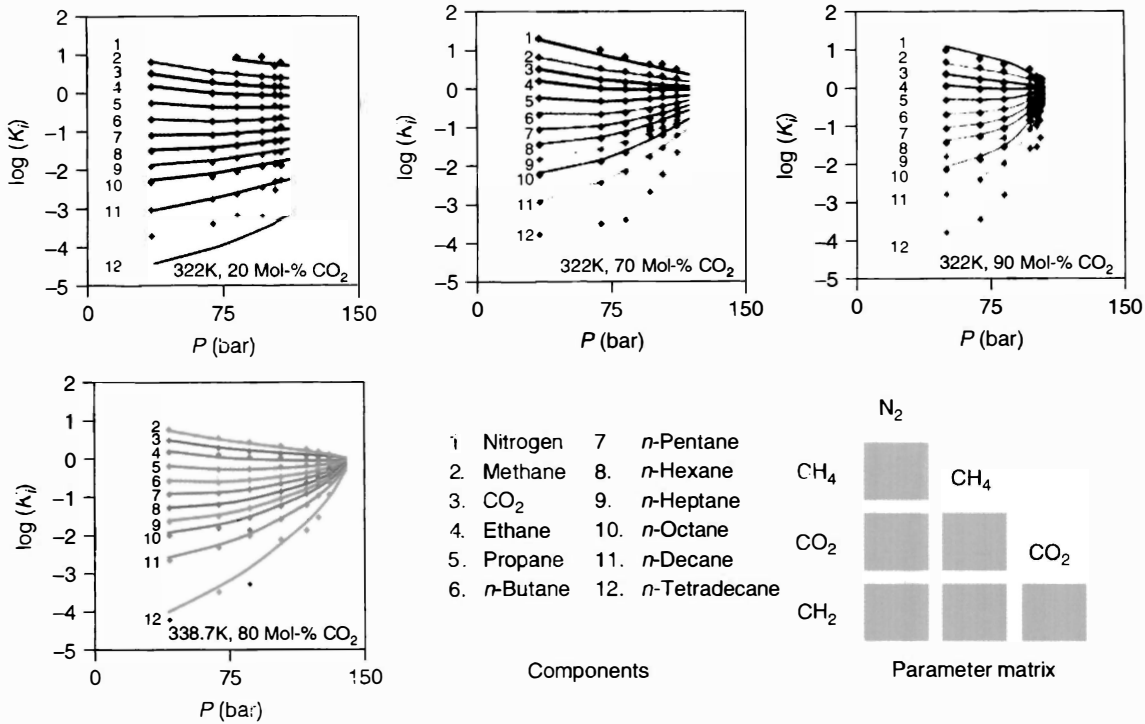

Figure 5.105 Experimental [65] and predicted K-factors for a 12 component system.

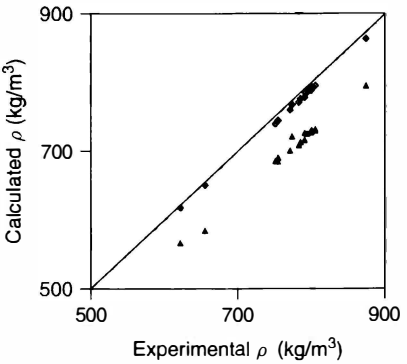

Figure 5.106 Experimental and calculated liquid densities using PSRK and VTPR for the quaternary system pentane–hexane–benzene–cyclohexane at 298.15 K: ▲ PSRK; ♦ VTPR.

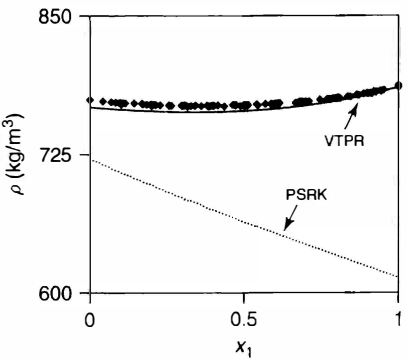

Figure 5.107 Experimental and predicted densities for the binary system acetone (1)–cyclohexane (2) at 298.15 K: ---- PSRK; — VTPR.

using VTPR is shown in Figure 5.102 together with the experimental data. It can be seen that the parameters fitted to a comprehensive data base can be successfully applied also at very low temperatures.

The next example (see Figure 5.103) shows the results of the group contribution equation of state VTPR in comparison to the results of modified UNIFAC for different VLE, excess enthalpies, SLE, azeotropic data, activity coefficients at infinite dilution for various alkane–ketone systems. It can be seen that with the group contribution equation of state VTPR similarly good results are obtained for the different phase equilibria and excess enthalpies as obtained with modified UNIFAC. But, besides the prediction of the different phase equilibria of subcritical compounds, the method can directly be applied for systems with supercritical compounds, for example, it can directly be applied for the calculation of gas solubilities. At the same time various other thermophysical properties (densities, enthalpies, for example, enthalpies of vaporization, heat capacities, Joule–Thomson coefficients, etc.) for pure compounds and mixtures for the liquid or gas phase can be predicted for the given condition (temperature, pressure, composition). The main disadvantage is that the available parameter matrix of the group contribution equation of state is still limited. But work is in progress to extend it.

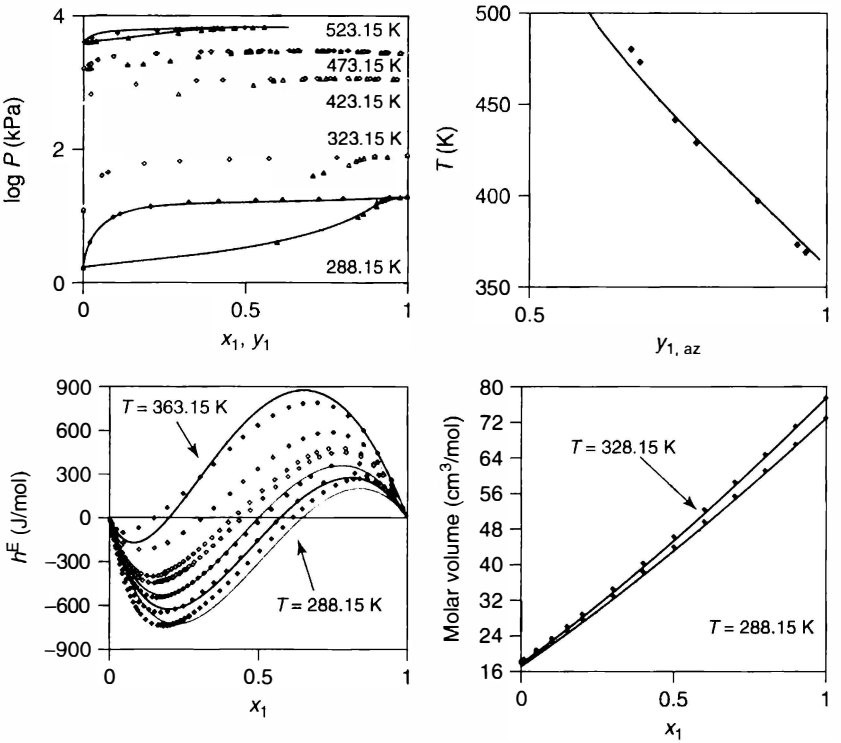

Figure 5.108 Correlation results of the equation of state VTPR for the system acetone(1)–water(2) using temperature dependent UNIQUAC parameters a_{12} = 472.46 K, a_{21} = −585.54 K, b_{12} = −0.40712, b_{21} = 2.5101, $c_{12} = 3.607 \cdot 10^{-4}$ K^{-1}, $c_{21} = 1.595$ 10^{-5} K^{-1}.

At the same time the group contribution equation of state VTPR in contrast to modified UNIFAC can be applied for the prediction of phase equilibria including compounds not covered by modified UNIFAC, for example, the various gases. The predicted LLE results for the ternary system nitrogen–CO_2–methane at 122 K and the binary system nitrogen–CO_2 as a function of temperature are shown in Figure 5.104 together with the experimental data.

A group contribution equation of state shows in particular great advantages compared to the usual equation of state approach in the case of multicomponent mixtures, when the multicomponent mixture consists of gases and various alkanes, alcohols, alkenes, and so on. The reason is that the same parameters can be used for all alkanes, alcohols, alkenes, so that the size of the parameter matrix is small in comparison to the typical equation of state approach. The results of VTPR for a 12 component system consisting of nitrogen–methane–CO_2–alkanes are shown in Figure 5.105. As can be seen, excellent results are obtained with the six required parameters (66 binary parameters would be required for the classical equation of state approach).

As mentioned already several times, using equations of state besides phase equilibria also other properties, such as densities, heat capacities, enthalpies, Joule–Thomson coefficients, and so on, for pure compounds and mixtures can be calculated. In Figure 5.106 the improvements in liquid densities for a four component system are shown, when instead of the PSRK the VTPR group contribution equation of state is used. The main reason for the improvements using VTPR comes from the fact, that the pure component densities are already much better described by the VTPR equation of state. In Figure 5.107 the predicted densities of the PSRK and the VTPR group contribution equation of state are shown together with the experimental densities. The improvement when going from PSRK to VTPR is significant.

VTPR can also be applied to correlate experimental data. Then instead of the group contribution method a g^E-model, for example, the UNIQUAC, Wilson, or NRTL equation can be applied. This is of great interest when reliable experimental data are available. For the system acetone–water the correlation results are shown in Figure 5.108. It can be seen that nearly perfect results are obtained for VLE, excess enthalpies and the azeotropic composition. Similarly good results can be obtained with the help of a g^E-model (see Figure 5.34). But as can be seen from the VLE data, now the model can be applied at supercritical conditions. At the same time other properties, for example, densities, and so on, can be calculated.

An overview about the development of group contribution methods and group contribution equations of state for the prediction of phase equilibria and other thermophysical properties can be found in [69].

Additional Problems

P5.1 Calculate the pressure and the vapor phase mole fraction for the system ethanol (1)–water (2) at 70 °C with the help of the different g^E-models (Wilson, NRTL, UNIQUAC) for an ethanol mole fraction of $x_1 = 0.252$ using the interaction parameters, auxiliary parameters, and Antoine constants given in Figure 5.30 and assuming ideal vapor phase behavior. Besides total and partial pressures and vapor phase composition, calculate also K-factors and separation factors. Repeat the calculation using the quantities defined in Eq. (5.15) $\phi_1 = 0.9958$ and $\phi_2 = 1.0070$.

P5.2 Regress the binary interaction parameters of the UNIQUAC model to the isobaric VLE data of the system ethanol (1) - water (2) measured by Kojima *et al.* at 1 atm and listed below. As objective function, use:

a. relative quadratic deviation in the activity coefficients
b. quadratic deviation in boiling temperatures
c. relative quadratic deviation in vapor phase compositions
d. relative deviation in separation factors.

Adjust the vapor pressure curves using a constant factor to exactly match the author's pure component vapor pressures.

x_1	y_1	T (K)	x_1	y_1	T (K)
0.0000	0.0000	373.15	0.5500	0.6765	352.57
0.0500	0.3372	363.15	0.6000	0.6986	352.28
0.1000	0.4521	359.08	0.6500	0.7250	352.00
0.1500	0.5056	357.12	0.7000	0.7550	351.75
0.2000	0.5359	356.05	0.7500	0.7840	351.57
0.2500	0.5589	355.29	0.8000	0.8167	351.45
0.3000	0.5794	354.67	0.8500	0.8591	351.37
0.3500	0.5987	354.14	0.9000	0.8959	351.35
0.4000	0.6177	353.67	0.9500	0.9474	351.39
0.4500	0.6371	353.25	1.0000	1.0000	351.48
0.5000	0.6558	352.90	–	–	–

Reference: Kojima, K., Tochigi, K., Seki, H., Watase, K., and Kagaku, Kogaku (1968) **32**, 149–153.

P5.3 Compare the experimental data for the system ethanol–water measured at 70 °C (see Figure 5.30 resp. Table 5.2) with the results of the group contribution method modified UNIFAC and the group contribution equation of state VTPR.

P5.4 Calculate the Pxy-diagram at 70 °C for the system ethanol(1)–benzene(2) assuming ideal vapor phase behavior using the Wilson equation. The binary Wilson parameters Λ_{12} and Λ_{21} should be derived from the activity coefficients at infinite dilution (see Table 5.6). Experimentally the following activity coefficients at infinite dilution were determined at this temperature:

$$\gamma_1^\infty = 7.44 \quad \gamma_2^\infty = 4.75$$

P5.5 Determine the azeotropic composition of the following homogeneous binary systems

a. acetone–water
b. ethanol–1,4-dioxane
c. acetone–methanol.

at 50, 100, and 150 °C using the group contribution method modified UNIFAC.

P5.6 In the manual of a home glass distillery (s. Figure P5.1) the following recommendation is given: "After some time liquid will drip out of the cooler. You are kindly requested to collect the first small quantity and not to use it, as first a methanol enrichment takes place." Does this recommendation make sense? The purpose of the glass distillery is to enrich ethanol. Consider the wine to be distilled as a mixture of ethanol (10 wt%), methanol (200 wt ppm), and water. The one stage distillation takes place at atmospheric pressure.

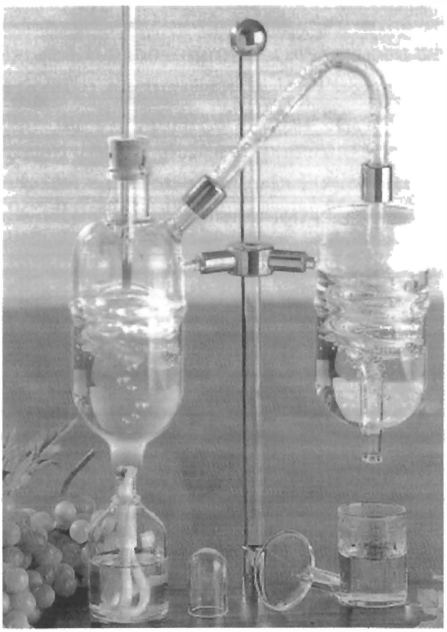

Figure P5.1 Home glass distillery

Calculate the percentages of methanol and ethanol removed from 200 g feed, when 10 g of the distillate is withdrawn. For the calculation the modified UNIFAC method should be applied. The constants for the Antoine equation for ethanol and water can directly be taken from Figure 5.30. For methanol the vapor pressure constants and the molar mass are given in Appendix A. For the calculation ideal vapor phase behavior should be assumed.

P5.7 Calculate the VLE behavior, h^E data, azeotropic data, and activity coefficients at infinite dilution for the system *n*-pentane–acetone at 373 K, 398 K, and 423 K using modified UNIFAC. The results are shown graphically in Figure 5.103.

The vapor pressure constants are given in Appendix A. Experimental data can be downloaded from the textbook material page on *www.ddbst.com*. For the calculation by modified UNIFAC ideal vapor phase behavior should be assumed.

P5.8 Using the free Explorer Version of DDB/DDBSP, search for mixture data for the system acetone–*n*-hexane.

a. Plot the experimental pressure as function of liquid and vapor phase composition together with the predictions using UNIFAC, modified UNIFAC, and PSRK for the data sets at 318 K and 338 K.

b. How large are the differences in the azeotropic composition as shown in the plot of separation factor vs. composition?
c. Plot the experimental heats of mixing data as function of liquid phase composition together with the predictions of UNIFAC, modified UNIFAC, and PSRK for the data sets at 243 K, 253 K, and 298 K. Interpret the linear part in some of the calculated heat of mixing curves.
d. Plot the experimental LLE data together with the results of UNIFAC and modified UNIFAC. What led to the improved results in case of modified UNIFAC?

P5.9 Using the free Explorer Version of DDB/DDBSP, search for mixture data for the systems CO_2–n-hexane and CO_2–hexadecane. Plot the experimental high pressure VLE data (HPV) together with the predictions using PSRK. Compare the results to those of VTPR (Figure 5.99d) and examine the results for SLE in the binary mixture CO_2–n-hexane.

P5.10 Calculate the activity coefficients in the system methanol (1)–toluene (2) from the data measured by Ocon *et al.* [71] at atmospheric pressure assuming ideal vapor phase behavior. Try to fit the untypical behavior of the activity coefficients of methanol as function of composition using temperature independent g^E-model parameters (Wilson, NRTL, UNIQUAC). Explain why the activity coefficients of methanol show a maximum at high toluene concentration.

The vapor pressure constants are given in Appendix A. Experimental data as well as molar volumes, r and q values can be downloaded from the textbook page on *www.ddbst.com*. For the calculation, ideal vapor phase behavior should be assumed.

P5.11 Predict the Henry constants of methane, carbon dioxide, and hydrogen sulfide in methanol in the temperature range −50 to 200 °C with the help of the group contribution methods PSRK and VTPR.

Compare the predicted Henry constants with experimental values from the textbook page on *www.ddbst.com*.

P5.12 Predict the solubility of methane, carbon dioxide, and hydrogen sulfide in methanol at a temperature of −30 °C for partial pressures of 5 bar, 10 bar, and 20 bar using the PSRK and VTPR group contribution equations of state. Compare the results with the solubilities obtained using Henry's law and the Henry constants predicted in problem P5.11.

P5.13 In the free DDBSP Explorer Version, search for data for all subsystems of the system methanol–methane–carbon dioxide.

a. Compare the available gas solubility data with the results of the PSRK method via the data prediction option in DDBSP.
b. Plot the available high pressure VLE data (HPV) for the system methanol–carbon dioxide together with the predicted curve using the PSRK method. Examine and familiarize yourself with the different graphical representations.

c. Regress the dataset 2256 using the Soave-Redlich-Kwong equation of state with the quadratic mixing rule and a g^E mixing rule with activity coefficient calculation via the UNIQUAC model. Explain the differences.

P5.14 In the free DDBSP Explorer Version, search for all mixture data for the system benzene–water. Calculate the solubility of benzene in water from the experimental activity coefficients at infinite dilution and compare the results to the experimental LLE data.

P5.15 Examine with the help of the regular solution theory, UNIFAC and modified UNIFAC if the binary systems benzene–cyclohexane and benzene–n-hexane show an azeotropic point at 80 °C. In case of the regular solution theory, calculate the solubility parameter from the saturated liquid density and the heat of vaporization using Eq. (5.70). All required data are given in Appendices A, H, and I.

References

1. Baerns, M., Behr, A., Brehm, A., Gmehling, J., Hofmann, H., Onken, U., and Renken, A. (2006) *Technische Chemie*, Wiley-VCH Verlag GmbH, Weinheim.
2. Hildebrand, J.H. (1949) *J. Phys. Coll. Chem.*, **53**, 944–947.
3. Dortmund Data Bank *www.ddbst.com*.
4. Parikh, J.S., Bukacek, R.F., Graham, L., and Leipziger, S. (1984) *J. Chem. Eng. Data*, **29**, 301–303.
5. Novak, J.P., Matous, J., and Pick, J. (1987) *Liquid – Liquid Equilibria*, Elsevier, Amsterdam.
6. Gmehling, J., Onken, U. *et al.* (1977) *Vapor–Liquid Equilibrium Data Collection*, DECHEMA Chemistry Data Series, 37 parts, Vol. **I**, DECHEMA, Frankfurt.
7. Gmehling, J. and Kolbe, B. (1992) *Thermodynamik*, Wiley-VCH Verlag GmbH, Weinheim.
8. Mertl, L. (1972) *Collect. Czech. Chem. Commun.*, **37**, 366–374.
9. Porter, A.W. (1921) *Trans. Faraday Soc.*, **16**, 336–345.
10. Redlich, O., Kister, A.T., and Turnquist, C.E. (1952) *Chem. Eng. Prog. Symp. Ser.*, **48** (2), 49–61.
11. Larkin, J.A. (1975) *J. Chem. Thermodyn.*, **7**, 137.
12. Chaudry, M.S. and Lamb, J.A. (1987) *J. Chem. Eng. Data*, **32**, 431–434.
13. Wilson, G.M. (1964) *J. Am. Chem. Soc.*, **86**, 127.
14. Renon, H. and Prausnitz, J.M. (1968) *AIChE J.*, **14**, 135.
15. Abrams, D. and Prausnitz, J.M. (1975) *AIChE J.*, **21**, 116.
16. Flory, P.J. (1941) *J. Chem. Phys.*, **9**, 660.
17. Huggins, M.L. (1941) *J. Phys. Chem.*, **9**, 440.
18. Huggins, M.L. (1942) *Ann. Acad. N. Y. Acad. Sci.*, **43**, 1.
19. Hiaki, T., Kurihara, K., and Kojima, K. (1994) *J. Chem. Eng. Data*, **39**, 714–719.
20. Voňka, P., Novák, J.P., Suška, J., and Pick, J. (1975) *Chem. Eng. Commun.*, **2**, 51.
21. Nelder, J.A. and Mead, R. (1965) *Comput. J.*, **7**, 308.
22. Hoffmann, U. and Hofmann, H. (1971) *Einführung in die Optimierung*, Wiley-VCH Verlag GmbH, Weinheim.
23. Gmehling, J., Menke, J. *et al.* (1986) *Activity Coefficients at Infinite Dilution*, DECHEMA Chemistry Data Series, 6 parts, Vol. **IX**, DECHEMA, Frankfurt.
24. Van Ness, H.C. (1995) *Pure Appl. Chem.*, **67**, 859–872.
25. (a) Redlich, O. and Kister, A.T. (1948) *Ind. Eng. Chem.*, **40**, 345; (b) Herington, E.F.H. (1947) *Nature*, **160**, 610; (c) Herington, E.F.H. (1951) *J. Inst. Petrol.*, **37**, 457.
26. Van Ness, H.C., Byer, S., and Gibbs, R.E. (1973) *AIChE J.*, **19**, 238.
27. Fredenslund, Aa., Gmehling, J., and Rasmussen, P. (1977) *Vapor–Liquid*

Equilibria Using UNIFAC, Elsevier, Amsterdam.

28. Margules, M. (1895) Akad. S.-B. *Wiss. Wien, Math. Naturwiss. Kl. II*, **104**, 1234.
29. van Laar, J.J. (1910) *Z. Phys. Chem.*, **72**, 723.
30. Fenske, M.R. (1931) *Ind. Eng. Chem.*, **24**, 482.
31. Rarey-Nies, J.R., Tiltmann, D., and Gmehling, J. (1989) *Chem. Ing. Tech.*, **61**, 407–410.
32. Tochigi, K., Rarey, J., and Gmehling, J. (2009) *J. Chem. Eng. Jpn.*, **42**, 376–380.
33. Peneloux, A., Rauzy, E., and Freze, R. (1982) *Fluid Phase Equilib.*, **8**, 7–23.
34. Diedrichs, A., Rarey, J., and Gmehling, J. (2006) *Fluid Phase Equilib.*, **248**, 56–69.
35. Huron, M.-J. and Vidal, J. (1979) *Fluid Phase Equilib.*, **3**, 255.
36. Knapp, H., Döring, R., Oellrich, L., Plöcker, U., and Prausnitz, J.M. (1982) *Vapor – Liquid Equilibria for Mixtures of Low Boiling Substances*, DECHEMA Chemistry Data Series, Vol. **VI**, DECHEMA, Frankfurt.
37. Gmehling, J., Menke, J., Krafczyk, J., and Fischer, K. (2004) *Azeotropic Data*, 3 parts, Wiley-VCH Verlag GmbH, Weinheim.
38. Novak, J.P., Matous, J., and Vonka, P. (1991) *Collect. Czech. Chem. Commun.*, **56**, 745–749.
39. Zieborak, K. (1966) *Z. Phys. Chem.*, **231**, 248–258.
40. Gmehling, J. and Möllmann, C. (1998) *Ind. Eng. Chem. Res.*, **37**, 3112–3123.
41. Hochgesand, G. (1970) *Ind. Eng. Chem.*, **62**, 37–43.
42. Sada, E., Kito, S., and Ito, Y. (1976) 170th Meeting ACS, Chicago, August 27–28, 1975, pp. 374–380.
43. (a) Holderbaum, T. and Gmehling, J. (1991) *Fluid Phase Equilib.*, **70**, 251–265; (b) Horstmann, S., Fischer, K., and Gmehling, J. (2000) *Fluid Phase Equilib.*, **167**, 173–186.
44. (a) Ahlers, J. and Gmehling, J. (2001) *Fluid Phase Equilib.*, **191**, 177–188; (b) Ahlers, J. and Gmehling, J. (2002) *Ind. Eng. Chem. Res.*, **41**, 3489–3498; (c) Ahlers, J. and Gmehling, J. (2002) *Ind. Eng. Chem. Res.*, **41**, 5890–5899.
45. Prausnitz, J.M. and Shair, F.H. (1961) *AIChE J.*, **7**, 682.
46. Horiuti, J. (1931) *Sci. Pap. Inst. Phys. Chem. Res. (Jpn.)*, **17**, 125–256.
47. Sørensen, J.M., Arlt, W., Macedo, E., and Rasmussen, P. (1979) *Liquid–Liquid Equilibrium Data Collection*, DECHEMA Chemistry Data Series, 4 parts, DECHEMA, Frankfurt.
48. (a) Scatchard, G. (1931) *Chem. Rev.*, **8**, 321–333; (b) Hildebrand, J. and Wood, S.E. (1933) *J. Chem. Phys.* **1**, 817–822.
49. Prausnitz, J.M. and Gmehling, J. (1980) *Thermische Verfahrenstechnik – Phasengleichgewichte*, Krausskopff Verlag, Mainz.
50. Derr, E.L. and Deal, C.H. (1969) *Inst. Chem. Eng. Symp. Ser.*, **32**, 40–51.
51. Kojima, K. and Tochigi, K. (1979) *Prediction of Vapor–Liquid Equilibria by the ASOG Method*, Kodansha-Elsevier, Tokyo.
52. Fredenslund, Aa., Jones, R.L., and Prausnitz, J.M. (1975) *AIChE J.*, **21**, 1086–1099.
53. Hansen, K.H., Schiller, M., Fredenslund, Aa., Gmehling, J., and Rasmussen, P. (1991) *Ind. Eng. Chem. Res.*, **30**, 2352–2355.
54. Bondi, A. (1967) *Chem. Rev.*, **67**, 565.
55. Weidlich, U. and Gmehling, J. (1987) *Ind. Eng. Chem. Res.*, **26**, 1372–1381.
56. Nebig, S. and Gmehling, J. (2011) *Fluid Phase Equilib.*, **302**, 220–225.
57. UNIFAC Consortium *www.unifac.org*.
58. Gmehling, J., Li, J., and Schiller, M. (1993) *Ind. Eng. Chem. Res.*, **32**, 178–193.
59. Wienke, G. and Gmehling, J. (1998) *Toxicol. Environ. Chem.*, **65**, 57–86. (Erratum: (1998) **67**, 275.)
60. Gmehling, J. and Rasmussen, P. (1982) *Ind. Eng. Chem. Fundam.*, **21**, 186.
61. Banerjee, S. (1985) *Environ. Sci. Technol.*, **19**, 369–370.
62. Jakob, A., Grensemann, H., Lohmann, J., and Gmehling, J. (2006) *Ind. Eng. Chem. Res.*, **45**, 7924–7933.
63. Soave, G. (1972) *Chem. Eng. Sci.*, **27**, 1197.
64. Peng, D.Y. and Robinson, D.B. (1976) *Ind. Eng. Chem. Fundam.*, **15**, 59–64.

65. Turek, E.A., Metcalfe, R.S., Yarborough, L., and Robinson, R.L. (1984) *Soc. Petrol Eng. J.*, **24**, 308–324.
66. Yan, W., Topphoff, M., Rose, C., and Gmehling, J. (1999) *Fluid Phase Equilib.*, **162**, 97–113.
67. Chen, J., Fischer, K., and Gmehling, J. (2002) *Fluid Phase Equilib.*, **200**, 411–429.
68. Jensen, R.H. and Kurata, F. (1971) *AIChE J.*, **17**, 357–364.
69. Gmehling, J. (2009) *J. Chem. Thermodyn.*, **41**, 731–747.
70. Anderson, T.F., Abrams, D.A., Grens, E.A., (1978) *AIChE J.*, **24**(1), 20–29.
71. Ocon, J., Tojo, G., Espada, L., (1969) *Anal. Quim.*, **65** 641–648.